2025-06

Geo-Information Science Program Developing an Earth Observation-Derived Combined Drought Index for Agricultural Drought Monitoring In Amhara Region, Ethiopia

Banchayehu, Molla

BAHIR DAR UNIVERSITY

FACULTY OF SOCIAL SCIENCES

DEPARTMENT OF GEOGRAPHY AND ENVIRONMENTAL STUDIES

GEO-INFORMATION SCIENCE PROGRAM

DEVELOPING AN EARTH OBSERVATION-DERIVED COMBINED DROUGHT INDEX FOR AGRICULTURAL DROUGHT MONITORING IN AMHARA REGION, ETHIOPIA

BY

BANCHAYEHU MOLLA

JUNE 2025

BAHIR DAR, ETHIOPIA

BAHIR DAR UNIVERSITY

FACULTY OF SOCIAL SCIENCES

DEPARTMENT OF GEOGRAPHY AND ENVIRONMENTAL STUDIES

GEO-INFORMATION SCIENCE PROGRAM

DEVELOPING AN EARTH OBSERVATION-DERIVED COMBINED DROUGHT INDEX FOR AGRICULTURAL DROUGHT MONITORING IN AMHARA REGION, ETHIOPIA

BY

BANCHAYEHU MOLLA

EMAIL: banchayehu.2022@gmail.com

A THESIS SUBMITTED TO THE DEPARTMENT OF GEOGRAPHY AND ENVIRONMENTAL STUDIES OF SOCIAL SCIENCE FACULTY, BAHIR DAR UNIVERSITY, IN PARTIAL FULFILLMENT OF THE REQUIREMENTS FOR THE DEGREE OF MASTERS OF SCIENCE IN GEO-INFORMATION SCIENCE

ADVISOR

SIMACHEW BANTIGEGN (PhD)

JUNE 2025

BAHIR DAR, ETHIOPIA

DECLARATION

I, Banchayehu Molla Getie, certify that the work embodied in this M.Sc. thesis is my own original work carried out by me under the supervision of Simachew Bantigegn (PhD) at the Faculty of Social Science, Department of Geography and Environmental Studies, Bahir Dar University, Bahir Dar, Ethiopia. The matters embodied in this M.Sc. thesis haven't been submitted for the award of any degree or diploma. I declare that I've faithfully conceded, given credit, and appertained to the exploration workers wherever their works have been cited in the textbook and the body of the thesis. I further certify that I haven't completely lifted some others' work, such as paragraphs, textbooks, data, and results, etc., reported in journals, books, magazines, reports, compositions, thesis, etc., and websites included them in this M.Sc. thesis and cited them as my own work. I also declare that I've conformed to all principles of academic honesty and integrity, and I haven't misrepresented, fabricated, or falsified any idea or data source in my submission. I understand that any violation of the academic rule will be cause for correctional action by the university.

Researcher Name	Signature	Date
Banchayehu Molla Getie	……………	------------------------

Place: Bahir Dar

BAHIR DAR UNIVERSITY

FACULTY OF SOCIAL SCIENCES

DEPARTMENT OF GEOGRAPHY AND ENVIRONMENTAL STUDIES

GEO-INFORMATION SCIENCE PROGRAM

THESIS APPROVAL SHEET

As a members of the Board of Examiners of the Master of Science (M.Sc.) thesis open defenses examination, we have read and evaluated this thesis prepared by Mrs. Banchayehu Molla Getie entitled **"Developing an Earth Observation Derived Combined Drought Index for Agricultural Drought Monitoring in Amhara Region, Ethiopia.''** We here by certify the award of the degree of Master of Science (M.Sc.) in Geo Information Science (GIS).

Board of Examiners

Internal Examiner: Mehretie Belay (PhD) Signature: _______ Date: _______

Chairperson: Birhanu Mengist (PhD) Signature: _______ Date: _______

External Examiner: Habitu W. (PhD) Signature: _______ Date: ______

ABSTRACT

Drought is one of the most devastating natural disasters in the world, affecting millions of people in various ways. Effective monitoring and assessment are therefore essential. This study aimed to develop an Earth observation-derived combined agricultural drought index (CADI) for agricultural drought monitoring in the Amhara Region. The development of CADI for the entire study period, that is, from 2000 to 2021, was constructed using a substantial machine learning (ML) algorithm, i.e., Random Forest (RF), by using SPI data calculated from selected fifty-one stations of the study area for each summer month. SPI values of each month were used to train the RF model and test the model; thus, 70% of the value of SPI was utilized for training the RF algorithms, and 30% of the value of SPI was utilized for testing. For the entire study period (2000 to 2021), remote sensing-based input parameters, which are Land Surface Temperature (LST), Temperature Condition Index (TCI), Evapotranspiration (ET), Normalized Difference Vegetation Index (NDVI), Vegetation Condition Index (VCI), Enhanced Vegetation Index (EVI), Precipitation Condition Index (PCI), and Soil Moisture Condition Index (SMCI), in addition to these, three topographic variables (Elevation, Slope, and Aspect) were utilized to develop CADI on a monthly scale for the entire study period (2000 to 2021). Crop yield and the Emergency Events Database (EM-DAT) drought periods were utilized to assess the effectiveness of the Combined Agricultural Drought Index. The result of CADI indicated that temporal and spatial variations of agricultural drought records have been observed in the study period with different severity levels. Hence, during the 22 years, 14, 16, 12, & 13 in June, July, August, and September were affected by droughts of different severity levels, respectively. Particularly, the CADI-derived maps depict that 2002, 2009, and 2015 were the years most affected by drought in terms of area coverage and severity levels (severe-to-extreme drought cases) in the Amhara region, Ethiopia. During these years, drought has affected about 77.14%, 83.04%, and 86.93% of the study area in 2002, 2009, and 2015, respectively, and 2007 was the wettest year during the entire study period as well as seasonally. The correlation coefficient results between the combined agricultural drought index and crop yield were very good, ranging from $r = 0.51$ to 0.95, indicating the index's utility for agricultural drought monitoring. From these, the highest correlation was observed in the East Gojam Zone and the lowest in the Wag Himra Zone. Overall, the combined agricultural drought index performed well in capturing the spatiotemporal patterns of the historic agricultural drought occurrences. CADI also performed well in distinguishing between drought and non-drought years, with higher sensitivity and spatial resolution than traditional drought indices. Thus, to mitigate the negative effects of drought in the region, the model can be used to develop an early warning system and agricultural drought monitoring. The CADI-based spatial analysis confirms its utility as a reliable tool for detecting and managing agricultural drought, aiding policymakers and stakeholders in developing region-specific drought preparedness and mitigation strategies. As a conclusion, this study confirms that CADI is a robust and adaptable index that enhances early warning capabilities and supports informed decision-making for agricultural drought risk management.

Keywords: *Agricultural Drought, Combined Agricultural Drought Index, Earth Observation, Amhara Region, Ethiopia.*

ACKNOWLEDGMENTS

First and foremost, I would like to praise Almighty God for giving me the strength and perseverance to complete this thesis.

Secondly, I express my deep gratitude to my advisor, Dr. Simachew Bantigegn, for his consistent supervision, invaluable advice, insightful comments, and systematic guidance throughout the development of this research. I am also sincerely thankful to Assistant Professor Daniel Asfaw (Bahir Dar University, Ethiopia) for his constructive feedback and evaluation of my research proposal, which greatly contributed to refining the overall direction of this thesis.

My heartfelt thanks also go to all my classmates, with special appreciation to Yonas Tesfay for your critical technical support. Whenever I needed help, you were always there. Thank you.

I extend my sincere thanks to Zerihun Chere (PhD student at Entoto Observatory and Research Center, Space Science and Geospatial Institute) and the staff of the Department of Geography and Environmental Studies at Dire Dawa University, Ethiopia. Your valuable advice, technical assistance, continuous encouragement, and constructive suggestions were instrumental in shaping this study. I truly appreciate your unwavering support and readiness to help whenever needed. I would also like to thank all my former teachers at Dire Dawa University, Ethiopia, for their foundational contributions to my academic journey.

Furthermore, I am deeply grateful to my family, especially my father, Molla Getie; my mother, Bizuayehu Setaregie; and all my brothers and my sister, for their moral and financial support throughout my academic years. A special thanks goes to my beloved husband, Belete Misgie, whose endless love, encouragement, and support have been the driving force behind my achievements.

Finally, I would like to thank the National Meteorological Agency of Ethiopia for providing ground station datasets; the Amhara Regional State Agricultural Office and the Amhara Regional State Disaster Risk Management Office for their cooperation in responding to interview questions; and the United States Geological Survey (USGS) Earth Explorer for making satellite datasets freely accessible.

TABLE OF CONTENTS

Contents Page

LIST OF TABLES

LIST OF FIGURES

ABBREVIATION AND ACRONYMS

CADI	Combined Agricultural Drought Index
CDI	Combined Drought Index
CDI-E	Combined Drought Index for Ethiopia
CHIRPS	Climate Hazard Group Infrared Precipitation with Station
CSA	Central Statistical Agency
EM- DAT	Emergency Events Database
EMDH	Ethiopia Mini Demographic and Health Survey
ENSO	El Niño-Southern Oscillation
ERDAS	Earth Resource Data Analysis System
ESA-CCI	European Space Agency-Climate Change Initiative
ET	Evapotranspiration
EVI	Enhanced Vegetation Index
FCE	Fuzzy Comprehensive Evaluation
FEWS-NET	Early Warning Systems Network
FLDAS	Famine Early Warning Systems Network Land Data Assimilation System
GEE	Google Earth Engine
GIS	Geographic Information System
GLDAS	Global Land Data Assimilation System
ICDI	Integrated Combined Drought Index
LST	Land Surface Temperature
ML	Machine Learning

MODIS	Moderate Resolution Spectra Radiometer
NDVI	Normalized Difference Vegetation Index
NIR	Near-Infrared
NMA	National Meteorological Agency
PCA	Principal Component analysis
PCI	Precipitation Condition Index
PET	Potential Evapotranspiration
PSNP	Productive Safety Net Program
RF	Random Forest
RS	Remote Sensing
SDCI	Scaled Drought Condition Index
SM	Soil Moisture
SMAP	Soil Moisture Active Passive products
SMCI	Soil Moisture Condition Index
TCI	Temperature Condition Index
USGS	United States Geological Survey
VCI	Vegetation Condition Index

CHAPTER ONE

1. INTRODUCTION

1.1. Background of the Study

One of the most devastating challenges of our day is climate change (Malhi et al., 2020), which has a significant impact on global ecosystems, economics, and civilizations (Kikstra et al., 2022). Global food security, livelihoods, the economy, the availability of water, and human health are all seriously threatened by these changes (Sikhwari, 2019). Climate change, driven by human activities such as greenhouse gas emissions, has led to significant alterations in global weather patterns, including shifts in precipitation, increased temperatures, and changes in hydrological cycles (Nema, 2012). These changes have profound implications for drought occurrence, severity, and duration, posing substantial risks to ecosystems, agriculture, water resources, and human well-being. Drought is a natural event characterized by prolonged periods of abnormally low precipitation and water scarcity (Slette et al., 2019). However, the influence of climate change has the potential to exacerbate the impacts of drought, making it a more frequent and severe occurrence in many regions of the world (Huijgevoort et al., 2013).

Drought is a prevalent natural disaster in various parts of the world (Mutsotso et al., 2018). It affects an integral component of ecosystems and is a common climatic phenomenon. The far-reaching and cumulative impacts of drought, covering extensive geographical areas, render it more potent than many other natural disasters (Haile et al., 2020). Particularly in developing and food-insecure settings, drought can inflict significant devastation across large regions over prolonged periods (Anderson et al., 2021). The effects of drought on vegetation conditions have serious repercussions for agriculture, ecosystems, food security, human health, water resources, and the economy (Wilhite, 2000). Furthermore, drought is an extremely destructive force, leading to pain, population displacement, food shortages, human and animal fatalities, diminished agricultural productivity, the drying of rivers and lakes, deteriorating water quality, wildfires, and permanent vegetation failure (Mekonnen & Gokcekus, 2020). Therefore, the multifaceted impact of drought underscores its far-reaching consequences on both the environment and human well-being (Congress et al., 2011).

Drought can be categorized into meteorological, hydrological, agricultural, and socioeconomic categories based on the length of time and the influence of the water cycle component (Tijdeman et al., 2022). The study's main topic, agricultural drought, is especially caused by a lack of moisture for the growth of vegetation. This inadequacy is attributed to deficits in precipitation, soil water, and evapotranspiration (ET) on the land surface and within the root zone (Zeleke et al., 2017). Moreover, agricultural drought happens when the soil's moisture content is insufficient to support optimal crop growth (Narasimhan & Srinivasan, 2005). Thus, agricultural drought hinders crop growth, which lowers yields (Dietz et al., 2021). Furthermore, lack of precipitation and decreased levels of soil moisture have had a detrimental impact on crop production and the regular public food supply in the majority of agricultural regions that depend on little rainfall, such as Ethiopia (Merga & Ahmed, 2019). Agriculture is significantly impacted by both hydrological and meteorological droughts because low rainfall, depleted soil moisture, and declining groundwater all lower agricultural yields (Wilhite, 2000). Thus, the emphasis on agricultural drought underscores the significance of understanding and monitoring the specific conditions that affect vegetation growth, which has direct implications for food security, ecosystems, and the broader agricultural sector (Belal et al., 2014).

Globally, drought have become more severe and now rank second among the top eight natural disasters. Drought frequency and severity are increasing due to human-caused global climate change (Zhang et al., 2023). Furthermore, it is predicted that by 2030, the frequency of drought events will increase by about 30% if the current trend continues (Wen et al., 2023). Drought has a destructive impact on the society, environment, and economy (Schreiner et al., 2018). Thus, drought was made worse by climate unpredictability, population expansion, changes in land use, wars, and political instability (Raleigh & Urdal, 2007).

In Africa, numerous countries consistently face the impact of severe and prolonged drought, resulting in substantial socioeconomic and environmental consequences (Kogan et al., 2019). The pronounced non-productive losses and the unpredictable nature of rainfall exert a significant impact on the rain-fed agricultural system of sub-Saharan Africa, including Ethiopia, where drought is a recurrent occurrence (Wolka et al., 2023). This has repercussions for various sectors, with agriculture being the most affected (Temam et al., 2019).

In Ethiopia, the recurrence of drought is a persistent phenomenon with far-reaching impacts across various sectors, notably agriculture. Agricultural drought is the primary hazard to human life (Tadesse, 2018). Ethiopia's economy, primarily reliant on agriculture, has faced challenges due to the country's vulnerability to drought (Alarifi et al., 2016). Additionally, Bewket and Conway (2007) stated that historically, drought in Ethiopia has been the primary cause of famines and food shortages in the country. For instance, the major drought occurrences during the years 1964-1966, 1972-1974, 1982-1984, 1987–1988, 1990, 1999, 2000, 2002, 2003, 2006, 2009, 2011, 2015, 2016, 2018, 2019, 2020, 2021, and 2022 (Degefu & Bewket, 2015; Deressa et al., 2010; Hirko et al., 2021). Thus, the most severe events in the last 30 years were the drought in 2015, which significantly impacted a substantial portion of the nation and worsened food insecurity (Chere & Debalke, 2024). This highlights the profound impact of drought on both the agricultural sector and the overall socioeconomic conditions in Ethiopia.

Even though a significant majority, more than 85% of the population in Ethiopia, relies on income generated from agricultural activities (Bayissa et al., 2019), the agricultural practices in the country are largely traditional and heavily dependent on annual precipitation (Gebregziabher et al., 2006). Consequently, the agricultural sector is highly susceptible to the adverse effects of insufficient and poorly timed rainfall, leading to decreased crop yields, concerns regarding food security, and substantial economic losses (Kassaye et al., 2021). Moreover, in Ethiopia and other eastern African nations, dry spells have become a repetitive marvel that can happen without caution, without border restrictions, and without financial or political contrasts. In this way, insufficient precipitation has shown up in large-scale nourishment security emergencies in the past, influencing the entire country (Wassie et al., 2022). In addition, in the years 2002–2003, Ethiopia experienced widespread food shortages; the impact was severe, leading to the loss of 1.4 million animals. In 2008-2009, also, nearly 15 million people were affected across various regions. In addition, repercussions continued in 2015–16, affecting around 5 million people in Northern, Southern, and Eastern Ethiopia (Liou & Mulualem, 2019; Mera, 2018). Moreover, reports by Kassaye et al. (2021) estimate that a staggering 10.2 million people were affected by these events.

The Amhara region, which is an important part of Ethiopia, is grappling with a severe and persistent climatic disaster attributed to ongoing drought conditions (Weldlul, 2016). The impact of this climatic event has been catastrophic, specifically causing destitution or extreme poverty for the population in North and South Wollo (Mekonen et al., 2020). Thus, during the drought of 2002 and 2009, a substantial proportion of the population in the weredas (administrative divisions) of Legambo, Desie Zurie, and Jamma in South Wollo, along with Bati in the Oromiya Zone, faced severe conditions; approximately 75% of the affected population in these areas required food assistance (Goyet et al., 2012). Thus, the gravity of the impact of drought on these communities emphasizes the urgent need for significant intervention measures (Mohamed, 2017). Addressing these challenges requires concerted efforts and targeted strategies to alleviate the suffering of the impacted communities. In light of the recurrent drought in Amhara's drought-prone areas, effective drought management has become a crucial priority. Specifically, an effective strategy to minimize the impacts of drought involves the application of a drought monitoring system (Mera, 2018). Such a system plays a key role in early identification and warning of impending dry spells (Dalezios et al., 2020). Moreover, appropriate drought monitoring and early warning systems are essential for reducing the overall impact of drought (Abdulkadir et al., 2016).

1.2. Statement of the Problem

Ethiopia's drought-affected areas are growing as a result of climate change, climate variability, and other human-caused variables (Siname et al., 2016). A prolonged drought that devastated Ethiopia's northern, southern, southeastern, and eastern regions resulted in an enormous food crisis (Mekonen et al., 2020). Ethiopia's primary food production, particularly in the Amhara Region, is nearly entirely dependent on rain-fed agriculture, and the region experiences recurrent droughts (Wassie et al., 2022). The primary causes of drought are insufficient management of water and a deficiency of precipitation relative to the demand for water (Rockström, 2003). Ethiopia's predominant economic activity, agriculture, has been significantly impacted by the recurrent drought that the country experiences (Mera, 2018). However, this sector is expected to play a pivotal role in driving the overall development of the nation, as well as specifically contributing to the economy of the Amhara region, Ethiopia (Shumuye, 2015). Despite the Amhara region's reputation for being a significant producer of food, its agricultural activities heavily rely on seasonal rainfall, which exhibits considerable variability (Demeku et al., 2015). Consequently, the impact of drought is severe, exacerbated by high rainfall variability both in space and time (Chere & Debalke, 2024).

Recurrent periods of drought have profound effects on the environment, society, and the economy (Schreiner et al., 2018). For example, during the drought of 2002 and 2009, a substantial proportion of the population in the weredas (administrative divisions) of Legambo, Desie Zurie, and Jamma in South Wollo, along with Bati in the Oromiya Zone, faced severe drought conditions (Goyet et al., 2012). As an illustration, the 2014 Ethiopia Mini Demographic and Health Survey (EMDHS) revealed that approximately 14.8% of rural households in Amhara faced persistent food shortages, prompting their inclusion in the Productive Safety Net Program (PSNP) in 2014. Therefore, to monitor agricultural drought, it is imperative to maintain regular and internally consistent records of data related to various biophysical variables (Kogan et al., 2019).

Agricultural drought, which occurs when there is a prolonged deficiency in precipitation that leads to a shortage of water for crops, has been a recurring challenge in the Amhara region. The impact of agricultural drought is far-reaching, affecting crop yields, livestock productivity, and the overall socioeconomic well-being of the communities in the region (Bogale & Erena, 2022). In recent years, there has been a growing body of research focused on understanding the dynamics of agricultural drought in the Amhara region. Major studies have highlighted the need for sustainable water management practices, improved irrigation infrastructure, and climate-resilient farming techniques to mitigate the impact of agricultural drought on local farmers. To address the complex challenges posed by agricultural drought in the region, it is essential to consider the interdisciplinary nature of the problem and explore holistic solutions that integrate scientific research, traditional knowledge, and community-based adaptation strategies.

In the Amhara Region, numerous research projects have been carried out to track agricultural drought utilizing GIS and remote sensing techniques. For instance, Wassie et al. (2022) determine and characterize agricultural droughts in North Wollo, Ethiopia, utilizing a number of MODIS-based metrics. Gebre et al. (2017) utilized GIS and RS methods to evaluate the state of the agricultural drought in the northern Wollo zone. Senamaw et al. (2021) utilized geospatial approaches to map the agricultural and climatic drought's temporal and spatial variations in Ethiopia's Waghimra Zone. Kebede (2019) evaluates the Waghimra Zone's agricultural drought situation using GIS and remote sensing methods. Demisse and Suryabhagavan (2016), in the east Amhara region, evaluate vegetation indices for agricultural drought monitoring. Together, the research deepens our understanding of the intensity of agricultural drought in the region.

However, until recently, there were very few comprehensive drought studies carried out in the Amhara Region that combined different environmental parameters that influence agricultural drought intensities. Prior studies have focused on applying a specific type of drought index separately for monitoring agricultural drought in the region, such as NDVI, SPI, VCI, LST, VHI, TCI, and SPEI, neglecting to apply them in a combined way. The overall drought condition cannot be assessed in a better way by drought indices separately rather by considering several agro-climatological settings in a combined way (Immerzeel et al., 2020). Therefore, for enhanced drought monitoring capabilities that can more effectively inform agricultural practices, the integration of many relevant environmental factors is required (Ji & Peters, 2003). Hence, in order to improve drought monitoring capacities and give further informed insights for agrarian practices, it is necessary that a number of applicable environmental indicators need to be integrated (Kulkarni et al., 2020). Thus, most studies demonstrated that the applicability and performance of the CADI in drought characterization and monitoring at the local scale compared to the being drought indicators (Bayissa et al., 2019; Cai et al., 2023 ; Karimi et al., 2022; Kulkarni et al., 2020; Lee et al., 2021). However, there aren't many studies like these in Ethiopia overall, and the Amhara region in particular. Therefore, the study aims to address the existing limitations in operational drought monitoring methods in the Amhara region. Specifically, it was sought to develop a Combined Agricultural Drought Index (CADI) for monitoring agricultural drought in the Amhara region.

1.3. Objectives of the Study

1.3.1. General Objective

The general objective of the study was to develop an Earth observation-derived combined drought index for agricultural drought monitoring in the Amhara Region, Ethiopia.

1.3.2. Specific Objectives

The following were the specific objectives of the study:

- To develop an Earth observation-based Combined Agricultural Drought Index (CADI) for the Amhara region.
- To examine the spatial and temporal agricultural drought status based on CADI in the Amhara region.
- To evaluate the performance of CADI in detecting the historic agricultural drought events in the study area.

1.4. Research Questions

1. How to develop an Earth Observation-based Combined Agricultural Drought Index (CADI) for the Amhara region?
2. What methods can be used to examine the spatial and temporal agricultural drought status based on CADI in the Amhara region?
3. How to evaluate the performance of CADI to detect the historic agricultural drought events in the study area?

1.5. Significance of the Study

The study is anticipated to furnish both quantitative and qualitative information crucial for monitoring agricultural drought, facilitating a prioritized response based on the severity and duration of hazard in the study area. This information is not only valuable for decision- and policymakers but also essential for formulating pre- and post-drought risk management plans. The identification of the most drought-vulnerable areas has a significant role in safeguarding the communities. This information is pertinent not only for the regional state government but also for the federal government of Ethiopia. The study will provide baseline information on the most vulnerable areas, enabling systematic surveillance and monitoring of drought and its effects. Given that agriculture is the primary economic activity in the Amhara Region, dependent on annual rainfall and subject to variability, the sectors have been significantly affected by drought. This impact extends to water scarcity, livestock mortality, economic fluctuations, and other related problems. Hence, the identification of the most drought-vulnerable areas is poised to play a crucial role in local community adaptation and mitigation strategies against the stated challenges. In general, the study was anticipated to offer an effective technique for monitoring agricultural drought, namely CADI, which will improve agricultural drought monitoring systems.

1.6. Scope of the Study

The geographic scope of the investigation was limited to the Amhara region. Temporally, by considering the summer season, which is the main rainy season of the study area (June to September), the study covers the years 2000 to 2021. The content scope of the study was to develop an Earth observation-derived combined drought index for agricultural drought monitoring in the Amhara Region, Ethiopia. CADI was developed using the Random Forest Model by using specified code on the GEE Platform. CADI was developed using eight independent variables, i.e., PCI, LST, TCI, NDVI, VCI, EVI, ET, and SMCI, and SPI for training and validation of the RF model. In addition, three topographic variables (elevation, aspect, and slope) were considered for CADI development.

1.7. Limitations of the Study

In conducting this study, numerous challenges were encountered. The primary challenge was the security problem in the Amhara Region; this security issue has an adverse impact, limiting the extent of fieldwork and data collection that could be conducted. To address these challenges, communication with the Amhara Region Agricultural Office and Disaster Risk Management of the Region was established to get data about the overall agricultural drought conditions in the region. The other limitation is that the availability of missing values for station data in the study area, even though the researcher demands to use all station rainfall data for this study that are found in the study area, the existence of more missing values of the rainfall data hinders it, so that the researcher utilizes only 51 station rainfall data that have less percent of missing values for this study. In addition, the absence of internet connectivity to do this study had an immense impact; the need for high-speed internet access to download large datasets further complicated the timely acquisition of the data. Despite these challenges, every effort was made to ensure that the study was as comprehensive and reliable as possible within the available resources. Furthermore, a trip to Addis Abeba for nearly two months and another trip to Dire Dawa resolved this issue.

1.8. Organization of the Paper

This thesis has five major components. The first chapter was about the background of the study, the statement of the problem, the objectives of the study, research questions, the scope of the study, and the significance of the study. The second chapter of the study was about reviewing related literature. Chapter three was about the research methodology and materials as well as a description of the study area. The result and discussion are carried out in the fourth chapter. The last chapter, Chapter Five, states the conclusions and recommendations parts of the study.

CHAPTER TWO

2. RELATED LITERATURE REVIEW

2.1. Definition and Concepts of Drought

Even though it is incorrectly believed to be an erratic and unusual occurrence, drought is a typical, recurring aspect of the climate (Slette et al., 2019). Contrary to aridity, which is only present in areas with little rainfall and is a recurring aspect of the climate, it is distinct from aridity (Wilhite, 2000). Additionally, according to Sivakumar (2010), it has to do with when and how well the rains fall. When precipitation falls below average over a length of time, drought is a harmful natural phenomenon that is characterized by making human activities and natural processes insufficient (Viste et al., 2013). Moreover, drought is a perilous natural phenomenon that develops when precipitation is less than normal for a length of time, resulting in a lack of resources for both human practices and natural activities (Sivakumar, 2010). Furthermore, it is a recurring extreme climate event characterized by under-normal precipitation over a period of months to years (Dalezios et al., 2020). Thus, it leads to serious economic and environmental issues, especially in agricultural production operations, which have an impact on the supply and demand balance for food (Boken, 2009).

Furthermore, Wilhite and Glantz (1985) stated that there are two types of definitions of drought: conceptual and operational. Conceptual definitions are defining the boundaries of the concept of drought and thus are holistic in their description of the phenomenon (Beltman, 2019). There is insufficient precipitation to meet the demands of human activities, resulting in economic, social, and environmental impacts (Mera, 2018). Additionally, drought frequency, severity, and duration for a specific historical time can be examined using operational definitions (Trenberth et al., 2014). The probabilities of droughts with different levels of intensity, duration, and regional features are computed using these definitions (Wilhite & Vanyarkho, 2000). Even though the term drought, has many different meanings, the best way to define drought is, it is an extended period of abnormally dry weather brought on by a serious hydrological imbalance that affects both human activity and environmental functions (Narasimhan, 2004).

2.2. Types of Drought

Even though, in the context of the proposed study, the primary emphasis of the study is agricultural drought, it's critical to comprehend the types of drought in order to evaluate and monitor them. Moreover, comprehensive understanding of various drought types is paramount due to the interconnected nature of agricultural drought with other forms (Beltman, 2019). The classification of drought extends beyond its type, encompassing considerations of intensity, duration, spatial extent, and perceived impact (Zargar et al., 2011). This definition is dynamic, continuously evolving to incorporate impacts and intricate interactions with the environment and society (Mukherjee et al., 2018). Classifying drought is complex, taking into account the length of time and the influence of the water cycle component. Thus, drought falls into four primary categories: meteorological, hydrological, agricultural, and socioeconomic (Tijdeman et al., 2022). Aligning with the framework proposed by Wilhite and Glantz (1985), a comprehensive understanding of these distinct drought types is imperative for a holistic examination of their impacts on agriculture and their broader implications for the environment and society.

2.2.1. Meteorological Drought

Meteorological drought alludes to a delayed period of below-average precipitation or an amplified nonappearance of precipitation in a specific locale (Sivakumar, 2010). It is ordinarily characterized by a shortage within the sum of precipitation compared to the long-term normal for that locale (Patel et al., 2007). Moreover, meteorological drought, as articulated by Viste et al. (2013), arises due to insufficient precipitation, focusing on the physical aspects of drought rather than its consequential impacts. The region-specific occurrence is characterized by the extent of dryness concerning a defined normal or average quantity and the duration of the dry period (Sivakumar, 2010).

2.2.2. Agricultural Drought

Agriculture, being the largest consumer of water, is particularly susceptible to drought, with moisture shortage often posing a significant obstacle to crop productivity (Rosegrant et al., 2009). The primary rainy season in Ethiopia, known as Kiremt, holds paramount importance for agricultural activities, contributing to approximately 95% of crop production (Belal et al., 2014). Consequently, agricultural drought during this crucial period significantly impacts the country's food production (Mera, 2018). When there is not enough moisture in the soil to support the best possible crop development, agricultural drought occurs (Zeleke, 2017). Additionally, agricultural drought is defined by erratic rainfall distribution over time, with crop production and the regular supply of food being negatively impacted in areas like Ethiopia that rely largely on little rainfall due to the lack of moisture (Chere & Debalke, 2024). This condition impedes crop development, leading to reduced yields. Both meteorological and hydrological drought exert a substantial influence on agricultural drought by causing low rainfall, soil water deficits, and diminishing groundwater levels, all contributing to decreased agricultural yields (Wilhite, 2000).

2.2.3. Hydrological Drought

Hydrological drought is distinguished by a shortage of surface or subsurface water, primarily arising from inadequate precipitation (Van Loon, 2015). This form of drought occurs when groundwater recharge diminishes or when there is a substantial deficit in surface runoff compared to normal conditions (Tallaksen & van Lanen, 2023). While the lack of precipitation is the fundamental cause of all droughts, hydrological drought places emphasis on how this scarcity of precipitation affects specific elements within the hydrological system, such as soil moisture, stream flow, groundwater levels, and reservoir capacities (Bayissa et al., 2019). Hydrologists are particularly concerned with understanding how the deficiency of precipitation unfolds through the hydrological system, making hydrological drought a specialized focus within the broader context of drought studies (Avanzi et al., 2024). Significantly, hydrological droughts typically occur after or out of sync with agricultural and meteorological droughts, indicating a delay in the effects on the hydrological system relative to the times when drought conditions first appeared (Van Loon, 2015).

2.2.4. Socio-economic Drought

According to Cerveny et al. (2017), socio-economic drought is intricately connected with the availability and demand of water, considering water as an economic good. These droughts occur when water resource systems fall short of meeting the demands for water (Sivakumar, 2010). In contrast to other forms of drought, socio-economic drought brings together elements of hydrological, agricultural, and meteorological dryness with the dynamics of supply and demand for particular economic goods or services (Schuldt et al., 2020). This can include critical resources like water, cattle fodder, or hydroelectric power. The distinctive feature of socio-economic drought lies in its integration of meteorological, agricultural, and hydrological factors with the economic implications of failing to meet specific demands for essential goods and services (Haile et al., 2020).

2.3. Causes of Drought

Distinct geographic elements, local oceanic circulations, and coastal influences are only a few examples of the many distinct factors that contribute to drought (Lyon, 2014). El Niño Southern Oscillation (ENSO), unusual patterns of sea surface temperature in regions other than the equatorial eastern Pacific, soil moisture desiccation, and nonlinear behavior of the climate system are all highlighted as potential causes of drought in eastern Africa (Masih et al., 2014). According to Dai (2011), there is also evidence that the climate is changing and that drought is becoming more frequent or more severe. Additionally, Lyon (2014) determined that anthropogenic factors and multi-decadal oscillations in the global sea surface temperature were the primary causes of drought.

2.3.1. Anthropogenic Factors

Under the circumstances of a growing population, anthropogenic environmental consequences have altered drought patterns (Masih et al., 2014). Land use change, land degradation, deforestation, fires, and mining are a few examples of these consequences (Gebremeskel et al., 2019). Additionally, drought is impacted by human activities such as the extension of grazing and farming lands, overuse of water resources, new settlements, and urbanization (Rosenzweig et al., 2014).

2.3.2. Natural Climate Variability

The considerable seasonal and interannual variability of the climatic system is one of the primary causes of drought. Drought in East Africa is intimately correlated with the complexity and variability of the El Niño-Southern Oscillation (ENSO) and land-atmosphere feedbacks (Matsumura et al., 2014). According to Tierney et al. (2013), the climate of East Africa is influenced by climate dynamics in the Indian Ocean and the Intertropical Convergence Zone (ITCZ), which are aggravated by the region's complicated topography. El Niño, a component of the Southern Oscillation, is an unusual warming of the ocean's surface water in the eastern tropical Pacific. Between the eastern and western tropical Pacific, there is an oscillating pattern of retreating surface air pressure known as the Southern Oscillation.

2.4. Historical Background of Drought in Ethiopia

Drought has been a part of the climate, and it has affected many countries in the world and this included Ethiopia (Dai, 2011). Thus, the country, has experienced the devastating impact of drought, in the country; the population has endured repeated periods of drought and significant fluctuations in climate conditions (Meze-Hausken, 2000). Moreover, Ethiopia has suffered from a

succession of severe droughts over the past 35 years, predominantly attributed to the failure of its primary rainy season known as "kiremt" (Hirko et al., 2021). This has had a profound impact on the country, considering that the majority of the population relies on rain-fed agriculture and related economic activities as their main source of livelihood (Bayissa et al., 2019).
According to O'Connor et al. (2017) in Ethiopia, drought is a phenomenon that happens in different parts of the country throughout different seasons when seasonal rainfall falls by roughly 30% to 50% below normal. It has shown a spatiotemporal distribution over the last fifty years and certain regions in the country are affected by drought regularly; the eastern and southeastern and rift valley regions (Feyisa, 2017). Devastating droughts have been reported in three consecutive years, and the frequency of droughts has recently been found to be decreasing 2015–2017 (Mera, 2018) .

Ethiopia has seen an increase in the frequency of droughts over time, especially in the second half of the 20th century (Viste et al., 2013). These findings highlight the recurring nature of drought events in the region and the growing challenges posed by their increased occurrence in recent decades. Since the mid-1970s, the severity and magnitude of drought have increased due to factors like climate change, deforestation, land degradation, and population growth.

In the year 1999-2000, a significant portion of Ethiopia's population, which consisted of approximately 10.5 million individuals, experienced adverse effects. Moving forward to 2002-2003, the number of affected people increased to over 15 million, and sadly, 1.4 million livestock perished. Similarly, in 2004-2005, more than 13 million people in Ethiopia were impacted by adverse conditions. In 2006, the Borena region alone witnessed the effects on about 7.4 million individuals, leading to the death of 247,000 livestock. In 2008, Borena reported the death of approximately 26,000 livestock. During the period of 2008-2009, all regions of Ethiopia experienced the consequences, affecting around 5 million people. Moreover, moving forward to 2011, the southern, southeastern, and eastern parts of Ethiopia were affected, with an estimated 4.5 million individuals experiencing the consequences. In addition, in 2015-2016, the northern, southern, and eastern regions of Ethiopia faced the impact, affecting approximately 10.2 million people (Degefu & Bewket, 2015; Deressa et al., 2010; Hirko et al., 2021).

These changes have been primarily managed by communities, highlighting the need for better preparedness and mitigation strategies (van Aalst et al., 2008). Climate change, deforestation, and land degradation in Ethiopia have increased vulnerability to droughts, affecting food security and livelihoods (Zegeye, 2018). The Ethiopian government and international organizations are implementing measures to enhance preparedness, response, and resilience, including early warning systems, community-based adaptation strategies, water resource management initiatives, and sustainable agricultural practices (van Ginkel & Biradar, 2021).

2.5. Historical Background of Drought in Amhara Region

Dry spells have been a repeating issue within the region for a long time, with extreme and destructive impacts on crops, animals, and the lives of the individuals. The recurrence and intensity of dry season occasions within the region have expanded over time, with critical dry spells recorded in 1984, 1985, and 2015 (Amsalu et al., 2019). In addition, nearly half of the woredas of the North Wollo Zone have been especially influenced, confronting serious and inveterate nourishment frailty as a result (Goyet et al., 2012). These dry seasons have led to nourishment deficiencies, lack of healthy sustenance, and financial hardship for the communities within the region (Mohamed, 2017). On the other hand, much of the western portion of the region has great soils and satisfactory precipitation and regularly produces rural surpluses (Asaye et al., 2025).

In this way, in reaction to the repeating dry seasons, the Ethiopian government, in collaboration with universal accomplices, has started different mediations to address the effect of the dry season within the locale (Tsige, 2019). These incorporate the arrangement of crisis nourishment help, the improvement of water sources through water system ventures, and the advancement of drought-resistant edit assortments. Moreover, universal organizations have bolstered activities pointed at building the strength of communities through vocation expansion and capacity-building programs. Be that as it may, continued collaboration, long-term arrangements, and ventures in sustainable advancement are fundamental to guaranteeing the long-term versatility of the Amhara region in the face of repetitive dry season occasions (Marthews et al., 2015).

2.6. Role of Remote Sensing and GIS in Drought Studies

Before, during, or after a disaster, the present situation can be monitored using satellite or remote sensing techniques (Wilhite, 1993). While the GIS approaches offer an appropriate framework for integrating and analyzing the several types of data sources required for catastrophe monitoring, they can be utilized to provide baseline data against which future changes can be evaluated (Tsatsaris et al., 2021). Recent years have seen a rise in major areas of concern related to the ever-increasing population and the overuse of natural resources, soil erosion, dwindling water supplies, and projected future climate change scenarios.

Recently, remote sensing and Geographic Information Systems (GIS) play a crucial role in agricultural drought studies by providing valuable information on drought monitoring, assessment, and mitigation strategies (Belal et al., 2014). In addition, remote sensing enables the monitoring of various drought-related indicators, such as vegetation health, soil moisture, and evapotranspiration (Aghakouchak et al., 2015). Moreover, GIS platforms help in integrating and analyzing the remote sensing data, facilitating the creation of drought monitoring systems (Anderson et al., 1997). In support of this, GIS platforms facilitate the integration of various datasets, including remote sensing data, topographic information, and socio-economic data (Gerland et al., 1996). By overlaying these datasets, researchers can assess the potential impact of drought on agricultural productivity, crop yield, and water availability. Such assessments support early warning systems and help in developing strategies for drought mitigation and adaptation (Wardlow et al., 2007).

Overall, by analyzing satellite imagery and GIS data layers, researchers can quantify vegetation indices, land surface temperature, precipitation patterns, and other relevant parameters. These assessments provide valuable insights into the spatial and temporal dynamics of drought, helping policymakers and farmers make informed decisions (Thenkabail et al., 2002). In addition, remote sensing and GIS can be used to develop drought risk maps, which identify areas prone to drought events based on historical climate data and satellite imagery (Anderson et al., 1997). Thus, these maps help in prioritizing resource allocation, implementing drought management strategies, and reducing vulnerability in agricultural systems (Peng et al., 2019).

2.7. Empirical Studies on Developing Combined Agricultural Drought Index (CADI) to Monitor Agricultural Drought

Several studies have been conducted around the globe to create and deploy integrated agricultural drought indices for the purpose of monitoring agricultural drought. For example, Agricultural Drought Assessment Using the Combined Drought Index: A Study in Northwest China by Cai et al. (2023) The study creates a Scaled Drought Condition Index (SDCI), also known as the Combined Drought Index, for agricultural drought assessment based on multi-source remote sensing data in a major grain-producing region of Northwest China. It integrates multiple indicators based on the combination of the PCI, VCI, and TCI using four different weight determination methods: Criteria relevance employing the Analytic Hierarchy Process (AHP), fuzzy comprehensive evaluation (FCE), entropy approach, and intercriteria correlation (CRITIC). Finally, a weighted sum approach is used. The result demonstrated the effectiveness of the SDCI in capturing agricultural drought dynamics and provided insights for drought disaster prevention and mitigation strategies.

Another study by Lee et al. (2021) entitled " Development of Integrated Crop Drought Index by Combining Rainfall, Land Surface Temperature, Evapotranspiration, Soil Moisture, and Vegetation Index for Agricultural Drought Monitoring" in the State of Illinois, a crucial region of the U.S. Corn Belt, the quantification and analysis of the failure were undertaken on a county size during the June to August months of 2004 to 2019. The rainfall factors (PCI), hydrological elements (PET and SM), and vegetating factors (improved vegetation index, or EVI) were combined to create the study's Drought Index (ICDI). According to the author, the ICDI accurately represents agricultural drought in terms of land surface dryness/wetness and its relationship to crop productivity.

In addition, a study by Karimi et al. (2022) entitled on, meteorological and agrarian failure monitoring in Southwest of Iran using a remote seeing- grounded combined failure indicator, they develop Combined Drought Index (CDI). The star element Analysis (PCA) system was employed, to develop CDI, therefore, combination of meteorological and agrarian information was used to develop a Combined Drought Indicator (CDI), i.e. Vegetation Condition Index (VCI), Temperature Condition Index (TCI), the Soil Water Index (SWI) and the precipitation condition indicator (PCI). The study demonstrated, that CDI indicator has a strong capacity for drought monitoring.

Also, a study by Kulkarni et al. (2020) between 2001 and 2018, monthly assessments of land surface temperature (LST), soil moisture (SM), and normalized difference vegetation index (NDVI) were conducted in Marathwada, India, to create an integrated Combined Drought Indicator Approach for Agricultural Drought Monitoring. The input parameters were standardized precipitation index (SPI-3). To integrate the input parameters for generating the CDI_M, two quantitative methods, PCA and expert judgment weighting of each parameter were tested. The study's findings indicated that the CDI_M is a useful tool for tracking India's agrarian failure and offers better data to support agricultural drought monitoring strategies.

In Ethiopia, few studies were taken to develop an integrated drought index, thus, one of the studies done for the end of developing a combined indicator is the study by Bayissa et al. (2019) Ethiopia as a case study for developing a composite drought indicator based on remote sensing to track agricultural drought. Standardized Precipitation Index (SPI), Land Surface Temperature (LST) anomaly, Standardized Normalized Difference Vegetation Index (stdNDVI), and Soil Moisture (SM) anomalies from 2001 to 2015. CDI-E were generated utilizing a quantitative methodology, namely the principal component analysis method (PCA), which assigns weights to each input parameter. The study's findings report, that the CDI- E efficiently maps the indigenous and temporal patterns of former failure and non-drought times effectively.

Likewise, Kebede et al. (2020) created two drought indices by taking into account indicators both with and without the contribution of climate signals, that is, both indicators that incorporate SST into the meteorological variables (MVDIstS) and those that do not (MVDIst0). To validate the quality and performance of the developed indicators the authors were enforced statistical technique i.e. RMSE, MAE and bias with the existing indicator of SPI across different time scales. The study revealed that the performance of the recently developed indicators for drought characterizing is best solution compared to SPI.

Most of the reviewed papers report the significance of integrating multiple indicators and data sources to develop a comprehensive Combined Drought Index (CDI) (Kulkarni et al., 2020 ; Lee et al., 2021; Cai et al., 2023; Karimi et al., 2022 ; Bayissa et al., 2019). They showcase different methodologies and approaches for CDI development and demonstrate the connection of these indicators in monitoring and assessing agricultural drought conditions. Also, the study demonstrated the connection and performance of the CDI in drought characterization and monitoring at the local scale compared to the existing indicators. However, there aren't many studies like these in Ethiopia overall, and the Amhara region in particular. Thus, this study was focusing on developing an Earth observation-derived combined drought index for agricultural drought monitoring in Amhara Region, Ethiopia.

2.8. Earth observation satellites derived drought indices for monitoring agricultural drought

The advancement of satellite remote sensing technologies over the past few decades has made a number of satellite-based drought indices available, including the precipitation index, vegetation index, and SM products index. In the last decades, numerous satellite-based drought indices, such as precipitation index, vegetation index, and SM products index, have become available through the development of satellite remote sensing technology (Martínez-Fernández et al., 2016). Thus, these drought indices are tools used to monitor and assess agricultural drought conditions using satellite remote sensing data (Crocetti et al., 2020). Moreover, Earth observation-based indices are valuable tools for monitoring and assessing drought conditions, offering valuable insights for agricultural management and decision-making (Running et al., 2019). These indices provide valuable information about the vegetation health and water availability, allowing for early detection and monitoring of drought impacts on agriculture.

Moreover, Earth observation indices provide a deeper understanding of the complex interactions between climate, soil, and vegetation, which are crucial for assessing drought impacts on agriculture (Liu et al., 2016). Thus, the ability to monitor various environmental parameters, such as vegetation health and moisture levels, allows for better prediction and management of drought-related risks in agricultural areas (Liu et al., 2016). Furthermore, the use of satellite remote sensing enables real-time and large-scale monitoring, offering a comprehensive and detailed assessment of drought conditions over a wide geographical area (Senay et al., 2014). This information can support farmers and agricultural stakeholders in making informed decisions regarding crop selection, irrigation strategies, and land management practices to mitigate the impacts of drought (Gautam & Pagay, 2020).

2.8.1. Normalized Difference Vegetation Index (NDVI)

The NDVI, which takes into consideration all green vegetation, is derived from the combination of near-infrared (NIR) and red band wavelengths (Stamford et al., 2023). Due to the tight connection between vegetative vigor and moisture state, the use of NDVI-based indicators for tracking and recognizing drought is justified (de Paul Obade et al., 2023; Gelata et al., 2023; Usman et al., 2015). NDVI has been used for a variety of applications, including monitoring vegetation cover and health, assessing the impacts of climate variability and change, and informing natural resource management strategies (Kogan & Guo, 2016). NDVI gives information on the spatial and temporal patterns of vegetation cover, as well as changes in vegetation cover over time.

Monitoring the effects of drought on ecosystems and human systems is made possible by the NDVI's sensitivity to changes in vegetation cover and health (Gelata et al., 2023). Reduced soil moisture and water availability during drought circumstances can result in less vegetation cover, which can be identified using NDVI. The effects of climate variability and change on vegetation cover and production have also been evaluated using NDVI. For example, studies have shown that NDVI can be used to detect changes in vegetation cover and productivity associated with changes in temperature and precipitation patterns (Stamford et al., 2023).

2.8.2. Vegetation Condition Index (VCI)

Vegetation Condition Index (VCI) is a measure of environmental stress that describes the vegetation's moisture content (Kogan, 2001). In addition, Vegetation Condition Index (VCI) is a valuable indicator for evaluating the health and condition of vegetation based on satellite imagery and remote sensing data, providing insights into changes in vegetation cover, growth, and stress levels over time (Pei et al., 2018). Moreover, VCI is an indicator used to assess the health and condition of vegetation, particularly in agricultural and ecological contexts (Dutta et al., 2015). Additionally, because VCI distinguishes between climate signals and long-term biological signals, it provides a more accurate measure of moisture shortage than NDVI (Dikici & Aksel, 2021).

The VCI is typically calculated using a combination of vegetation indices, such as the Normalized Difference Vegetation Index (NDVI), and statistical methods. The NDVI is calculated based on the contrast between near-infrared (NIR) and red-light reflectance, which provides an estimate of the vegetation's greenness and density. A VCI value nearer 100 denotes healthier and more abundant vegetation, whereas lower values signify vegetation stress or degeneration. The VCI value ranges from 0 to 100 (Tran et al., 2017). In support of this, very low and very high VCI values, respectively, show unfavorable and favorable situations (Kane et al., 2016).

2.8.3. Temperature Condition Index (TCI)

These days, due to global warming, temperature plays a critical role in monitoring drought, the NDVI-based VCI index alone is insufficient to adequately characterize droughts in agriculture (Rahman, 2016). Drought and the rise in land surface temperature are highly correlated, and the temperature increase is the first sign that crops are experiencing moisture stress and drought. The

TCI uses temperature-related drought situations as a thermal stress indicator (Adou et al., 2024). As a result of, TCI is a crucial metric in the material science of land surface processes at both regional and global levels, utilizing TCI is essential for drought monitoring (Parviz, 2016). Furthermore, the TCI is able to identify vegetative stress brought on by temperature (Chere et al., 2022). TCI gives opportunity to capture dry spell due to warm impact and recognize identify change s in vegetation wellbeing due to high temperature accompanied by moisture deficiency (Kogan & Guo, 2016). Moreover, Temperature Condition Index plays a crucial role in understanding and predicting various environmental phenomena (Dash et al., 2002). Thus, it provides valuable insights into the temperature of land surfaces, including both vegetation and bare soil (Kogan, 1997).

2.8.4. Precipitation Condition Index (PCI)

An important component of environmental and meteorological research, the Precipitation Condition Index provides important information about the distribution and variability of rainfall over various geographic areas (Schuldt et al., 2020). The PCI is designed to quantify the dispersion of precipitation over a defined area within a specific time frame (Carle et al., 2016). Numerous applications, such as agricultural planning, water resource management, and forecasting possible flood and drought conditions, depend on an understanding of the PCI (Shawul & Chakma, 2020). Moreover, rainfall concentration, the likelihood of drought or floods, and the erosivity of rainfall are all highly important indicators that were determined on an annual and monthly basis for each climatic station.

2.8.5. Soil Moisture

Soil moisture is a crucial factor in predicting both water storage levels and agricultural drought (Shao et al., 2018). It regulates water availability during transpiration, providing a direct indication of the agricultural drought state (Wei et al., 2021). Even though only a small percentage of precipitation is kept in the soil when evapotranspiration (ET), surface runoff, and deep percolation are taken into account, the soil's moisture reserve is crucial for the upkeep of crops, pastures, and forests (Narasimhan, 2004). Overall, Soil moisture is an important parameter in drought monitoring because; it controls the availability of water during transpiration, which directly reflects the state of drought (Brocca et al., 2011; Ford & Quiring, 2019; Shahzaman et al., 2021; Winker et al., 2009). Therefore, incorporating of these and related soil moisture indices, for drought detection, a more comprehensive characterization of drought conditions can be achieved (Khampeera et al., 2018).

CHAPTER THREE

3. MATERIALS AND METHODS

3.1. Description of the Study Area

3.1.1. Location

The Amhara Regional State is situated in northwestern and central Ethiopia, located between latitudes 8°36'0"N and 13°48'0"N and longitudes 35°12'0"E and 40°24'0"E. It shares borders with various regions, including the Republic of Sudan to the west, Tigray to the north, Afar to the east, Oromia to the south, and Benishangul-Gumuz to the southwest. The region has a total area of 155,275.224 km².

The region is blessed with numerous water resources, including rivers, lakes, and reservoirs. One of the primary water sources in the Amhara Region is Lake Tana, the largest lake in Ethiopia, which is located in its northwest. The Blue Nile River originates there, and it serves as a major water reserve for the region (Lilienthal et al., 2023). On its islands, the lake is home to a number of monasteries and is renowned for its beautiful splendor. The Blue Nile, also known as the Abbay River, originates from Lake Tana and passes through the Amhara Region. It is one of the Nile River's principal tributaries and is essential for supplying water for hydroelectric power production and agriculture. The Ribb River is another important water resource in the Amhara Region; it runs through the central and northeastern parts of the region, contributing to agriculture and providing water for domestic use (Bezabih, 2021).

Despite being endowed with abundant water resources, such as Lake Tana, the Blue Nile (Abbay) River, and the Ribb River, the Amhara Region continues to face recurrent agricultural drought. This apparent contradiction highlights the gap between water availability and effective water utilization. Factors such as limited irrigation infrastructure, uneven distribution of water sources, topographic challenges, soil degradation, and inefficient water management practices hinder the full use of available water for agriculture. Additionally, much of the rain-fed farming in the region remains highly vulnerable to seasonal rainfall variability. Thus, addressing agricultural drought in Amhara requires not only recognizing its rich hydrological potential but also investing in sustainable water management, irrigation development, and land restoration to bridge the gap between water abundance and agricultural resilience.

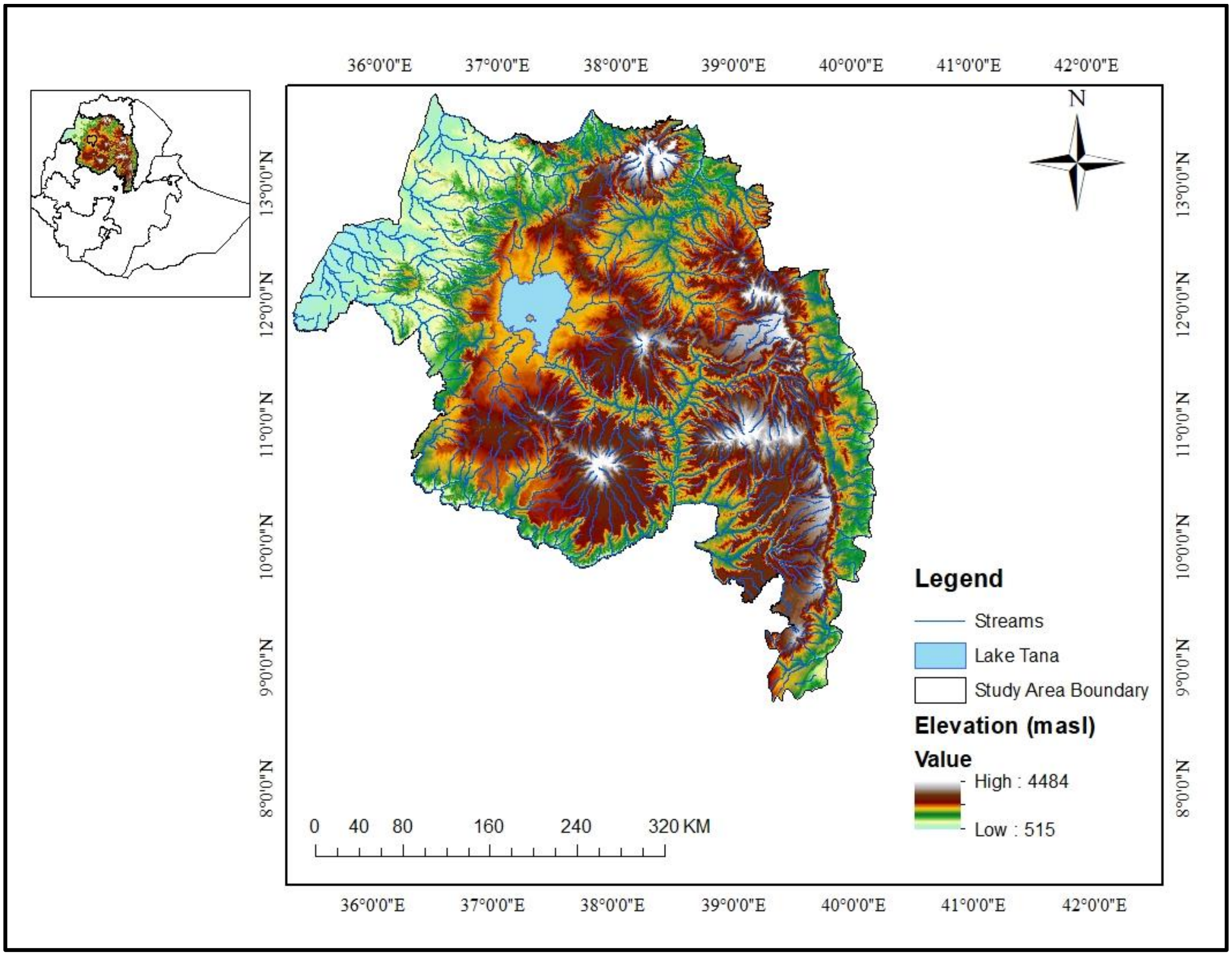

Figure 1: Map of the Study Area *(Source: Author,2025)*

3.1.2. Climate

The region exhibits diverse climate types due to its varied topography. The region encompasses both highland areas and lowland plains, resulting in a significant variation in climatic conditions. The study area is endowed with five agro-ecological zones based on Gorfu and Ahmed (2012) altitudinal classification; these are Kolla, which is between 500 and 1500 m above sea level; Woina Dega, which is between 1500 and 2300 m; Dega, which is between 2300 and 3200 m; Wurch, which is between 3200 and 3700 m above sea level; and Kur, which is over 3700 m. Having such different agroecology is very important for agricultural practices. Based on figure 2, the Kolla agro-ecological zone covers about 27.62% (43166.00 km²) of the study area, Woina Dega regions cover 45.11% (70591.31 km²), the Dega agro-ecological zone covers 24.12% (36841.63 km²), and Wurch and Kur cover 2.70% (4333.25 km²) and 0.45% (630.70 km²) of the area, respectively.

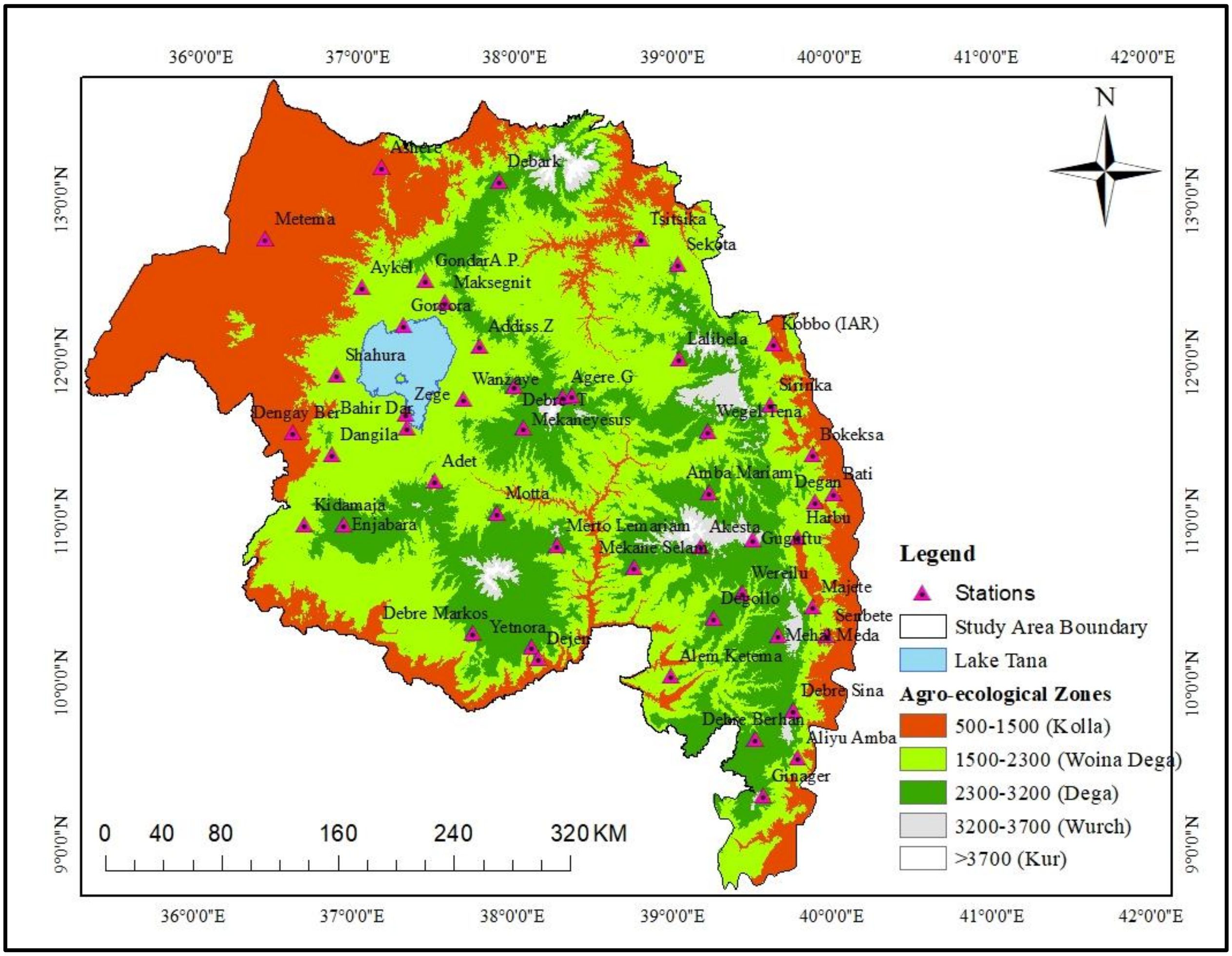

Figure 2: Agro-ecological Zones of Amhara Region Based on Altitudinal Classification and Location of Selected Stations *(Source: Author,2025)*

Thus, the highland areas of the Amhara region, including the Simien Mountains and parts of the region’s highland areas, encompass a highland climate. This climate type is characterized by cool to mild temperatures and relatively high precipitation.

Precipitation is significant throughout the year, with a distinct wet season from June to September. Rainfall varies from 1,000 to 2,500 mm on average per year. In addition, the average annual temperature is between 20 and 30 °C, and the average annual precipitation is between 300 and 800 mm. Moreover, some parts of the southern lowlands in the Amhara region have a subtropical steppe climate.

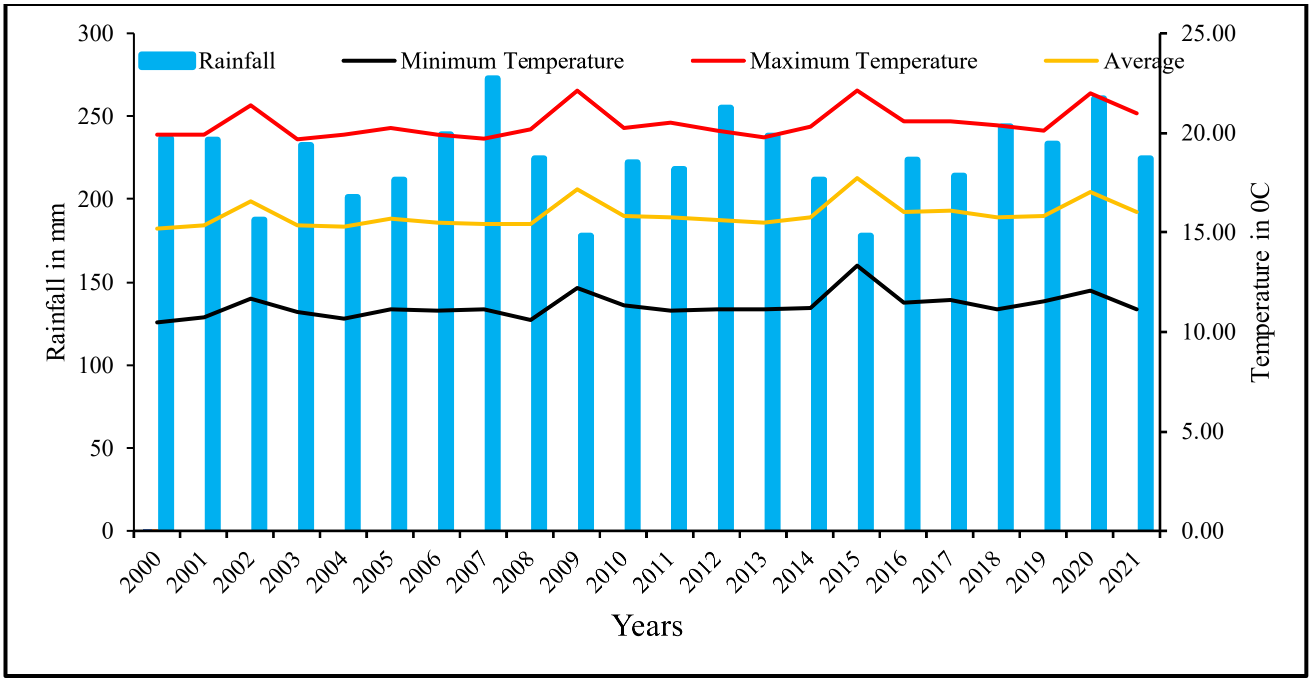

Figure 3: Rainfall and Temperature Distributions of the Amhara Region from 2000 to 2021

Source: -National Meteorological Agency (NMA))

3.1.3. Slope

Slope gradient analysis constitutes a fundamental parameter in agricultural practices, as it directly influences soil erosion and farming activities (Zhao et al., 2015). This study utilized Digital Elevation Model (DEM) analysis to classify the study area's topography into six distinct slope categories, each representing different degrees of vulnerability to soil erosion and results for agricultural production (Latocha & Migon, 2006). The analysis identified that flat to very gentle slopes (0-2) and gentle slopes (2-5) represent very low and low susceptibility to soil erosion, respectively, offering minimal land degradation challenges and maximum soil fertility. These areas demonstrate high suitability for crop production due to their favorable characteristics for the existence of developed soil type. Sloping (5-10) represents a medium level of susceptibility for soil erosion. A strongly sloping slope (10-15) represents high susceptibility, and moderately steep (15-30) and steep slopes (>30) represent very high and extremely high susceptibility areas for soil erosion.

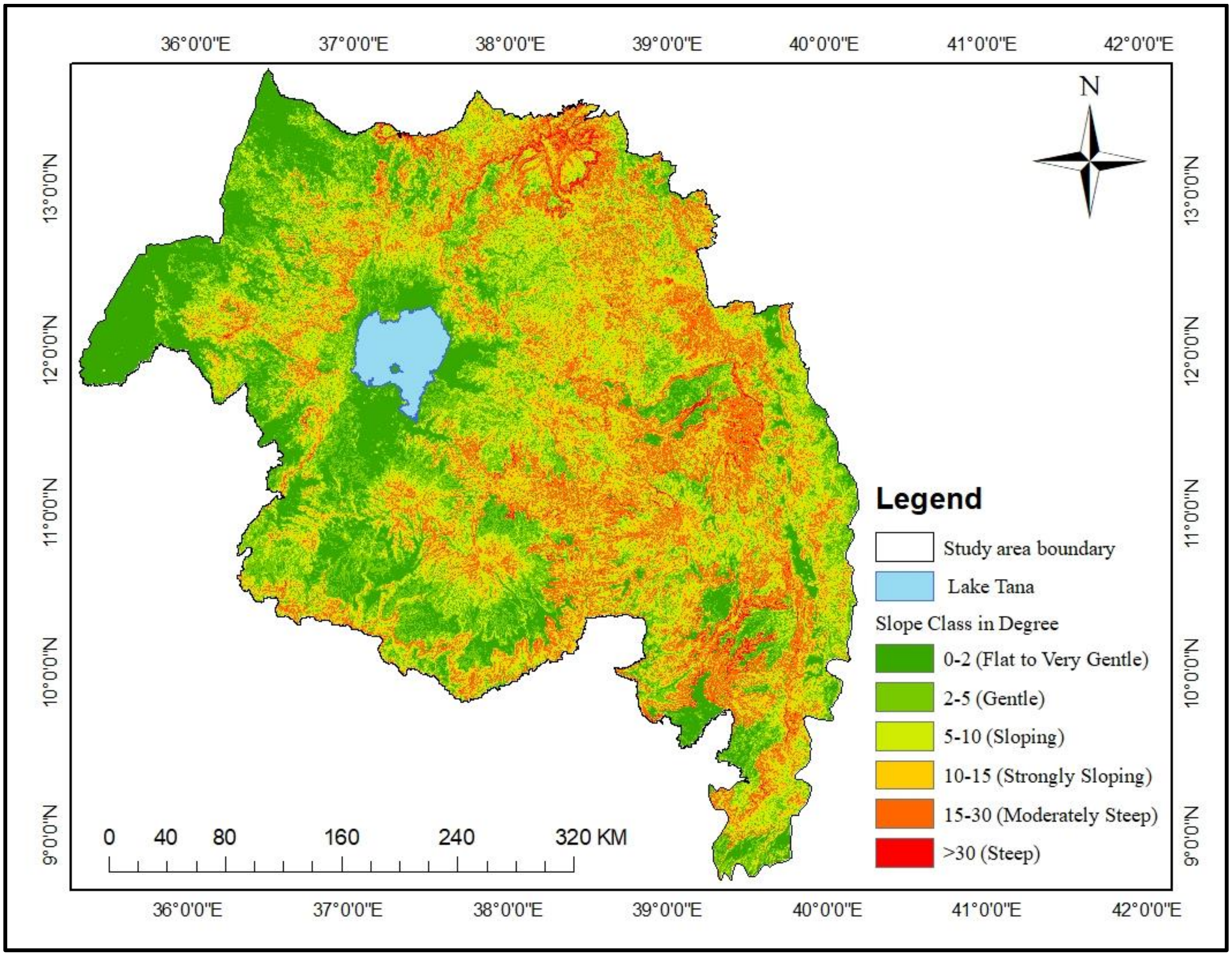

Figure 4: Slope Map of the Study Area *(Source: Author,2025)*

After dividing the digital elevation model (DEM) into six classes based on Nut et al. (2021), 23.22% of the total area has a slope of 5-10, whereas 22.02% and 21.42% of the entire area are characterized as flat to very gentle (0-2) and gentle slope (2-5). 15.72% (10-15), 16.58% (15-30), and 1.04% (>30) of the remaining land slopes were classified as strongly sloping, moderately steep, and steep slope, respectively.

3.1.4. Soils

The region is mostly home to Vertisols, Nitisols, Luvisols, and Cambisols. Vertisols (30%): Vertisols are soils that are high in clay content and have a high capacity to hold moisture. Their distinctive feature is their capacity to inflate when moist and create deep fractures when dry. These are very productive soils that can be farmed, particularly for crops like oilseeds, pulses, and cereals. Nitisols: 25% Deep, well-drained soils, nitisols are rich in organic matter and clay. They are very fruitful and have an excellent capacity to hold water. Thus, nitisols in the region are regarded as among the most productive soils for agriculture. They can be used to cultivate teff, sorghum, maize, and other crops. Luvisols (20%): Luvisols are medium-textured, well-drained soils that have a moderate fertility content.

The proportions of clay, silt, and sand for this type of soil are well-balanced. Hillsides and plateaus are just two of the environments where luvisols can be found. Numerous crops, including grains, legumes, vegetables, and fruits, can be grown in these soils. Cambisols (15%): Weak soil horizon development is a characteristic of cambisols, which are immature, shallow soils. Their textures vary, from sandy to clayey, and they are made of weathered parent materials. Low-rainfall regions are home to cambisols, which are ideal for cultivating crops resistant to drought, such as wheat, barley, and millet. The aforementioned soil types are the most common, while there can be other minor soil types in the area. Local variables such as drainage, fertility management techniques, and land use patterns can also have an impact on the properties of the soil and its appropriateness for particular crops.

Generally, the soils of the Amhara Region exhibit considerable spatial variability, which significantly influences the region's vulnerability to agricultural drought. Fertile and deep soils such as Nitisols and Vertisols generally have better moisture retention capacities, offering some resilience against short-term dry spells. However, the widespread presence of shallow and erosion-prone soils like Leptosols and Cambisols, particularly in highland and degraded areas, limits water-holding capacity and increases sensitivity to drought. These soil-related constraints highlight the importance of soil conservation, moisture management, and region-specific drought mitigation strategies to sustain agricultural productivity under increasingly variable climatic conditions.

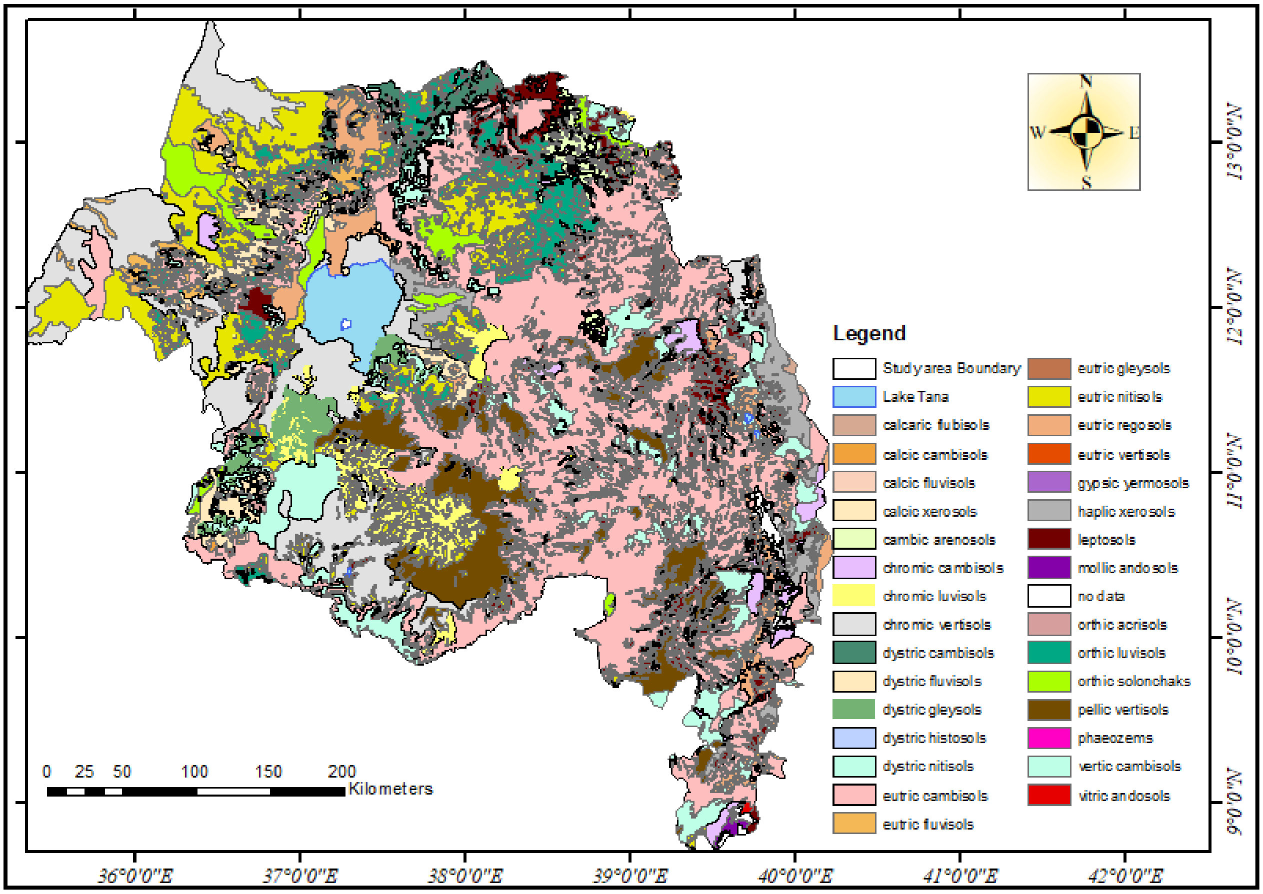

Figure 5: Soil type map of the study area, extract from Ethio-Soil shapefile

3.1.5. Major economic activity

Agriculture continues to be the predominant economic sector in the area, serving as the primary source of sustenance, raw materials for local industries, and income from exports. The region, characterized by its expansive landmass and diverse agro-ecology, possesses significant potential for producing a wide range of agricultural products intended for both domestic consumption and exportation. Additionally, the abundant water resources derived from Lake Tana and the region's rivers offer substantial opportunities for the development of irrigation systems. The extensive utilization of land to meet the increasing demands for food and feed, driven by the growing human and livestock population, has resulted in environmental degradation. Practices like overgrazing, deforestation, and suboptimal agricultural methods, including cultivating slopes unsuitable for agriculture, have significantly contributed to substantial soil erosion, particularly in the highland areas of the region.

3.1.6. Land Use/Cover Type

Understanding land use is crucial to comprehending how human activity interacts with the environment. The land use types within the study area were classified into nine major classes using the MODIS Land Cover type product (MCD12Q1). The MODISMCD12Q1 land cover product was chosen due to its long-term time series availability of the land cover data; it is available from 2001 to present. Land cover data sets that map the world's land cover at a 500-meter spatial resolution on an annual time period are available through the MODIS Land Cover type product (MCD12Q1).

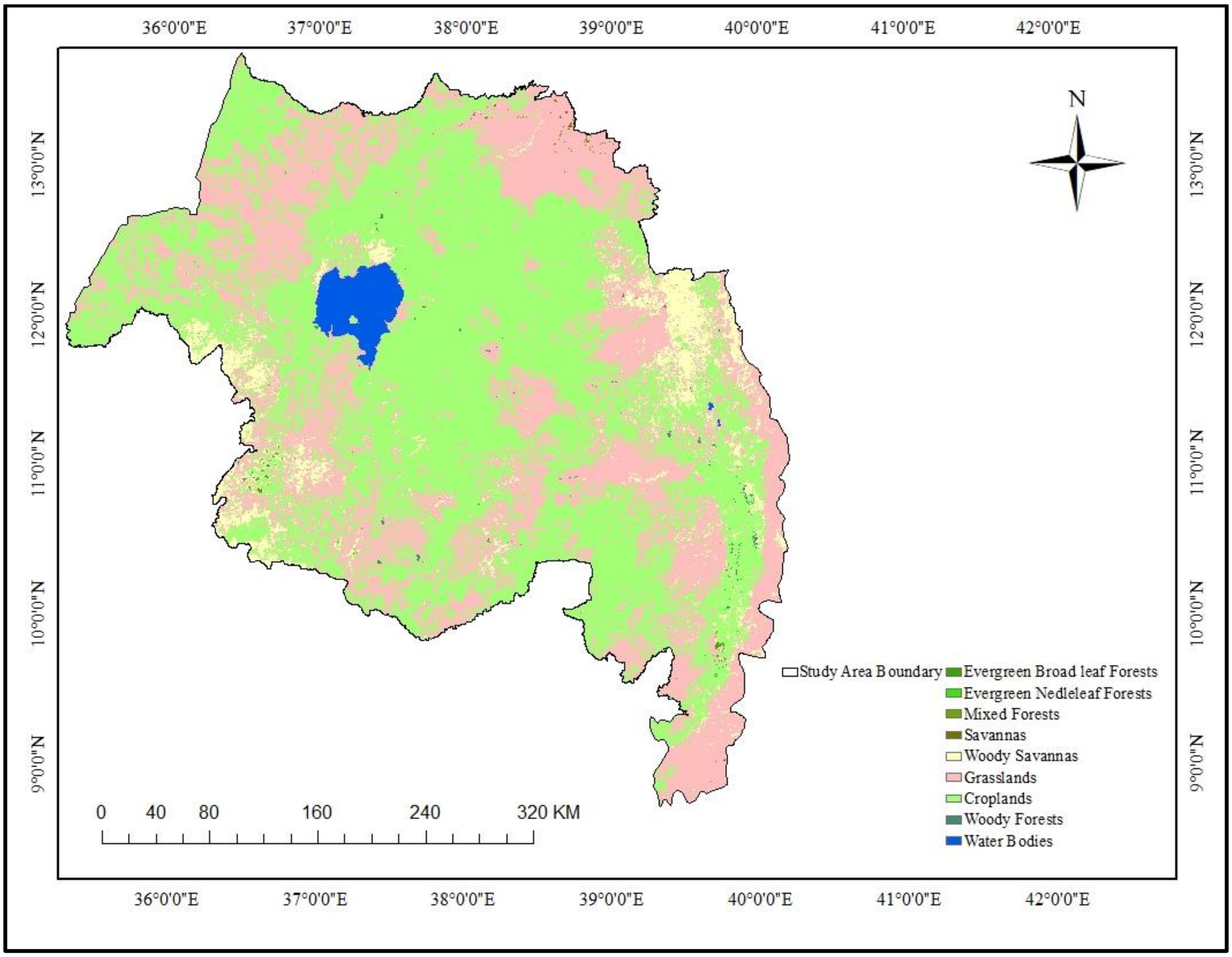

Figure 6: Land Cover Map of Amhara Region (*Source: MODIS Land Cover Type Product (MCD12Q1), 2021)*

The land cover map of the Amhara Region was extracted from the MODIS Land Cover Type Product MCD12Q1 for the recent year (2021). To show the land cover of the study area during this specified year, all land cover data from the year 2001 to 2021 was downloaded via the GEE platform. For this study, croplands (excluding other land uses) were taken into consideration as agricultural land and used to mask the developed agricultural drought index (CADI) for the study area for the entire study year (2000-2021). For CADI during 2000, agricultural land from 2001 was utilized because land cover data was available starting from 2001. Based on this LC map, cropland occupies 57.50% (89459.075 km^2), evergreen broadleaf forest area covers 0.01% (15.5581 km^2), evergreen needleleaf forests occupy 0.02% (31.1162 km^2), grasslands cover 36.68% (57063.4428 km^2), woody forests cover 0.03% (46.6713 km^2), mixed forests cover 0.02% (31.1142 km^2), woody savanna covers 3.58% (5553.885 km^2), savanna covers 0.22% (342.2562 km^2), and water bodies make up 1.94% (3018.0774 km^2).

3.2. Research Design

Descriptive research design was utilized to examine agricultural drought conditions in the Amhara region. It was employing a developed drought index (CADI) to generate reports on the severity of agricultural drought in different parts of the region. Additionally, the research incorporated a correlational research design to establish connections between developed drought indices and crop yield. This analysis aims to evaluate the effectiveness of the newly developed Combined Agricultural Drought Index (CADI).

3.3. Research Approach

Mixed research methods were used in the study to guarantee a thorough investigation of agricultural drought evaluation. The emphasis is on a quantitative approach, supplemented by the integration of a qualitative approach. This mixed research approach allows for the researcher to comprehensively explore various aspects related to agricultural drought monitoring.

3.4. Data Type and Sources

To carry out the study, various data sets were used. Primary and secondary data sources were therefore being used. Primary information was collected through an interview with key informants and from meteorological station data. Secondary data was collected from different existing sources such as published and unpublished literature like published and unpublished institutional reports, books, and other online data. Additionally, necessary secondary data were collected from different local and national government departments. In addition, RS and ancillary data on the study area were collected from different open-source websites and purchased from data providers.

Table 1: Data Types and Sources

Data Type	Data Set	Source	Variable(s)	Spatial Resolution	Temporal Resolution
Remote Sensing	MOD13Q1	NASA Earth data (MODIS)	NDVI, EVI	250 m	16 days
Remote Sensing	MOD11A2	NASA Earth data (MODIS)	Land Surface Temperature (LST)	1 km	8 days
Remote Sensing	MOD16A2GF	NASA Earth data (MODIS)	ET, PET	500 m	8 days
Remote Sensing	MCD12Q1	NASA Earth data (MODIS)	Land Cover	500 m	Annual
Satellite Rainfall	CHIRPS v2.0	Climate Hazards Group (CHG)	Precipitation (PCI)	5 km	Monthly
Reanalysis + Satellite	FLDAS NOAH01	NASA/USGS (MERRA-2$CHIRPS)	Soil Moisture (SM)	10 km	Monthly
Agricultural Data	Crop Yield	Central Statistical Agency (CSA), Ethiopia	Crop Yield	---	Annual
Ground Observation	Station Rainfall	National Meteorology Agency (NMA), Ethiopia	Rainfall	Point-based	Monthly

The details of these data sources and data types are explained in the following section.

3.4.1. Metrological Station Data

Meteorological station rainfall data were collected from fifty-one (51) meteorological stations for the period 2000-2021 from the NMA of Ethiopia to derive SPI for training and validation of the RF model by using the GEE platform. These stations and years were selected based on long-term data records and low percentages of missing data.

Table 2: List of Stations with their Location in Different Zones of the Study Area

No	Station	Latitude	Longitude	Location (Zone)
1	Addisszemene	12.116517	37.77313	South Gonder
2	Adet	11.2745	37.49312	West Gojam
3	Ageregenet	11.8005	38.2987	South Gonder
4	Akesta	10.867253	39.176667	South Wollo
5	Alem Ketema	10.064444	38.986667	North Shewa
6	Aliyu Amba	9.55	39.783333	North Shewa
7	Amba Mariam	11.203035	39.224444	South Wollo
8	Artuma	10.5861	40.014444	North Wollo
9	Ashere	13.2238	37.1488	North Gonder
10	Aykel	12.48	37.03	North Gonder
11	Bahir Dar	11.6027	37.322	West Gojam
12	Bati	11.196389	40.01539	Oromia
13	Bokeksa	11.443687	39.880661	South Wollo
14	Dangila	11.4337	36.846	West Gojam
15	Debark	13.14213	37.8979	North Gonder
16	Debre tabor	11.8666	37.9954	South Gonder
17	Debre Berhan	9.670278	39.513056	North Shewa
18	Debre Markos	10.3257	37.7392	East Gojam
19	Debre Sina	9.847778	39.756944	North Shewa
20	Degan	11.14453	39.89728	South Wollo
21	Degollo	10.42427	39.2529	South Wollo
22	Dejen	10.17115	38.150667	East Gojam
23	Dengay Ber	11.568	36.599	Awi/Agew
24	Enjabara	10.9954	36.9193	Awi/Agew
25	Ginager	9.316667	39.566667	North Shewa
26	Gondar Airport	12.52115	37.4319	North Gonder
27	Gorgora	12.243	37.292	North Gonder

28	Guguftu	10.912584	39.502035	South Wollo
29	Harbu	10.923375	39.786991	South Wollo
30	Kidamaja	10.9989	36.679	Awi/Agew
31	Kobbo (IAR)	12.133333	39.633333	North Wollo
32	Lalibela	12.038995	39.039839	North Wollo
33	Majete	10.496944	39.880278	North Shewa
34	Maksegnit	12.3884	37.5551	North Gonder
35	Mehal Meda	10.3146	39.66025	North Shewa
36	Mekane Selam	10.74311	38.756691	South Wollo
37	Mekaneyesus	11.6076	38.05422	South Gonder
38	Merto Lemariam	10.878	38.268	East Gojam
39	Metema	12.7746	36.4139	North Gonder
40	Motta	11.074	37.89	East Gojam
41	Nefas Mewcha	11.81	38.36	North Wollo
42	Sekota	12.625615	39.031013	Wag Himra
43	Senbete	10.316667	39.966667	North Shewa
44	Shahura	11.9286	36.8737	North Gonder
45	Sirinka	11.750998	39.614281	North Wollo
46	Tsitsika	12.783778	38.799889	Wag Himra
47	Wanzaye	11.7862	37.67503	South Gonder
48	Wegel Tena	11.590343	39.221215	North Wollo
49	Wereilu	10.579488	39.436719	South Wollo
50	Yetnora	10.2449	38.1083	East Gojam
51	Zege	11.68878	37.312433	South Gonder

3.4.2. Crop Yield Data

The accuracy of the satellite-derived resultant combined agricultural drought index (CADI) necessitates validation through ground truth data. Crop production served as the study's main source of validation. For validation, crop yield data were obtained from the Central Statistics Agency (CSA) of Ethiopia for the period 2000 to 2021 at the zonal level, focusing on major cereal crops (maize, wheat, and teff). This comprehensive approach aims to increase the reliability of the developed agricultural drought index used for agricultural drought monitoring by conducting cross-validation. Crop yield data for ten crop-growing zones of the study area were collected for the period 2000-2021. The crop yield data for the years 2004, 2005, 2006, 2007, 2008, 2010, 2011, 2012, 2013, 2014, 2015, 2016, 2019, and 2020 were collected and used for validation. However, data for eight years (2000, 2001, 2002, 2003, 2009, 2017, 2018 and 2021) were missing and therefore discarded.

3.4.3. Satellite Data

3.4.3.1. Climate Hazards Group Infrared Precipitation with Stations (CHIRPS) data

The researcher utilized the Climate Hazards Group Infrared Precipitation with Station data (CHIRPS) to assess drought conditions. The data set was created by the US Geological Survey (USGS) and the Climate Hazards Group at the University of California, Santa Barbara, and covers the years 1981-present. The selection of CHIRPS data is based on the recommendations of previous studies conducted by Bayissa et al. (2019) and Dinku et al. (2018). CHIRPS data have demonstrated their effectiveness in various research projects conducted in Ethiopia, a country known for its complex topography. One of the notable advantages of CHIRPS data is its longer record length, which allows for the analysis of historical precipitation patterns. Additionally, its high spatial and temporal resolution makes it a valuable resource for understanding precipitation patterns, monitoring drought conditions, and assessing climate variability and change (Bayissa et al., 2019).

3.4.3.2. Moderate Resolution Imaging Spectroradiometer (MODIS) Data

MODIS (Moderate Resolution Imaging Spectroradiometer) is a multispectral medium- and high-resolution sensor consisting of Terra and Aqua satellites with a wide range of applications in the field of earth and environmental science (Maselli et al., 2020). MODIS is a useful tool for studying Earth's biological, meteorological, and hydrological aspects since it can detect electromagnetic energy in a wide spectrum range (Wang et al., 2023).

The MODIS products include the vegetation index (normalized difference vegetation index, NDVI) product MOD13Q1, the land surface temperature product (MOD11A2), and the evapotranspiration product (ET/PET, MOD16A2GF). NDVI and LST were downloaded via Google Earth Engine (GEE). MOD13Q1 is a vegetation index product with 16-day temporal and 250-meter spatial resolution. A surface temperature product with a spatial resolution of 1 km and a temporal resolution of 8 days is MOD11A2. Furthermore, the Enhanced Vegetation Index (EVI) is regarded as a modified version of the Normalized Difference Vegetation Index (NDVI) with higher sensitivity to biomass, atmospheric background, and soil condition. EVI is particularly useful in global vegetation studies and improves the detection of vegetation changes and extraction of canopy biophysical parameters (Jiang et al., 2008).

In this research, the researcher utilizes 16-day and 250m spatial resolution MODIS EVI data specifically for the summer months of each year within the study period. Moreover, evapotranspiration (ET), an important component of the water and energy cycle, reflects mass and energy exchange between ecosystems and the atmosphere (Velpuri et al., 2013). A unique feature of ET for drought monitoring is that it describes both water or moisture availability and the rate at which it is consumed (Wang et al., 2023). In addition, evapotranspiration (ET) is closely related to drought conditions because it reflects energy and water exchanges among vegetation, soil, and the atmosphere and considers the characteristics of soil moisture (Maselli et al., 2020). Evapotranspiration (ET) holds a close relationship with drought conditions as it mirrors the exchange of energy and water among vegetation, soil, and the atmosphere. This process also takes into account the characteristics of soil moisture, as highlighted by Wang et al. (2023). Given its connection to the intricate dynamics of water movement and energy exchange, ET serves as a valuable indicator for assessing drought.

Deficits in ET are a direct measure of crop stress and can be integrated into agricultural drought monitoring systems (Marshall et al., 2012). ET, providing a more comprehensive understanding of crop water stress and drought conditions (Narasimhan & Srinivasan, 2005). By considering factors such as vegetation type and phonology, antecedent soil moisture conditions, and soil properties, these ET provide a more accurate representation of crop water stress and contribute to improved decision-making in water resource management and agricultural planning. Thus, evapotranspiration (ET) provides valuable insights into water demand, crop water stress, irrigation scheduling, drought impacts, drought forecasting, and regional comparisons, making it a valuable tool for agricultural drought monitoring and management (Allen et al., 2011).

3.4.3.3. Soil Moisture (FLDAS NOAH)

Soil moisture is a crucial factor in predicting both water storage levels and agricultural drought. It is crucial to the general growth of vegetation, particularly in the root zone. Additionally, soil moisture regulates water availability during transpiration, providing a direct indication of the agricultural drought state. To account for the readily available water at the plant root zone level, the NOAH soil moisture (SM) model (NASA/FLDAS/NOAH01/C/GL/M/V001') data was used in this investigation. Soil moisture in the midst of four soil layers, 0–10, 10–40, 40–100, and 100–200 cm, is simulated by the land surface model NOAH (Xu et al., 2019). The soil moisture at a depth of 10 to 40 cm was considered in this study. Monthly time series data of soil moisture were gathered from the Early Warning Systems Network and the Land Data Assimilation System (FLDAS) for the designated study period. Then the soil moisture condition index (SMCI) was derived from these data. Previous studies have verified that soil moisture is an effective indicator for monitoring agricultural drought since it affects plant growth and productivity (AghaKouchak et al., 2015; Maselli et al., 2020).

3.4.3.4 Topographic Factors Affecting Agricultural Activities

Topographic factors significantly influence the viability and nature of agricultural activities. Therefore, understanding these factors is essential for effective agricultural planning, helping farmers optimize crop selection, irrigation, and soil conservation for improved productivity and sustainability. For this study, three major topographic factors (aspect, elevation, and slope) that directly or indirectly affect agricultural activities were considered.

Drought's spatial distribution is correlated with many topographical features. By altering the geographical distribution of solar radiation intake, aspect can have an indirect impact on regional evapotranspiration and plant transpiration (Huryna & Pokorný, 2016). Plant transpiration is influenced by the slope direction through the distribution of nutrients, water content, temperature, and lightness (Singh, 2018). Evapotranspiration, precipitation, light intensity, and soil organic matter of a soil are spatially dependent on elevation differences. Land use type and elevation had an impact on the SOM content; soil organic matter (SOM) concentration clearly increased with elevation (Li et al., 2015).

3.5. Data Collection Instruments

The data collection instruments to be utilized encompass a range of methods and tools to gather and record information for this study. These instruments include interview items for in-depth investigation of issues related to agricultural drought conditions in the study area. Furthermore, the integration of satellite imagery, GIS tools, and remote sensing techniques enables the assessment of agricultural drought dynamics. The secondary data collection involves sourcing information from diverse sources such as books, thesis's, dissertations, articles, office reports, and websites, supplementing the primary data collection with comprehensive and varied sources of information.

Interview

The research instrument employed to gather information on the occurrence, challenges, and problems associated with agricultural drought in various parts of the study area involved key informant interviews. Thus, key informant interviews for the study were used to supplement the information gathered from the earth observation-derived drought index. For this purpose, the data were collected from experts of the Amhara region agricultural office and from Amhara region disaster risk management offices. Specifically, the data were collected from the expert of agriculture from the agricultural office of the region and disaster risk management office experts. Thus, six interviews of key informants were carried out until data saturation was reached. The interview was done face-to-face with the agricultural and disaster risk management experts of the Amhara region.

The data were collected by a semi-structured format of interview questions, allowing for flexibility and in-depth exploration of relevant topics for them. The interviews were recorded to ensure accurate representation of the information provided by the key informants. Following the interviews, careful transcription was conducted. This careful transcription process aims to substantiate the data gathered through interview and secondary data collection techniques, enhancing the overall reliability and comprehensiveness of the research findings. Furthermore, secondary data were collected from searching information from diverse sources such as books, thesis's, dissertations, articles, office reports, and websites.

3.6 Software Packages

The software that has been mainly used for data preprocessing, data preparation, data analysis, and final output preparation was ArcGIS 10.8.2, R-Studio, Google Earth Engine (GEE), and Microsoft Excel 2016. Overall, the software used for this study is summarized in table 3 below.

Table 3: Software used with its purpose

No	Software Type	Purpose
1	ArcGIS 10.8	Map layout preparation, spatial data processing for drought analysis
2	R. Software v.4.4	For the purpose of calculating the SPI (standard precipitation index)
3	Google Earth Engine	Accessing large-scale satellite data and analysis data for agricultural drought monitoring, process for CADI development within the study area boundary.
4	Microsoft Excel 2016	Data organization, preprocessing, Graphical analysis, basic statistical analysis for rainfall data for different drought indices and CADI, crop yield, and correlation analysis

3.7 Data Processing and Analysis Techniques

Following important data processing and analysis techniques is crucial in order to achieve the objectives of the study. The input parameters to develop CADI, i.e., CHIRPS, Land Surface Temperature (LST), Soil Moisture (SM), Evapotranspiration (ET), Enhanced Vegetation Index (EVI), and Normalized Difference Vegetation Index (NDVI), have different spatial resolutions. Therefore, to ensure data consistency and harmonization, the initial step involved resampling all datasets to a spatial resolution of 250 meters using bilinear resampling method on a monthly time scale with the coordinate reference system of the WGS84 (World Geodetic System 1984), and then they were processed into monthly composites. By aligning the spatial properties of the input parameters, the resampling procedure aimed to promote consistency for integrated analysis and interpretation in later phases of the study.

Normalized Difference Vegetation Index (NDVI)

NDVI is the most popular index for tracking vegetation; it accounts for all the green vegetation and is based on the combination of red band and near-infrared (NIR) band wavelengths (Sanjerehei, 2017). The NDVI data were processed using the Google Earth Engine platform following a specified code. For this study, the researcher utilizes 16-day MODIS NDVI data specifically for the summer months of each year within the study period. Initially, the data was processed using the Google Earth Engine platform, which provides access to a vast array of satellite imagery and geospatial data, focusing only on the area of interest defined by the study area boundary. To obtain the final result, the scaled NDVI data were rescaled to get the actual NDVI data sets, thus multiplying the mean NDVI values with a scale factor of 0.0001 using GEE. This rescaling process ensures that the values are adjusted to their actual NDVI representation, taking into account the provided scale factor. To get the actual NDVI value, the scaled NDVI value was calculated by its scale factor.

$$\text{Thus, Actual NDVI} = \text{Scaled NDVI} * \text{Scale Factor} \quad (1)$$

The researcher transforms the data from its scaled representation to the true NDVI values, which accurately reflect vegetation density and health within the study area, by multiplying the scaled NDVI values by the scale factor of 0.0001. The next projection transformation was performed using a specified code because the original projection, i.e., geographical projection, should be converted into UTM zone 37, as the study area is found in this zone and it is essential for better spatial analysis of the study area.

Vegetation Condition Index (VCI)

MODIS NDVI data, i.e., MOD13Q1, a vegetation index product with 16-day temporal and 250-meter spatial resolution, was utilized to derive VCI for JJAS months of the specified study period. The minimum and maximum values of NDVI data were processed using the Google Earth Engine platform following a specified code. That means the researcher processed the scaled NDVI values using GEE, focusing only on the area of interest defined by the study boundary. Then, the VCI was computed from NDVI values by the study area boundary. Next to this, projection transformation was performed using a specified code on GEE because the original projection, i.e., the geographical projection, should be converted into UTM zone 37, as the study area is found in this zone, and it is essential for better spatial analysis of the study area. After these steps, VCI for JJAS months of the entire study period was computed based on the following formula:

$$\text{VCI} = (\text{NDVI i} - \text{NDVImin}) / (\text{NDVImax} - \text{NDVImin}) * 100 \quad (2)$$

Thus, for each pixel for the years 2000–2021, NDVImax and NDVImin represent the maximum and minimum NDVI, respectively, whereas NDVIi is the smoothed monthly NDVI. The estimated VCI values are in the range of 0 and 100. The value of the computed VCI falls within the range of 0 and 100. Very low and very high VCI levels indicate good and unfavorable circumstances, respectively (Kane et al., 2016).

Land surface temperature (LST)

Land surface temperature plays a crucial role in understanding and predicting various environmental phenomena (Dash et al., 2012). It provides valuable insights into the temperature of land surfaces, including both vegetation and bare soil. One of the most important factors in the material science of land surface processes at both regional and global sizes is land surface temperature, which makes it an excellent indication of the energy adjustments at the earth's surface (Parviz, 2016). In the climate system, land surface temperature (LST) is crucial because it affects a number of factors, including runoff, vegetation growth, snow cover, and human livelihoods. Understanding the dynamics of LST serves as an indicator for climate variability and change, as noted by Reiners et al. (2023). Consequently, incorporating temperature data derived from LST is crucial for a more comprehensive characterization of agricultural drought. According to Alemu and Zimale (2025), LST is particularly effective for assessing and monitoring agricultural drought.

The preference for these data is attributed to their superior spatial and temporal variations, as well as an up-to-date algorithm that includes factors like time of acquisition, satellite view zenith, azimuth angle, and quality flags, facilitating easy interpretation of the products compared to the AVHRR sensor (Coppin et al., 2004). Additionally, they state that Terra LST data offers more detailed information than Aqua (night) because significant changes in LST can be observed during the daytime. This choice enhances the study's capacity to capture and analyze the nuances of agricultural drought conditions more accurately. Then, the LST data were rescaled and converted into degrees Celsius, and projection transformations were performed.

Thus, $$\boldsymbol{LST} = (£ * \mathbf{0.02}) - \mathbf{273.15} \tag{3}$$

Where LST = land surface temperature in degrees Celsius, £ = row data sets, and 273.15 K is in kelvin, which is equivalent to one degree Celsius, and 0.02 is the scale factor to get the correct LST data value in kelvin.

Temperature Condition Index (TCI)

The land surface temperature product, which is MOD11A2 is a surface temperature product that has a temporal resolution of 8 days and a spatial resolution of 1 km was utilized to derive TCI for JJAS months of the specified study period. The LST data were processed using GEE platform following a specified code. The minimum and maximum value of LST also computed, then TCI were computed by the study area boundary next projection transformation was performed using code because the original projection i.e. Geographical projection should be converted into UTM zone 37, as the study area is found in this zone and it is essential for better spatial analysis of the study area.

Then TCI was calculated using the next equation:

$$\text{TCI} = (\text{LST Max} - \text{LST i})/(\text{LST Max} - \text{LST Min}) * 100 \quad (4)$$

Where LST i is the smoothed monthly LST; LST max and LST min represent maximum and minimum LST, respectively, calculated by multiyear smoothed monthly LST series for each pixel during the period 2000–2021.

Evapotranspiration (ET)

Evapotranspiration (ET), an important component of the water and energy cycle reflecting mass and energy exchange between ecosystems and the atmosphere, was used for this study. A unique feature of ET for drought monitoring is that it describes both water or moisture availability and the rate at which it is consumed (Wang et al., 2023). In addition, evapotranspiration (ET) is closely related to drought conditions because it reflects energy and water exchanges among vegetation, soil, and the atmosphere and considers the characteristics of soil (Senay, 2018). The MOD16A2GF files, which contain ET and PET datasets, were used for this study.

Then, ET were calculated as; = $\text{Actual ET} = \text{Scaled ET} * \text{Scale Factor}$ (5)

By multiplying the scaled ET values by the scale factor of 0.1, the researcher was converting the data from its scaled representation to the actual ET values, which accurately reflect vegetation health and density within the study area.

Enhanced Vegetation Index (EVI)

An advanced vegetation index that is more sensitive to changes in canopy structure, such as leaf area index (LAI), canopy type, plant physiognomy, and canopy architecture, is the Enhanced Vegetation Index (EVI). It is regarded as a modified version of the Normalized Difference Vegetation Index (NDVI) with higher sensitivity to biomass, atmospheric background, and soil condition. In this research, the researcher utilizes 16-day and 250m spatial resolution MODIS EVI data specifically for the summer months of each year within the study period. The researcher converts the scaled EVI into actual EVI values, focusing only on the area of interest defined by the study boundary. Once the actual EVI values have been processed, the next step is to re-project the data using the GEE platform. The purpose of re-projecting the data is to convert it from its original geographical projection to the UTM projection zone 37. Finally, to obtain the final result to prepare the EVI data as an input to develop CADI, the EVI data were rescaled by multiplying the mean EVI values with a scale factor of 0.0001 using the GEE platform. This rescaling process ensures that the values are adjusted to their actual EVI representation.

The following was the formula used to calculate the actual EVI values:

$$\text{Scaled EVI} * \text{Scale Factor} = \text{Actual EVI} \tag{6}$$

In the study, the scaled EVI values were transformed from their scaled representation to the actual EVI values, which accurately reflect the density and health of the vegetation within the study region, by multiplying them by the scale factor of 0.0001.

Soil Moisture (SM)

Soil moisture is a crucial factor in predicting both water storage levels and agricultural drought. Additionally, soil moisture regulates water availability during transpiration, providing a direct indication of the agricultural drought conditions. In this study, the researcher utilizes the NOAH soil moisture model to assess water availability at the plant root zone level. Monthly time series data of soil moisture were gathered from the Early Warning Systems Network and the Land Data Assimilation System for the designated study period. Then soil moisture condition index (SMCI) was derived from these data. Previous studies have verified that soil moisture is an effective indicator for monitoring agricultural drought since it affects plant growth and (AghaKouchak et al., 2015). The readily available water at the plant root zone level was taken into consideration in this study using the NOAH soil moisture (SM) model. NOAH is a land surface model that simulates soil moisture for the middle of four soil layers: 0–10, 10–40, 40–100, and 100–200 cm (He et al., 2023).

The soil moisture at a depth of 10–40 cm was considered in this study, because soil at a depth of 10-40cm reflects the moisture availability within the root zone of many crops, which directly impacts plant water uptake and growth (Li et al., 2023). In addition, soil moisture with a depth of 10-40cm allows for the identification of areas where drought stress is likely to impact crop yield, enabling timely interventions like irrigation or drought resistant crop selection. The Early Warning Systems Network (FEWS NET) Land Data Assimilation System (FLDAS) provided monthly time series data for the years 2000–2021 with a geographical resolution of approximately 10 km. Thus, SMCI were processed and downloaded using GEE platform.

Thus, SMCI was calculated as

$$\mathrm{SMCI} = (\mathrm{SMi} - \mathrm{SM\ min})/(\mathrm{SM\ max} - \mathrm{SM\ min}) * 100 \qquad (7)$$

Where; SM min and SM max are the minimum and maximum values of SM at each grid in i month; SM i, represents the soil moisture in i month during the period 2000–2021.

Precipitation Condition Index (PCI)

The researcher was calculating the maximum and minimum values of CHIRPS data to derive PCI data using GGE platform. Then, once the maximum and minimum values have been calculated, the next step is to re-project the data using GEE platform. The purpose of re-projecting the data is to convert it from its original geographical projection to the UTM projection zone 37. Finaly, for this study, by using the maximum and minimum values of CHIRPS-2 monthly rainfall data, PCI was calculated on the study area boundary for each month for the entire study period (2000-2021). Thus, the following equation was the formula to calculate PCI:

$$\frac{\mathrm{CHIRPS\ i - CHIRPS\ min}}{\mathrm{CHIRPS\ max - CHIRPS\ min}} * 100 = PCI \qquad (8)$$

Where; CHIRPS min and CHIRPS max are the minimum and maximum values of CHIRPS at each grid in i month; CHIRPS i, represents the precipitation in i month during the period 2000–2021.

Table 4: Formulas for Standardized Input Parameters

Drought Indices	**Formula**
VCI	(NDVI i – NDVI Min) / (NDVI Max – NDVI Min) * 100
TCI	(LST Max –LST i) / (LST Max-LST Min) *100
PCI	(CHIRPS i – CHIRPS min) / (CHIRPS max – CHIRPS min) *100
SMCI	(SM i-SM min) / (SM max-SM min) *100
EVI	Scaled EVI * Scale Factor (0.0001)
NDVI	Scaled NDVI * Scale Factor (0.0001)
LST	LST = (£*0.02) -273.15
ET	Scaled ET * Scale Factor (0.1)

Crop Yield Data

According to Kulkarni et al. (2020) drought variability and its spatiotemporal distribution are therefore largely to blame for variations in crop productivity and general agricultural conditions. As a result, the developed agricultural drought index (CADI), needs to be validated using field data, such as crop yield. Crop Yield data provides crucial information about agricultural productivity and the success of farming practices. Hence, drought variability and its spatio-temporal distribution are highly responsible for the fluctuations in crop productivity and overall agricultural conditions, the developed agricultural drought index i.e. CADI requires validation with ground data such as with crop yield. However, agricultural yields and productivity are affected by different factors, including scientific and technical breakthroughs and weather and climatic conditions; therefore, detrending the crop yield datasets was performed to avoid the contribution of other factors. This work employed a straightforward linear regression model to detrend crop yield by eliminating the rising linear trend of agricultural yields (Lu et al., 2017). Therefore, the collected 14 years crop yield data at zonal level was detrend using the following Equation;

$$\boldsymbol{Ydt} = \mathbf{Yat} - (\mathbf{Y(t)} = \boldsymbol{\alpha} + \boldsymbol{\beta X(t)}) \tag{9}$$

Where Ydt is detrained yield at time t; Yat is actual yield at time t; Y(t) is predicted yield at time t, α is the estimated value of the crop yield at time t, β is the average change in crop yield per year, and X(t) is the year that the yield is estimated.

Meteorological Station Data

Station data has faced missing problems, which will be related to extreme conditions, failures of instruments and observer inaccuracies (Yozgatligil et al., 2013). Therefore, to get continuous data, such missing values must be filled by using different filling techniques before being used in any study. Based on data availability and temporal coverage, daily rainfall data from fifty-one stations, found in different zones of Amhara region, Ethiopia, as displayed on table 2 gathered over 22 years were examined for this study. The missed value of station rainfall data was filled using the Normal Ratio (NR) method. Then after filling the missed recorded values of station rainfall data, station rainfall for this study were utilized for deriving station-based SPI to train and testing of the RF model to construct CADI using GEE.

Calculating Station-based SPI

SPI-1 to SPI-3: A measure of immediate effects such decreased soil moisture, snowpack, and flow in smaller creeks can be obtained by computing SPI for shorter accumulation periods (1 to 3 months). When SPI is computed for medium accumulation periods (3 to 12 months), it can be used as an indicator for reduced stream flow and reservoir storage (Uddameri et al., 2019). For this study SPI is calculated for 1 month i.e. for each Kirmet season months (JJAS) using R. Software v.4.4, then in the construction processes of CADI, these SPI values of each month were used to train the RF model and test the model. In this way, 70% of the SPI value was used to train the RF algorithms, and the remaining 30% was used for testing purposes.

3.8. Processes for construction of Combined Agricultural Drought Index (CADI)

CADI was developed using random forest algorithm (RF), the reason for using the RF model is that the effectiveness of the model for different drought monitoring related studies. For instance, the superior performance of RF was confirmed in studies by Rahmati et al. (2020) simulated drought situations and forecasted their severity in Australia's southeast Queensland region using five machine learning models, the outcomes demonstrated that the RF model performed better than the other models. In addition, RF model was highly accurate in predicting the period, duration and severity of agricultural droughts Wang et al. (2022). Moreover, one of the first effective algorithms for drought forecasting and assessment was RF (Nagre et al., 2024). Furthermore, several studies have been confirmed the effectiveness of combined drought indicator for drought monitoring (Kulkarni et al., 2020 ; Lee et al., 2021; Cai et al., 2023;Karimi et al., 2022 ; Bayissa et al., 2019). The development of CADI was constructed by integrating different variables these are ET/PET, LST, TCI, NDVI, VCI, PCI, SMCI, EVI, and considering three topographic variables i.e. Aspect, slope and Elevation these factors have an impact on agricultural activities directly or indirectly that is by affecting the spatial distribution of solar radiation input, aspect can have an indirect impact on plant transpiration and regional evapotranspiration. Through the distribution of lightness, soil temperature, water content, and nutrients, the slope direction influences plant transpiration. Evapotranspiration, precipitation and light intensity spatially depending on elevation differences. Therefore, these variables (Aspect, slope and Elevation) were also utilized in the process of CADI construction.

In addition, the monthly station-based value of SPI was utilized to train and test the RF model; the SPI data from 2000 to 2021 for all summer season months were divided into two parts, thus 70% were for training the model and the remaining 30% were for testing. CADI based on RF was built using the training data, and the model's accuracy was confirmed using the test data. Based on the typical drought episodes and the SPI value, drought was identified.

Table 5: Drought categories and classes

Drought Category	CADI Values
Extreme Drought	$\leq$ -2
Severe Drought	-1.50 to -1.99
Moderate Drought	-1.0 to -1.49
Slight Drought	0.0 to -0.99
No Drought	>0

Source: Mckee et al., (1993)

3.9. Validation of the Agricultural Drought Monitoring Performance of CADI Using Crop Yield Data and EM-DAT

The performance of CADI was done considering EM-DAT drought records and crop yield data. Considering that extended droughts are reported, the EM-DAT drought periods are used as a guide. In addition, the performance of CADI was evaluated using crop yield data; hence, drought variability and its spatio-temporal distribution are highly responsible for the fluctuations in crop productivity and overall agricultural conditions Kulkarni et al. (2020). Detrending the crop yield records was done to exclude the influence of other factors, such include weather and climatic circumstances, scientific and technology advancements, and other factors that affect agricultural yields and productivity.

A straightforward linear regression model that eliminates the crop yields' increasing linear trend (Lu et al., 2017) was used in this study. Finally, the capabilities of CADI for agricultural drought monitoring in the Amhara Region, Ethiopia, were evaluated through Pearson correlation methods. Pearson correlation was utilized to establish a relationship between the CADI time series and the mean of annual production of cereal crops. Both positive and negative results can be obtained via Pearson correlation. According to Evans (1996), there are three types of relationships between CADI and detrended crop yield data: strong ($r \geq 0.60$), moderate ($r = 0.40–0.59$), and weak ($r = -0.40$ to 0.40).

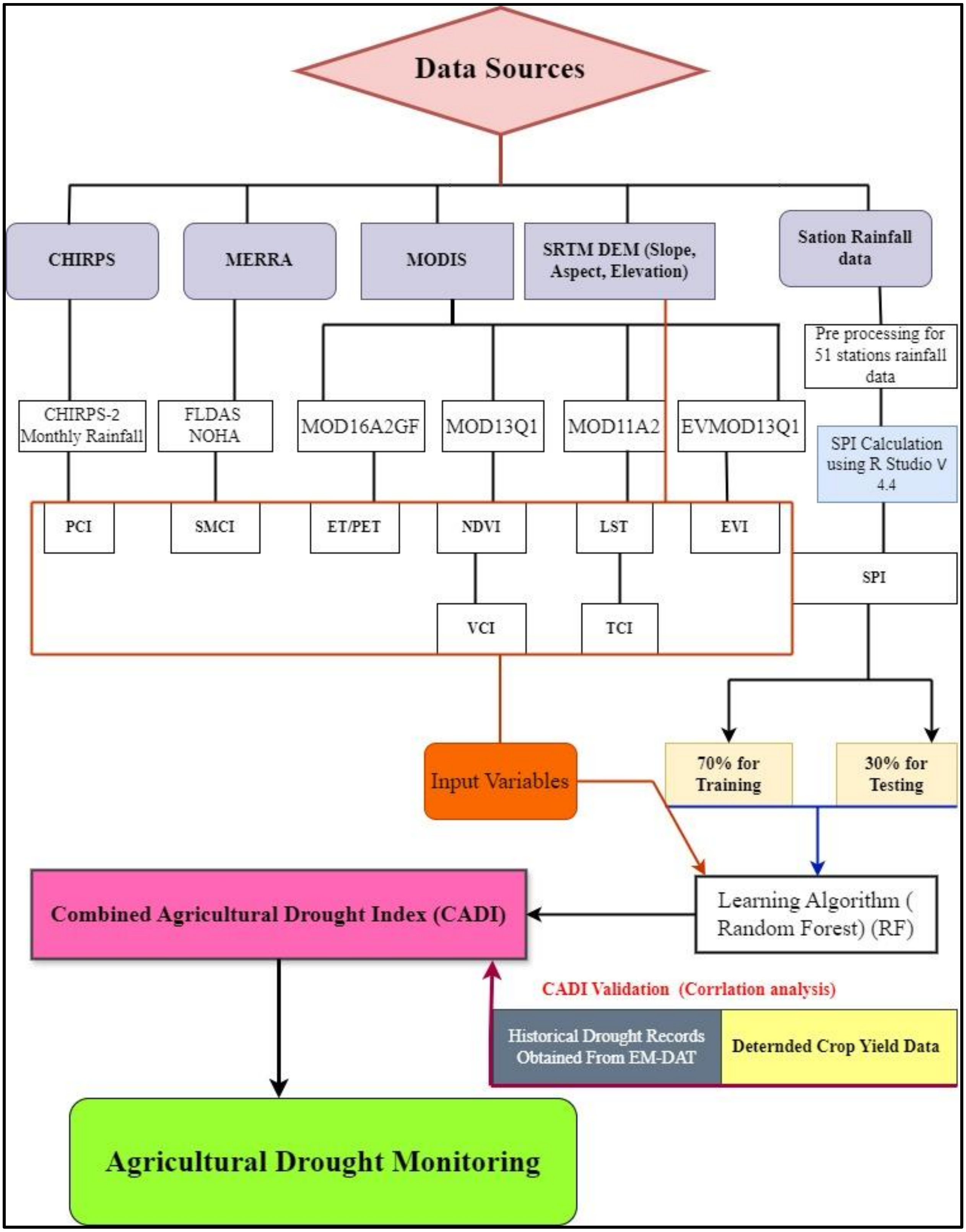

Figure 7: Methodological framework

CHAPTER FOUR

4. RESULTS AND DISCUSSIONS

This chapter deals with presenting the results and discussions of the Developed Combined Drought Index for agricultural drought monitoring in the Amhara Region, Ethiopia. The analysis of the obtained results incorporates the evaluation and validation of the developed index, which is the CADI series, in relation to crop yield. This evaluation aims to assess the accuracy and predictive potential of the CADI for monitoring agricultural drought.

4.1. Develop an Earth Observation-based Combined Agricultural Drought Index (CADI) to monitor agricultural drought.

The development of CADI, spanning from 2000 to 2021, was developed using a significant machine learning (ML) algorithm, i.e., Random Forest Algorithms (RF), by using SPI data calculated from selected fifty-one stations of the study area for each summer month, i.e., June, July, August, and September (JJAS). The SPI data were utilized for training and testing of the RF model. During the RF model's prediction stages, 70% of the SPI values for each month were used for training, and for validation, 30% of the SPI readings from each selected station were utilized. Then, by combining eight input variables representing different environmental variables (precipitation condition index, normalized difference vegetation index, vegetation condition index, enhanced vegetation index, land surface temperature, temperature condition index, evapotranspiration/potential evapotranspiration, and soil moisture), in addition, three topographical factors (elevation, slope, and aspect) were taken into account while creating CADI using RF models using a specific code in the Google Earth Engine (GEE) platform; the example is in the appendix portion (part two).

In the training phase of the RF model, the results for training range from 0.70 to 0.89 in June, 0.74% to 0.90% in July, 0.75% to 0.89% in August, and 0.78% to 0.90% in September; thus, as shown in Table 6, during the training phase of the model, all SPI values during all months (JJAS) of the study period give an acceptable result in terms of training. The RF had the highest values, ranging from 0.72 to 0.90 in all months. The values for testing are ranging from 0.63 to 0.86, 0.67 to 0.87, 0.71 to 0.86, and 0.66 to 0.88 in June, July, August, and September, respectively.

Table 6: R^2 Values for Training and Validation of Random Forest Model

Year	June		July		August		September	
	Training	Validation	Training	Validation	Training	Validation	Training	Validation
2000	0.82	0.73	0.85	0.83	0.80	0.78	0.88	0.86
2001	0.86	0.79	0.80	0.79	0.85	0.83	0.78	0.76
2002	0.82	0.77	0.84	0.80	0.83	0.80	0.90	0.88
2003	0.84	0.82	0.85	0.80	0.87	0.85	0.82	0.71
2004	0.80	0.71	0.82	0.74	0.83	0.81	0.87	0.76
2005	0.8	0.86	0.83	0.81	0.82	0.79	0.81	0.79
2006	0.82	0.81	0.82	0.69	0.85	0.75	0.82	0.81
2007	0.78	0.75	0.85	0.80	0.88	0.85	0.86	0.81
2008	0.83	0.75	0.80	0.74	0.83	0.80	0.83	0.81
2009	0.85	0.83	0.83	0.79	0.89	0.82	0.84	0.79
2010	0.80	0.74	0.80	0.78	0.75	0.71	0.85	0.82
2011	0.87	0.76	0.82	0.80	0.80	0.71	0.83	0.82
2012	0.77	0.75	0.74	0.67	0.75	0.74	0.85	0.78
2013	0.80	0.76	0.84	0.80	0.85	0.82	0.82	0.79
2014	0.81	0.75	0.80	0.79	0.79	0.75	0.88	0.85
2015	0.80	0.76	0.82	0.81	0.88	0.86	0.88	0.82
2016	0.70	0.66	0.83	0.74	0.84	0.73	0.80	0.66
2017	0.81	0.74	0.84	0.81	0.85	0.82	0.85	0.84
2018	0.89	0.82	0.90	0.87	0.80	0.77	0.83	0.79
2019	0.72	0.64	0.86	0.79	0.8	0.75	0.79	0.74
2020	0.73	0.63	0.78	0.73	0.84	0.83	0.85	0.79
2021	0.87	0.85	0.83	0.77	0.82	0.74	0.86	0.84

In the training phase, as shown in figure 8 below, for the summer season months of the study period, the RF demonstrated good performance, that is, R^2 ranging from 0.826, 0.806, and 0.856, respectively, in June 2002, 2009, and 2015. In July the values of R^2 were 0.847, 0.838, and 0.829 in 2002, 2009, and 2015, respectively; in August the values of R^2 were 0.835, 0.891, and 0.883; and in September the values of R^2 were 0.906, 0.849, and 0.889 in the years 2002, 2009, and 2015, respectively.

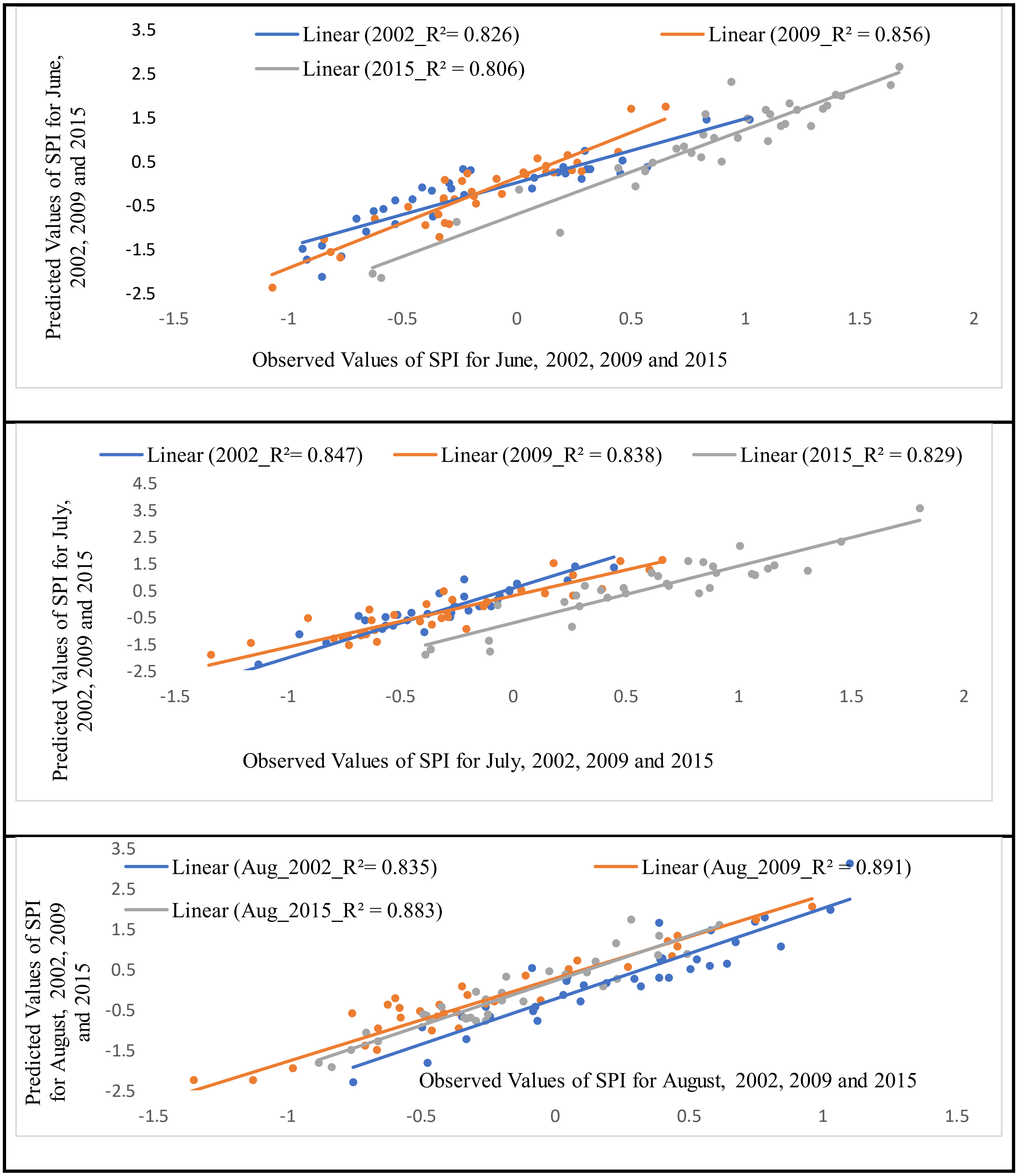
Linear (2002_R²= 0.826)
Linear (2009_R² = 0.856)
Linear (2015_R² = 0.806)
3.5
2.5
1.5
0.5
-0.5
-1.5
-2.5
-1.5
-1
-0.5
0
0.5
1
1.5
2
Predicted Values of SPI for June, 2002, 2009 and 2015
Observed Values of SPI for June, 2002, 2009 and 2015
Linear (2002_R²= 0.847)
Linear (2009_R² = 0.838)
Linear (2015_R² = 0.829)
4.5
3.5
2.5
1.5
0.5
-0.5
-1.5
-2.5
-1.5
-1
-0.5
0
0.5
1
1.5
2
Predicted Values of SPI for July, 2002, 2009 and 2015
Observed Values of SPI for July, 2002, 2009 and 2015
3.5
Linear (Aug_2002_R²= 0.835)
Linear (Aug_2009_R² = 0.891)
2.5
Linear (Aug_2015_R² = 0.883)
1.5
0.5
-0.5
-1.5
-2.5
-1.5
-1
-0.5
0
0.5
1
1.5
Predicted Values of SPI for August, 2002, 2009 and 2015
Observed Values of SPI for August, 2002, 2009 and 2015

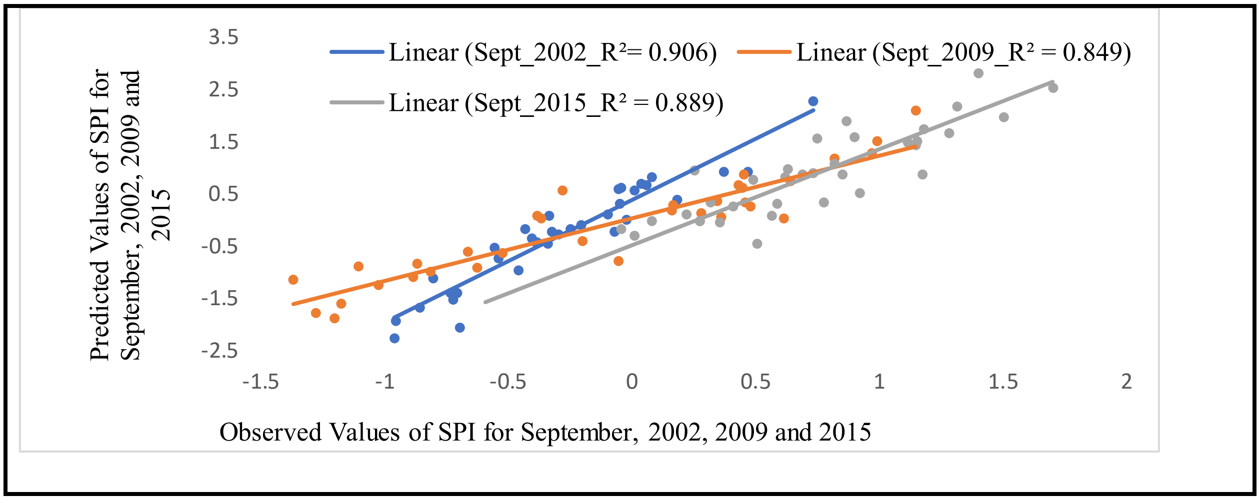

Figure 8: Sample scatter plot of observed and predicted values for selected stations using random forest algorithms for training

In the testing phase of the RF model, as shown in figure 9 below, for the summer season months of the study period, the RF demonstrated good performance, that is, R^2 ranging from 0.778, 0.834, and 0.769 in June 2002, 2009, and 2015, respectively. In July the values of R^2 were 0.804, 0.798, and 0.811 in 2002, 2009, and 2015, respectively; in August the values of R^2 were 0.807, 0.829, and 0.865; and in September the values of R^2 were 0.881, 0.799, and 0.823 in the years 2002, 2009, and 2015, respectively.

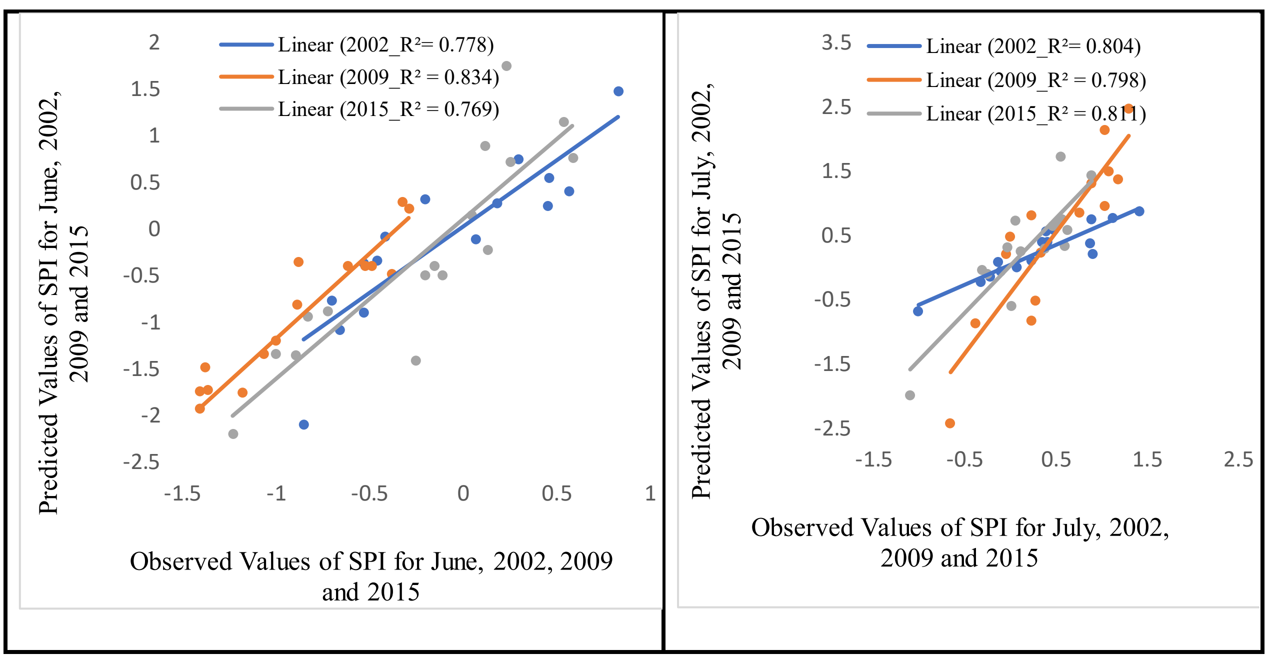

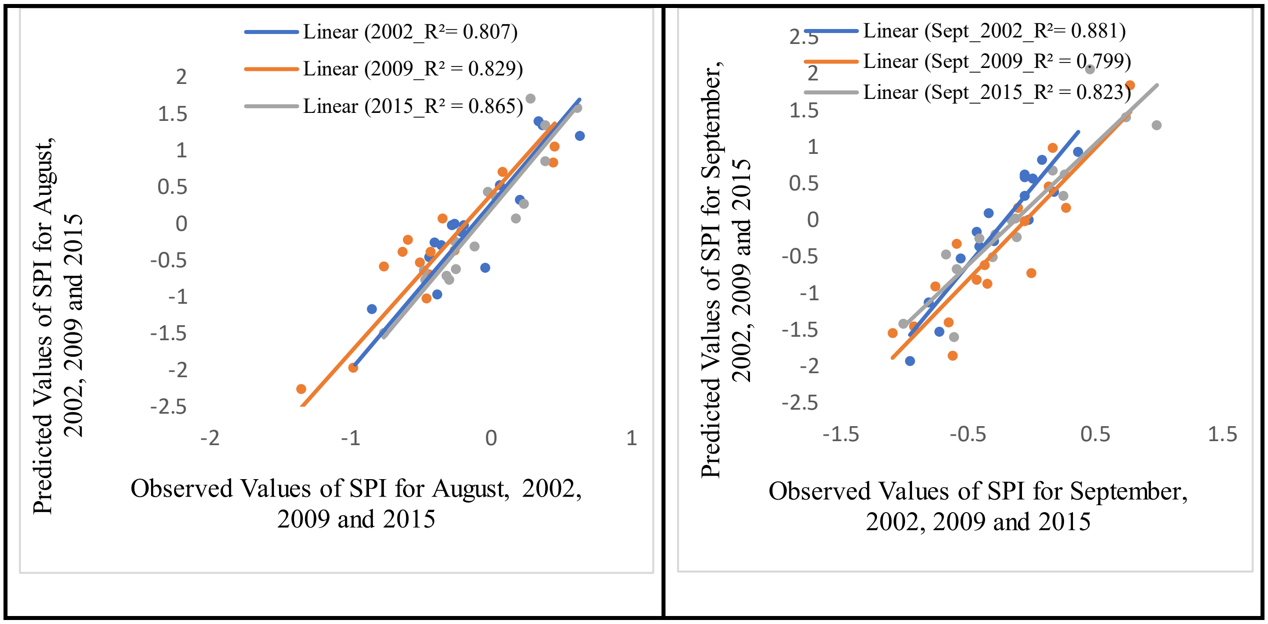

Figure 9: Sample scatter plot of observed and predicted values for selected stations using random forest algorithms for validation

The result of developed CADI precisely identified the historical drought years. From June to September of the summer season months, there was moderate to extreme drought in most eastern parts of the study area during 2000, 2002, 2004, 2008, 2009, 2012, 2013, 2014, 2015, 2016, 2018, 2019, 2020, and 2021 in June. In July 2000, 2002, 2004, 2005, 2006, 2008, 2009, 2012, 2013, 2014, 2015, 2016, 2017, 2019, 2020, and 2021, in August during 2000, 2002, 2006, 2008, 2009, 2012, 2013, 2014, 2015, 2016, 2017, 2019, 2020, and 2021 and during 2000, 2002, 2004, 2005, 2006, 2009, 2010, 2012, 2014, 2015, 2016, 2017, and 2020 in September, except the western portion of the study area specifically Awi/Agew zone, all parts particularly portions of northern Amhara, northeastern and southeastern parts of the study area were affected by moderate to extreme drought levels, but the spatial extent that is affected by moderate to extreme drought during 2002, 2009 and 2015 was larger than the remaining years, during these specified drought years, most eastern parts of the study area (North wollo, South wollo, Wag Himra, South Gonder, North Shewa and Oromia Zones of Amhara region) and parts of North Gonder as well as some parts of East Gojam Zone, were identified as drought-prone zones of the study area.

The results of this study are basically consistent with the historical drought occurrences over the years, i.e., the result of CADI indicating that the years 2002, 2009, and 2015 were primary drought occurrence years in the study area. The result of this study proves the result of previous studies that were conducted in different parts of the study area specifically and in Ethiopia in general. For instance, Gebre et al. (2017) studies on using GIS and remote sensing to describe agricultural drought conditions in Ethiopia's Amhara Regional State's North Wollo Zone discovered that while 2005 and 2015 were categorized as years of drought, the years 2009 and 2013 were classified as light drought years. In addition, Wassie et al. (2022), in their studies on trends and spatiotemporal patterns of meteorological drought incidence in North Wollo, northeastern highlands of Ethiopia, found that the years 2009 and 2015 were characterized by severe and extreme drought conditions.

Similarly, the studies by Mekonen et al. (2020) concluded that the driest years on record for the kirmet season were the rainy months of July 1987 and September 2009, when the most severe droughts were seen. Furthermore, another study by Enyew et al. (2025) shows that the Menna watershed in northwest Ethiopia was severely affected by droughts in 2002, 2009, and 2015, according to the spatiotemporal distribution of agricultural drought. In addition, repercussions continued in 2015–16, affecting around 5 million people in Northern, Southern, and Eastern Ethiopia (Liou & Mulualem, 2019; Mera, 2018). Moreover, reports by Kassaye et al. (2021) estimate that a staggering 10.2 million people were affected by these events. Furthermore, Tela et al. (2024) found that the years 2000, 2002, 2004-2005, 2009-2011, 2013-2015, 2017, and 2021-2023 were affected by different severity levels of drought and resulted in associated socioeconomic impacts. Furthermore, the results of this study also align with the findings of Kogan (2019), who has reported that Ethiopia was affected by drought in 2009 and 2015. He added that one of the regions with large grain crop areas, called Amhara, had droughts of severe-to-exceptional and extreme-to-exceptional (extremely severe) intensity that covered 50–75% and up to 25% of the grain crop area, respectively.

In addition, the result of this study was aligned with the results of several studies that found drought events in these specified drought years; for instance, a study by Gebrehiwot et al. (2011) noted that during the 2004 and 2009 monsoon seasons, the Tigray region saw the worst drought conditions, with 20.1% and 17.4% of the territory experiencing drought conditions, respectively, with VCI values below 35%.

Moreover, the study's findings are consistent with the results of interviews conducted with the agricultural offices in the Amhara region, which revealed that more than 50 woredas in their kola agroecological zones were agricultural drought-affected areas. These include parts of the East Gojam Zone as well as the majority of the eastern parts of the region, including North and South Wollo, Oromia, Wag Himra, South and North Gonder, and North Shewa.

Generally, the results of CADI based on the RF model in this study are basically in accordance with actual drought conditions and normal years, indicating the model has a strong monitoring capability in the study area. The result of this study showed that the RF model predicted agricultural drought well for each summer season's months. This result is aligned with the result of a study on A Random Forest Model for Drought Monitoring and Validation for Grassland Drought Based on Multi-Source Remote Sensing Data by Wang et al. (2022), which discovered that the model's monitoring results, which represent the growth and spatial evolution of drought conditions, were consistent with the real drought circumstances. In addition, the superior performance of RF was confirmed by Rahmati et al. (2020), who simulated drought situations and forecasted their severity in Australia's southeast Queensland region using five machine learning models; the outcomes demonstrated that the RF model performed better than the other models. This study also confirmed that the RF model was highly accurate in predicting the period, duration, and severity of agricultural droughts in this area.

Additionally, RF was among the earliest algorithms used for drought forecasting and evaluation (Nagre et al., 2024). Thus, the current study can provide a new application method for comprehensive monitoring of agricultural drought in the Amhara region of Ethiopia. In addition, good performance of RF-based CADI proves the study by another scholar Li et al. (2023), according to the findings of Remote Sensing Monitoring of Drought in Southwest China using random forest and extreme gradient boosting methods, the developed model can enhance the degree of dynamic drought monitoring and prediction for areas with complicated topography and terrain, as well as climatic formative factors and sparsely distributed weather stations. The RF-based agricultural drought monitoring index developed in this study can be used to assess the temporal and spatial evaluation of agricultural drought conditions in the Amhara region, Ethiopia.

4.2. Examine the spatial and temporal agricultural drought status based on CADI in the Amhara region.

The assessment of agricultural drought in the Amhara region, Ethiopia, spanning from the years 2000 to 2021, employed the Combined Agricultural Drought Index (CADI). The evaluation relied on the time series data of CADI to provide a comprehensive understanding of the prevalence and intensity of different levels of agricultural drought throughout the specified timeframe. By using CADI, the study aims to deliver a nuanced depiction of the agricultural drought scenario in the region, allowing for a detailed examination of its temporal variations and severity levels.

The spatial and temporal CADI-based investigation in the study area from 2000 to 2021 revealed a wide range of drought conditions. Thus, the study uses the developed new index, i.e., CADI, to examine the spatial and temporal agricultural drought situations in the study area. That means the spatial and temporal patterns of agricultural drought events in the Amhara Region were analyzed using this index. Based on the CADI results that were observed during the months of the summer season for each year of the study period, the drought status for each year can be determined by examining the drought status within different drought classes.

4.2.1. Temporal Status of Agricultural Drought Using CADI

Based on the trend of CADI displayed in figure 10, during the study periods in 2000, 2002, 2004, 2008, 2009, 2012, 2013, 2014, 2015, 2016, 2018, 2019, 2020, and 2021, in June, there was a moderate to severe drought. On the other hand, the years 2001, 2003, 2005, 2006, 2007, 2010, 2011, and 2017 show near-normal CADI values across the majority of the study areas during this month. In July the years 2000, 2002, 2004, 2005, 2006, 2008, 2009, 2012, 2013, 2014, 2015, 2016, 2017, 2019, 2020, and 2021. Conversely, the years 2001, 2003, 2007, 2010, 2011, and 2018 were recorded as near-normal years during this month. In August, the years 2000, 2002, 2006, 2008, 2009, 2010, 2012, 2013, 2014, 2015, 2019, and 2021 were recorded as drought years, and the years 2001, 2003, 2004, 2005, 2007, 2011, 2016, 2017, 2018, and 2020 were identified as near-normal years in this month. In September during 2000, 2002, 2004, 2005, 2006, 2009, 2010, 2012, 2014, 2015, 2016, 2017, and 2020, which were identified as relatively drought years, there was relatively little drought in the following years: 2001, 2003, 2007, 2008, 2011, 2013, 2017, 2018, 2019, and 2021. From these drought years, the years 2002, 2009, and 2015 consistently exhibit the lowest CADI values in all months of the entire study period.

The result of this study confirms the result of previous studies; for instance, a study by Chere and Debalke (2024) on modeling agricultural drought based on the earth observation-derived standardized precipitation evapotranspiration index and vegetation health index in the northeastern highlands of Ethiopia found that in the South Wollo administrative zone, there were agricultural droughts in 2002, 2004, 2009, 2010, 2014, and 2015 of various intensities.

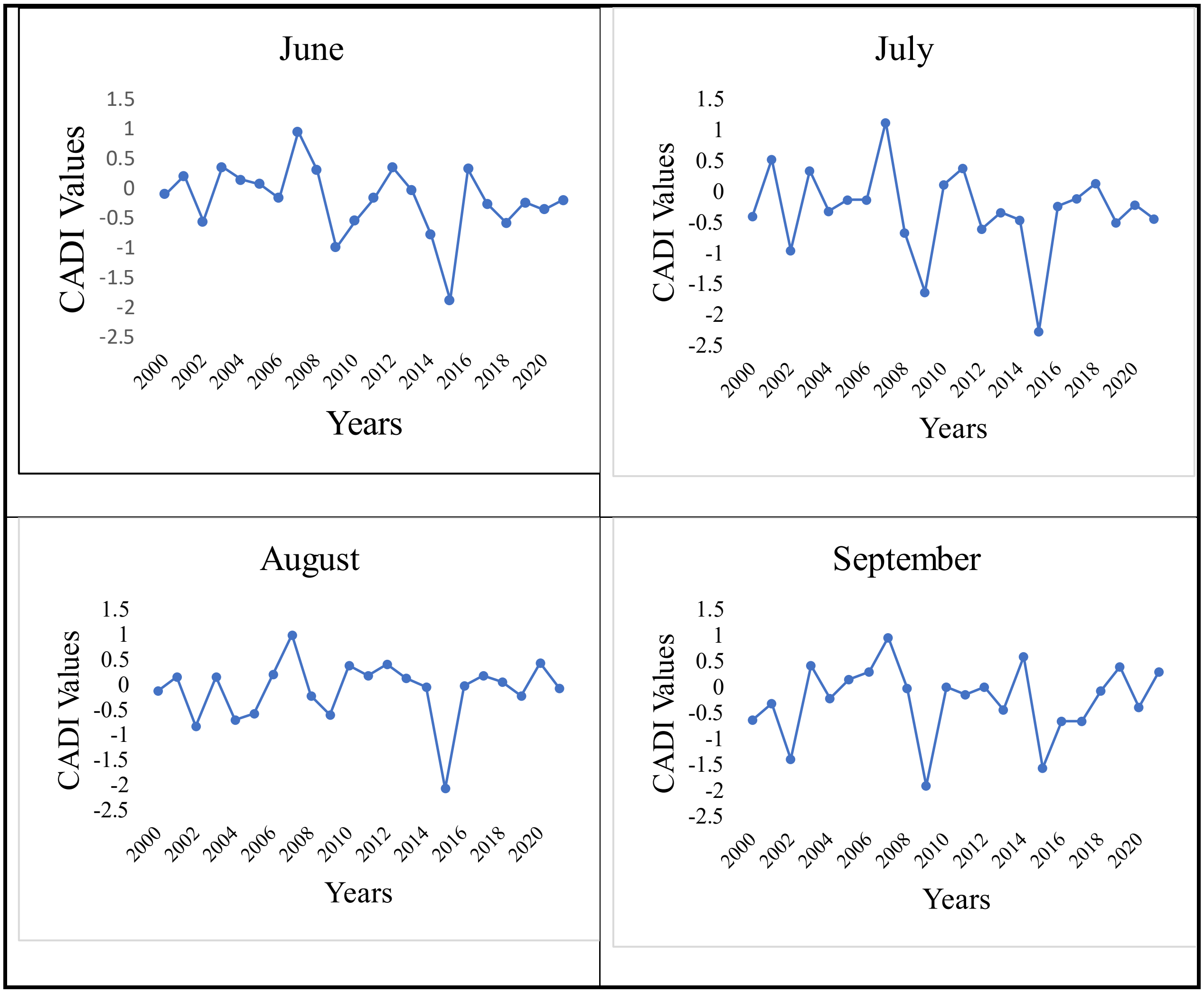

Figure 10: Trends of CADI for the entire study area over summer months from 2000 to 2021

In addition, Mohammed et al. (2022), in their studies on climate change repercussions on meteorological drought frequency and intensity in South Wollo, Ethiopia, found that the most severe and unique widespread drought episodes occurred in 2003, 2005, 2009, 2010, and 2012; these years had significant drought at all time scales in the study area. Furthermore, Wassie et al. (2022) found that the years 2002, 2004, 2009, 2011, 2014, 2015, and 2019 were under a rainfall deficiency with extreme drought events; the two years 2009 and 2015 were the driest years. Moreover, Shalishe et al. (2022), in studies on Meteorological Drought Monitoring Based on Satellite CHIRPS Product over Gamo Zone, Southern Ethiopia, show that the known historic drought years 2014, 2015, 2010, 2009, and 2008 were indicated very well; in addition, they report that severe and extreme droughts were observed in 2008 and 2009.

Generally, based on the result of the CADI time series trend displayed in figure 10 above during all summer months, the highest CADI values are consistently recorded in 2007 in all months. The high values of CADI in 2007 indicate that the study area was relatively drought-free during this year. Conversely, the low values of CADI observed in 2009 and 2015 imply that there was an occurrence of extreme drought conditions relatively during these years during all months of the study period in the Amhara region. The result is similar with a study on "Mapping the spatial and temporal variation of agricultural and meteorological drought using geospatial techniques, Ethiopia, by Senamaw et al. (2021), which states that the years 2009 and 2015 were drought years, while the years 2001 and 2007 were drought-free.

Based on the figure below, which illustrates the trend for the mean CADI during the summer season for each year of the study period, the drought status for each year can be determined. It was observed that the years 2009, 2002, and 2015 experienced moderate to extreme drought conditions. Conversely, the years 2001, 2003, and 2007 were categorized as relatively normal conditions without drought based on CADI.

The result of this study confirms the results of different studies; for instance, Liou and Mulualem (2019) and Senamaw et al. (2021) in their study on spatiotemporal assessment of drought in Ethiopia and the impact of recent intense droughts and Mapping the spatial and temporal variation of agricultural and meteorological drought using geospatial techniques, Ethiopia, respectively, discovered that there were notable nationwide droughts in 2009 and 2015, indicating that wet years were in 2001 and 2007, while drought years were in 2009 and 2015. Furthermore, this study's outcome is consistent with the findings of Gebrehiwot et al. (2016), Viste et al. (2013), and Chere et al. (2022), who identified Ethiopia's central and northern highlands, particularly the Amhara and Tigray regions, as the most vulnerable agriculturally producing areas.

The findings of this study also support the result of Gebre et al. (2017), who have reported that millions in the North Wollo zone have been affected due to the failure of crops, and hunger and malnutrition have risen sharply.

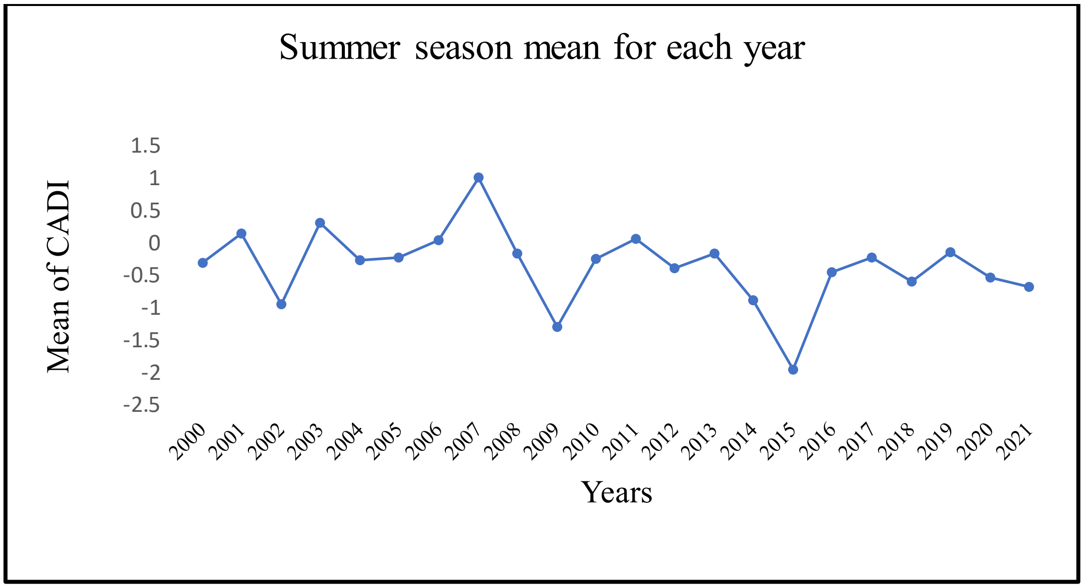

Figure 11: Trends of CADI for the entire study area over the mean of summer months from 2000 to 2021

4.2.2. Spatial Variations of Agricultural Drought Status Using CADI in June

As can be seen in figure 12 below, the eastern, central, northeastern, and southeastern parts of the study area were affected by moderate to extreme drought conditions during this month. During 2000, 2002, 2004, 2008, 2009, 2012, 2013, 2014, 2015, 2016, 2018, 2019, 2020, and 2021, excluding the western portion of the study area, the entire region experienced moderate to extreme drought conditions. However, compared to the other years, the regions hit by severe to extreme drought in 2002, 2009, and 2015 were larger. There were relatively near-normal CADI values across the majority of the areas during 2001, 2003, 2005, 2006, 2007, 2010, 2011, and 2017.

Based on the results mentioned on the map below, the years 2002, 2009, and 2015 were identified as the most severely drought-affected parts of the study area in June. In 2002, approximately 20.00% of the area experienced extreme drought conditions, 14.98% were classified as severe drought, 28.38% were considered moderate drought, 18.58% were slight drought, and the remaining 18.05% were drought-free. Similarly, in 2009, about 32.42% of the area was categorized as extreme drought, with 25.29% experiencing severe drought, 18.76% moderate drought, 15.49% slight drought, and 8.04% of the area drought-free. In 2015, the area under drought reached 34300.88, 33187.50, 12351.81, and 6629.13 for extreme, severe, moderate, and slight drought conditions, respectively, accounting for 38.50, 37.25, 13.86, and 7.44 percent of the area, respectively, while the drought-free area was 2629.13, representing 2.95 % of the total area only in this month. This suggests a severe drought situation during that particular year. On the other hand, there were relatively near-normal CADI values across the majority of the areas during 2001, 2003, 2005, 2006, 2007, 2010, 2011, and 2017. In 2007, for example, the area under drought in CADI was 3542.56, 7146.38, and 21434.50 areas for extreme, severe, and moderate drought areas, respectively, accounting for 3.92, 7.92, and 23.75 percent of the total area experiencing extreme, severe, and moderate drought conditions, respectively, while the mild drought and drought-free areas were 34203.69 and 23934.06, respectively, representing 37.89% and 26.52% of the total area, respectively, in this month. The level of drought condition at the zonal level in June, low CADI value (< 0), was observed in the Wag Himra Zone, North Wollo, Oromia, South Gonder, and most of the eastern, central, southeast, and northeastern parts of the Amhara area. In 2000, 2002, 2004, 2008, 2009, 2012, 2013, 2014, 2015, 2016, 2018, 2019, 2020, and 2021, almost all eastern parts of the study area and parts of east Gojam experienced moderate to extreme drought conditions, as can be shown on map 12 below.

Generally, a high prevalence of agricultural drought occurred in June 2002, 2009, and 2015, which is the start of the crop-growing season and the most critical period for crops to grow in the study area. The occurrence of drought in this month highly influences crop production, as it is the start of crop growth. On the other hand, in June during the years 2001, 2003, 2005, 2006, 2007, 2010, 2011, and 2017, most parts of the study area experienced drought-free conditions. The majority of the area was almost completely drought-free in 2007. But even in this typical year, there were still places that experienced moderate to severe drought conditions. Thus, the result was aligned with that of Sohnesen (2020), who claimed that Ethiopia's northern regions experienced drought in 2009 and 2015; 2009 had a notable decrease in precipitation in North Ethiopia. In addition, the results from interviews confirmed that there were delayed rains in the month of June, which impacted crop production. Thus, farmers fail to plant on time, crops fail to establish properly, and as a result the entire agricultural cycle is disrupted.

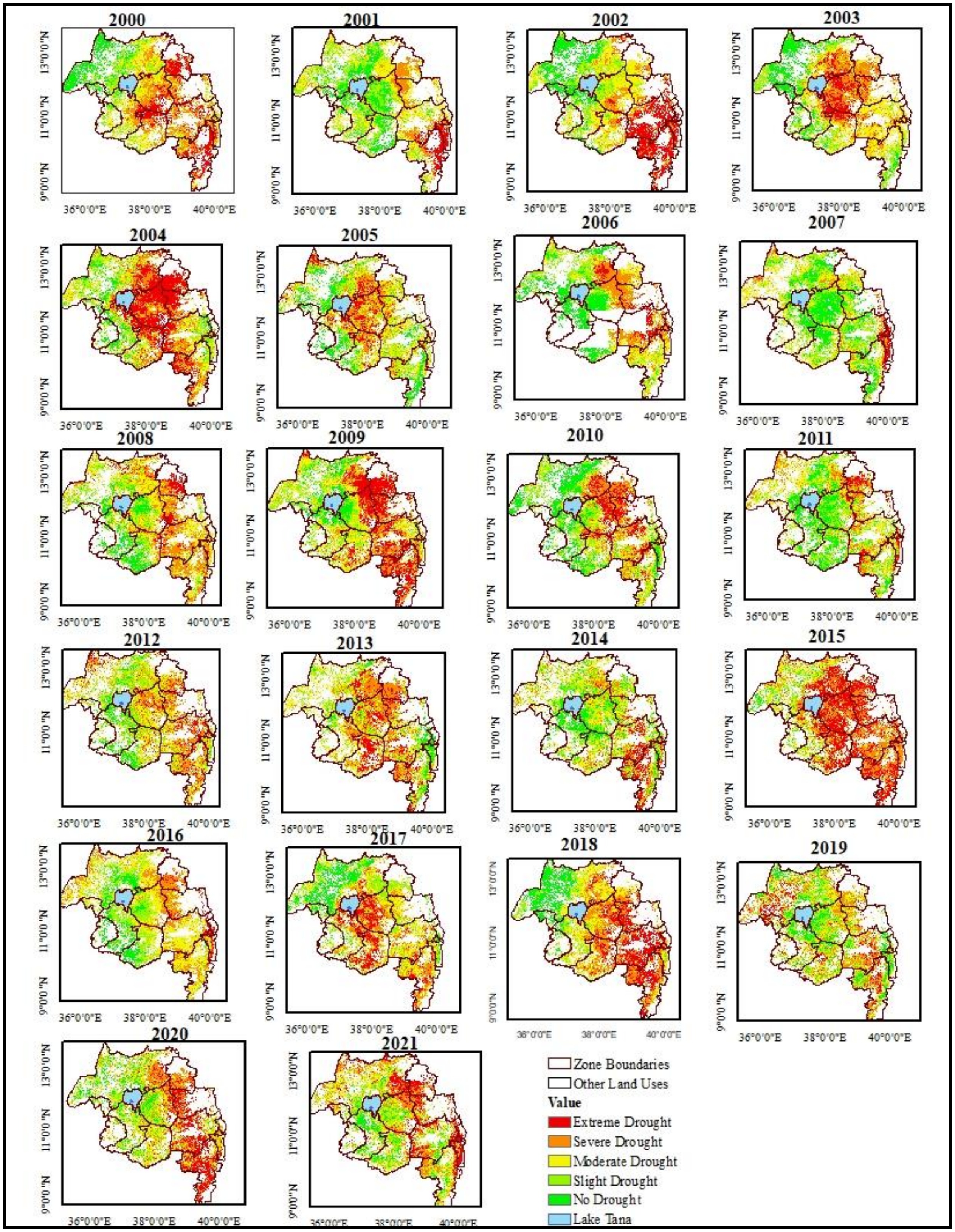

Figure 12: Spatial pattern of agricultural drought in the Amhara Region using CADI in June

The table provided below displays the areal coverages and percentages of drought based on CADI for each year from 2000 to 2021 in June. From the table, we can observe the variations in the extent of drought over the years. The fluctuations in these percentages indicate the dynamic nature of drought patterns. In 2007, for example, the area under drought based on CADI was 3542.56, 7146.38, and 21434.50 areas for extreme, severe, and moderate drought areas, respectively, accounting for 3.92, 7.92, and 23.75 percent of the total area experiencing extreme, severe, and moderate drought conditions, respectively, while the mild drought and drought-free areas were 34203.69 and 23934.06, respectively, representing 37.89% and 26.52% of the total area, respectively, in this month. This indicates that a significant portion of the region experienced drought conditions even during that wet year.

Table 7: Drought-Affected Areas Based on CADI Severity Level in June

Year	**Extreme Drought**		**Severe Drought**		**Moderate Drought**		**Slight Drought**		**No Drought**	
	Area (km^2)	%	Area (km^2)	%	Area (km^2)	%	Area (km^2)	%	Area (km^2)	%
2000	15702.50	17.30	25284.75	27.86	21872.13	24.10	15226.00	16.78	12657.88	13.95
2001	5081.44	5.62	12833.19	14.18	24478.81	27.05	30735.94	33.96	17363.88	19.19
2002	18788.88	20.00	14078.00	14.98	26670.00	28.38	17459.56	18.58	16964.00	18.05
2003	11629.56	11.92	24878.25	25.50	27237.81	27.92	17933.13	18.38	15889.19	16.29
2004	25530.94	27.24	20649.69	22.03	19737.75	21.06	18046.31	19.26	9753.81	10.41
2005	9040.13	10.03	20252.06	22.46	24985.50	27.71	21259.50	23.58	14626.75	16.22
2006	5307.25	7.16	19214.38	25.92	15272.31	20.60	15245.69	20.56	19097.75	25.76
2007	3542.56	3.92	7146.38	7.92	21434.50	23.75	34203.69	37.89	23934.06	26.52
2008	6292.94	6.70	27503.44	29.28	29320.19	31.22	17721.44	18.87	13079.50	13.93
2009	30920.31	32.42	24117.25	25.29	17890.69	18.76	14767.63	15.49	7670.06	8.04
2010	12184.38	13.16	20531.31	22.17	15427.81	16.66	21618.81	23.35	22827.88	24.65
2011	5591.25	6.23	14637.44	16.31	22256.81	24.80	27232.19	30.35	20021.13	22.31
2012	9055.75	10.17	23013.06	25.85	27449.88	30.83	20664.50	23.21	8850.69	9.94
2013	13253.00	15.08	28373.81	32.28	23717.19	26.98	16205.06	18.44	6342.81	7.22
2014	8299.81	9.44	15534.63	17.67	24494.19	27.87	23449.13	26.68	16119.88	18.34
2015	34300.88	38.50	33187.50	37.25	12351.81	13.86	6629.13	7.44	2629.13	2.95
2016	3169.06	3.50	21745.63	24.01	32389.94	35.76	21792.69	24.06	11475.63	12.67
2017	12025.81	13.12	22141.69	24.15	24818.19	27.07	19311.88	21.07	13375.06	14.59
2018	20297.38	21.70	28448.00	30.42	21488.69	22.97	9530.88	10.19	13767.00	14.72
2019	8602.50	9.36	22641.00	24.63	23160.44	25.20	22848.56	24.86	14671.56	15.96
2020	18547.31	20.91	22576.81	25.45	19984.38	22.53	19081.81	21.51	8519.63	9.60
2021	15783.69	17.48	23156.31	25.64	23110.75	25.59	19364.00	21.44	8887.00	9.84

The percentages of area under drought and drought-free areas fluctuate from year to year. For instance, in 2015, the area under drought reached 34300.88, 33187.50, 12351.81, and 6629.13 for extreme, severe, moderate, and slight drought conditions, respectively, accounting for 38.50, 37.25, 13.86, and 7.44 percent of the area, respectively, while the drought-free area was 2629.13, representing 2.95 % of the total area only in this month. This suggests a severe drought situation during that particular year.

4.2.3. Spatial Variations of Agricultural Drought Status Using CADI in July

As it has been shown in figure 13, based on CADI, moderate to extreme drought conditions occurred. During this month, the northeastern, central, eastern, and southeastern parts of the study area were affected by moderate to extreme drought conditions. During 2000, 2002, 2004, 2005, 2006, 2008, 2009, 2012, 2013, 2014, 2015, 2016, 2017, 2019, 2020, and 2021, almost the entire region experienced moderate to extreme drought conditions. However, compared to the other years, the regions hit by severe to extreme drought in 2009, 2015, and 2021 were larger. There were relatively near-normal CADI values across the majority of the areas during 2001, 2003, 2007, 2010, 2011, and 2018. Based on the results mentioned on the map below, in the years 2000, 2002, 2004, 2005, 2006, 2008, 2009, 2012, 2013, 2014, 2015, 2016, 2017, 2019, 2020, and 2021, most eastern parts of the study areas experienced drought conditions. For instance, in 2015, the area under drought of CADI in July was 32070.81, 36.27%; 30926.00, 34.98%; 11495.13, 13.00%; and 13908.69, 15.73%, accounting for extreme, severe, moderate, and slight drought areas in km^2 and percents of the total agricultural area, respectively, and the drought-free area in this year was 22.44 km^2 covering 0.03% of the study area. This indicates that there was a relatively extreme drought event in this year during this month. While the drought-free area in 2007 was recorded as 5398.00, 5.75%; 17753.25, 18.90%; 31309.00, 33.34%; 23773.06, 25.31%; and 15679.19, 16.70%, representing extreme, severe, moderate, slight, and drought-free areas, respectively. This indicates a relatively wet year in the entire study area and suggests that most of the region experienced moderate, slight, and drought-free conditions during that particular year. It implies that even if most of the region experienced drought-free conditions during this normal year (2007), to some extent some areas were experiencing moderate to extreme drought conditions even in this normal year. Additionally, in 2003 of this month, 31540.56, 32.38%, and 22783.31, 23.39%, exhibited slight drought and drought-free conditions, respectively.

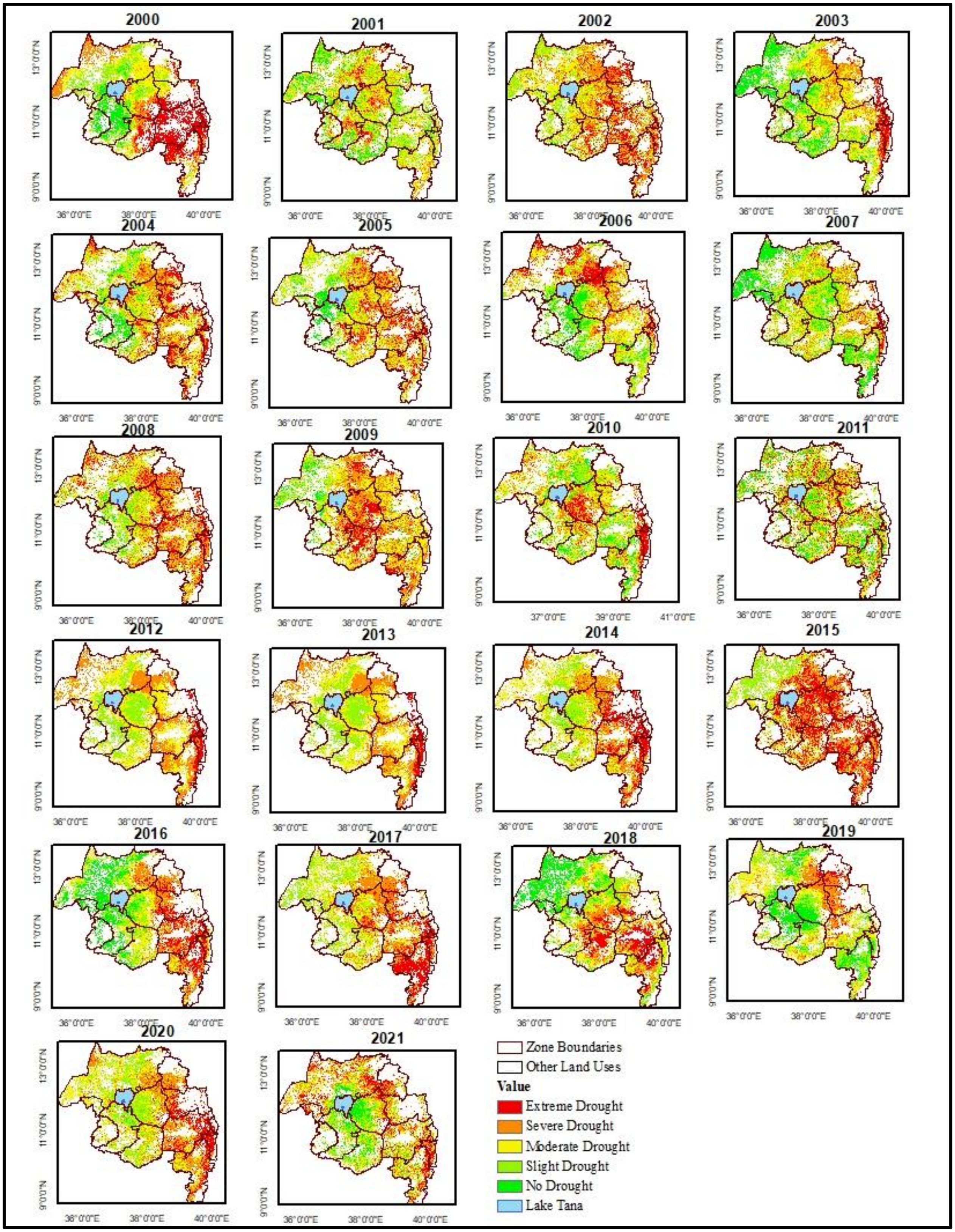

Figure 13: Spatial pattern of agricultural drought in Amhara Region using CADI in July

The level of drought condition at the zonal level in July, low CADI value (< 0), was observed in the Wag Himra Zone, the majority of the eastern, central, southeast, and northeastern Amhara region, as well as North and South Wollo, Oromia, and South Gonder. The result is confirmed by the interviewee with the region's agricultural office expertise; thus, one of the experts from the agricultural offices states that

> The droughts in 2002 and 2009 had a significant impact on the lives and food security of the residents of Bati in the Oromiya Zone and South Wollo Zone (Legambo, Dessie Zuria, and Jamma). The regions were highly susceptible to climatic shocks because they were already experiencing long-term food insecurity as a result of environmental degradation, over-dependence on rain-fed agriculture, and immense population pressure. The lack of rainfall during these times of drought resulted in significant failures of agricultural production and livestock loss, which increased the rate of hunger (August 01, 2024).

The table provided below displays the areal coverages and percentages of drought based on CADI for each year from 2000 to 2021 for July. The percentages of area under drought and drought-free areas fluctuate from year to year. For instance, in 2015, the area under drought of CADI in July was 32070.81, 36.27%; 30926.00, 34.98%; 11495.13, 13.00%; and 13908.69, 15.73%, accounting for extreme, severe, moderate, and slight drought areas in km^2 and percents of the total agricultural area, respectively, and the drought-free area in this year was 22.44 km^2 and 0.03%. This indicates that there was a relatively extreme drought event in this year during this month. While the drought-free area in 2007 was recorded as 5398.00, 5.75%; 17753.25, 18.90%; 31309.00, 33.34%; 23773.06, 25.31%; and 15679.19, 16.70%, accounting for extreme, severe, moderate, slight, and drought-free areas, respectively. This indicates a relatively wet year in the entire study area and suggests that most of the region experienced moderate, slight, and drought-free conditions during that particular year. It implies that even if most of the region experienced drought-free conditions during this normal year (2007), to some extent some areas were experiencing moderate to extreme drought conditions even in this normal year. Additionally, in 2003 of this month, 31540.56, 32.38%, and 22783.31, 23.39%, exhibited slight drought and drought-free conditions, respectively. Like that of 2007, it indicates a relatively wet year during 2003 in July.

Table 8: Drought-Affected Areas Based on CADI Severity Level in July

Year	Extreme Drought		Severe Drought		Moderate Drought		Slight Drought		No Drought	
	Area (km^2)	%	Area (km^2)	%	Area (km^2)	%	Area (km^2)	%	Area (km^2)	%
2000	22854.31	25.19	18136.88	19.99	19701.50	21.72	20927.38	23.07	9097.63	10.03
2001	3778.38	4.02	15280.63	16.26	29447.88	31.34	32861.13	34.97	12592.69	13.40
2002	14280.25	15.91	30524.31	34.01	31111.50	34.67	11222.94	12.51	2599.81	2.90
2003	2708.50	2.78	13875.25	14.24	26514.00	27.22	31540.56	32.38	22783.31	23.39
2004	14911.81	15.92	26234.56	28.00	28113.19	30.01	17239.38	18.40	7189.44	7.67
2005	13166.00	14.61	25106.75	27.86	26902.44	29.85	18417.63	20.44	6528.00	7.24
2006	11222.88	12.60	21859.50	24.55	24998.19	28.08	19460.88	21.86	11498.50	12.91
2007	5398.00	5.75	17753.25	18.90	31309.00	33.34	23773.06	25.31	15679.19	16.70
2008	23897.31	16.00	51106.50	34.22	45068.13	30.18	25571.06	17.12	3712.75	2.49
2009	16244.00	18.00	33387.50	36.99	27926.63	30.94	12681.50	14.05	25.00	0.03
2010	8765.56	9.49	21511.63	23.30	29078.81	31.50	23588.88	25.55	9383.44	10.16
2011	18380.81	12.27	25383.75	16.95	39554.81	26.41	32215.81	21.51	34229.88	22.86
2012	5708.94	6.42	30628.19	34.43	32181.94	36.17	20297.19	22.81	153.44	0.17
2013	5743.19	6.54	30229.13	34.42	31777.00	36.18	19935.44	22.70	144.13	0.16
2014	13579.38	15.50	26514.44	30.26	28268.75	32.27	18614.63	21.25	633.44	0.72
2015	32070.81	36.27	30926.00	34.98	11495.13	13.00	13908.69	15.73	22.44	0.03
2016	14211.06	15.69	21134.13	23.33	17786.81	19.64	16610.00	18.34	20830.94	23.00
2017	16498.75	18.07	29112.94	31.88	25149.63	27.54	20317.38	22.25	238.75	0.26
2018	13223.56	14.14	18228.88	19.49	21493.31	22.98	21981.25	23.50	18598.38	19.89
2019	4108.94	4.47	15366.38	16.72	24826.44	27.02	28841.50	31.39	18749.94	20.40
2020	12712.75	14.39	25576.44	28.94	29756.38	33.67	19660.38	22.25	659.25	0.75
2021	13061.75	14.63	25110.06	28.13	24095.13	26.99	18403.38	20.62	8596.81	9.63

4.2.4. Spatial Variations of Agricultural Drought Status Using CADI in August

Based on CADI as shown in figure 14, extreme to severe drought conditions have occurred. During this month, the northeastern, central, eastern, and southeastern parts of the study area were affected by moderate to extreme drought conditions. During 2000, 2002, 2006, 2008, 2009, 2012, 2013, 2014, 2015, 2016, 2019, and 2021, almost the entire region experienced moderate to extreme drought conditions. However, compared to other years, the region hit by severe to extreme drought in 2015 was larger than the remaining years. There were relatively near-normal CADI values across the majority of the areas during 2001, 2003, 2004, 2005, 2007, 2010, 2011, 2017, 2018, and 2020. Most parts of the northeastern, southeastern, and central portions of the study area were affected by moderate to extreme drought, specifically during the years 2002, 2009, and 2015.

When analyzing regional variations in agricultural drought status using the Combined Agricultural Drought Index (CADI) for the month of August, significant disparities in drought severity are observed across the research region. For agricultural production, Ethiopia's August crop growth peak is critical, and CADI effectively illustrated the regional impacts of drought stress during this period. In certain zones, particularly in most eastern parts of the study area, low CADI values indicate moderate to severe drought conditions. In contrast, higher CADI values in highland and western regions showed generally favorable conditions, with richer vegetation and enough moisture availability.

The spatial analysis of agricultural drought status using the Combined Agricultural Drought Index (CADI) in August reveals significant variability across the study area. Certain zones exhibited moderate to severe drought conditions, indicating localized moisture deficits affecting crop growth and agricultural productivity. Meanwhile, other regions showed normal or near-normal moisture conditions, suggesting heterogeneous climatic and soil moisture patterns. These spatial variations underscore the importance of targeted drought monitoring and management strategies to support effective agricultural planning and mitigate drought impacts at a regional level.

Analyzing the areal coverages and percentages of drought over time can provide valuable information for drought monitoring, water resource management, and agricultural planning. It allows policymakers, researchers, and stakeholders to assess the impact of drought on vegetation and make informed decisions regarding water allocation, crop management, and mitigation strategies.

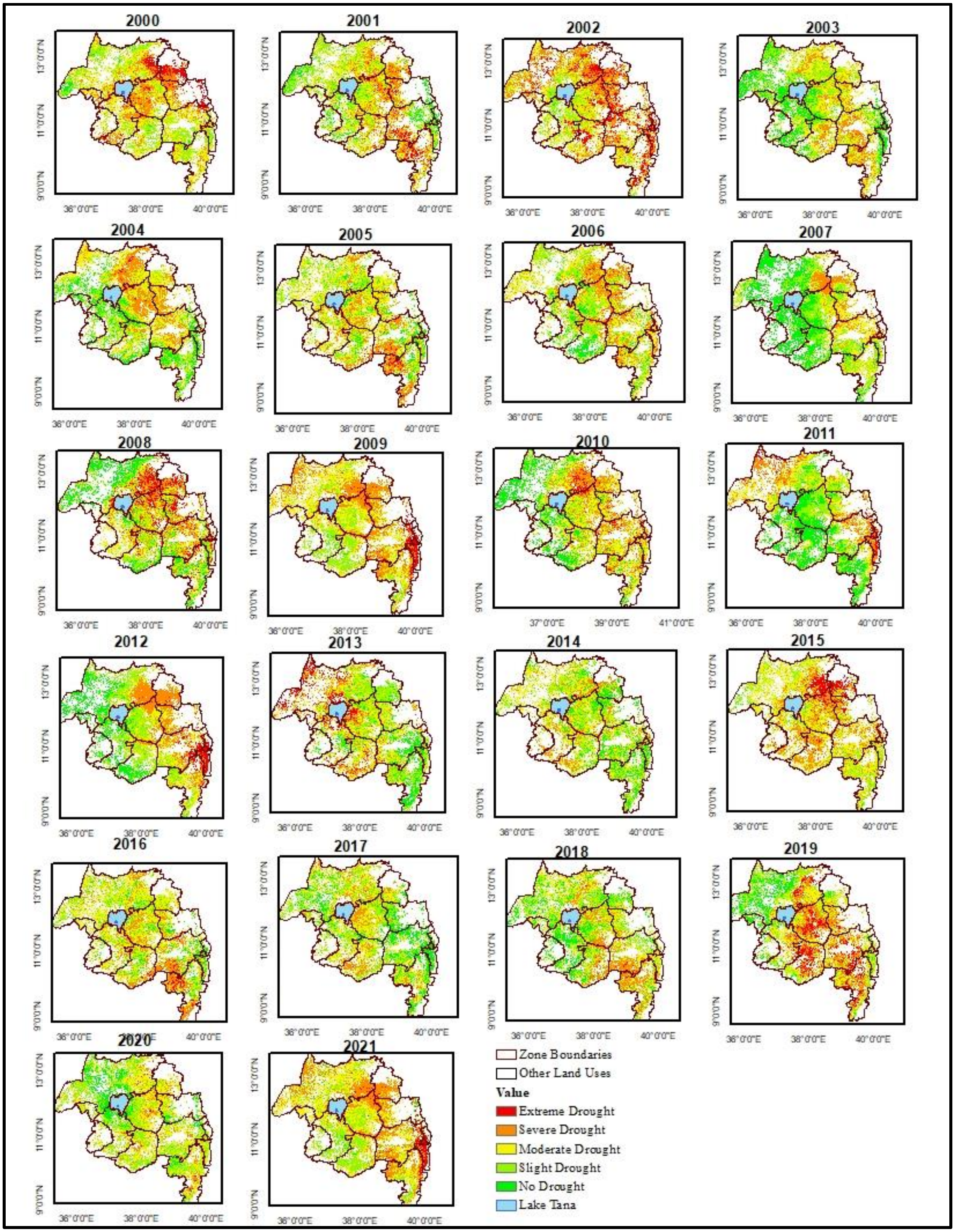

Figure 14: Spatial pattern of agricultural drought in Amhara Region using CADI in August

Table 9, provided below, presents a comprehensive overview of the areal coverages and percentages of drought based on CADI for each year in August, demonstrating the extent of the drought in the studied area. The years 2000, 2002, 2006, 2008, 2009, 2012, 2013, 2014, 2015, 2016, 2019, and 2021 were found to have experienced moderate to extreme drought conditions. The areas affected in these years were recorded as 7.46, 24.63, 5.10, 33.59, 1.72, 23.90, 11.71, 22.16, 15.93, 37.65, 4.50, 26.30, 8.22, 17.01, 0.06, 15.63, 31.63, 28.98, 1.17, 26.28, 11.33, 25.65, 7.64, and 28.18 percent of areas were affected by extreme and severe drought for each drought-experienced year, respectively.

Table 9: Drought-Affected Areas by Using CADI Severity Level in August

Year	**Extreme Drought**		**Severe Drought**		**Moderate Drought**		**Slight Drought**		**No Drought**	
	Area (km^2)	%	Area (km^2)	%	Area (km^2)	%	Area (km^2)	%	Area (km^2)	%
2000	7009.25	7.46	23143.31	24.63	35552.69	37.84	26560.69	28.27	1694.56	1.80
2001	4508.31	4.97	20403.56	22.48	28863.93	31.80	27629.18	30.44	9338.25	10.29
2002	4617.13	5.10	30420.00	33.59	35459.50	39.15	19492.31	21.52	583.81	0.64
2003	234.06	0.24	14524.69	14.89	28691.31	29.41	31660.94	32.45	22461.13	23.02
2004	413.44	0.44	19751.19	21.07	30111.13	32.13	26641.19	28.43	16805.56	17.93
2005	1579.75	1.78	19779.38	22.30	35180.06	39.66	24502.63	27.62	7668.06	8.64
2006	1532.19	1.72	21286.94	23.90	29925.00	33.60	28643.13	32.16	7684.75	8.63
2007	349.50	0.39	10478.06	11.62	18146.69	20.13	27810.31	30.84	33379.31	37.02
2008	10993.25	11.71	20813.13	22.16	23583.88	25.11	20577.38	21.91	17949.88	19.11
2009	14455.44	15.93	34164.13	37.65	26915.50	29.66	14720.63	16.22	487.44	0.54
2010	2613.00	2.82	23481.75	25.36	30638.25	33.09	16521.38	17.84	19331.88	20.88
2011	2877.50	3.21	15361.94	17.12	19762.81	22.02	26260.06	29.26	25476.38	28.39
2012	4005.06	4.50	23419.38	26.30	19232.25	21.60	24478.94	27.49	17899.75	20.10
2013	7224.13	8.22	14952.06	17.01	25078.69	28.53	28485.81	32.41	12151.06	13.83
2014	51.88	0.06	13742.38	15.63	30128.75	34.28	28649.00	32.59	15325.19	17.44
2015	28541.25	31.63	26155.50	28.98	22709.13	25.16	12813.75	14.20	27.88	0.03
2016	1117.31	1.17	25062.63	26.28	35685.69	37.42	23246.69	24.38	10254.81	10.75
2017	44.13	0.05	11410.31	12.45	27059.19	29.52	34112.00	37.21	19041.00	20.77
2018	647.44	0.69	19163.38	20.49	28855.75	30.85	28819.75	30.81	16044.75	17.15
2019	10592.81	11.33	23989.69	25.65	24079.94	25.75	21196.69	22.66	12031.69	12.86
2020	208.75	0.23	9165.50	10.15	30362.19	33.62	38078.88	42.17	12485.81	13.83
2021	6796.94	7.64	25056.81	28.18	37773.38	42.47	18828.88	21.17	474.88	0.53

On the other hand, the remaining years, 2001, 2003, 2004, 2005, 2007, 2010, 2011, 2017, 2018, and 2020, were found to have no drought conditions relatively based on the CADI drought classes.

The CADI values for no drought area coverage in percent for these years were recorded as 10.29, 23.02, 17.93, 8.64, 37.02, 20.88, 28.39, 20.77, 17.15, and 13.83 percent, respectively. This result indicates that the study area has experienced an increasing trend in drought conditions over time. Out of the 22-year study period, 12 years were found to have experienced drought conditions, while the remaining 10 years were relatively free from drought.

The percentages of the area under drought and the drought-free area provide valuable insights into the severity and distribution of drought conditions. Upon analysis, distinct trends in the areal coverages and percentages of drought occurrence in certain years, such as 2000, 2002, 2009, and 2015, show higher percentages of the area under drought, indicating more severe and widespread drought conditions. In contrast, lower percentages of the area experiencing drought were recorded in 2001, 2003, 2005, 2007, and 2018, indicating months that were comparatively typical. The result of this study was in line with other researchers results conducted in different parts of the study area; for instance, a study entitled "Monitoring agricultural drought using geospatial technologies, Menna Watershed, northwestern Ethiopia," conducted by Enyew et al. (2025). In addition, Tela et al. (2024), in Assessment of Meteorological and Socioeconomic Drought Conditions in the Tekeze Watershed, Northern Ethiopia, found droughts of various severity and associated socioeconomic effects occurred in 2000, 2002, 2004-2005, 2009-2011, 2013-2015, 2017, and 2021-2023.

4.2.5. Spatial Variations of Agricultural Drought Status Using CADI in September

As it has been shown in figure 15 below, based on CADI, extreme to severe drought conditions have occurred. During this month, the northern, central, eastern, and southern parts of the study area were affected by moderate to extreme drought, especially in the years 2000, 2002, 2004, 2005, 2006, 2009, 2010, 2012, 2014, 2015, 2016, 2017, and 2020. Except for the western part of the study area, specifically Awi/Agew, all parts, particularly the northeastern, southern, and southeastern parts of the study area, were affected by extreme drought. But the spatial extent that was affected by moderate to extreme drought in 2005, 2009, 2015, and 2017 was larger than the remaining years (almost all parts of the study area were affected in these years during this month). There were relatively near-normal years across the majority of the study areas during 2001, 2003, 2007, 2008, 2011, 2013, 2017, 2018, 2019, and 2021.

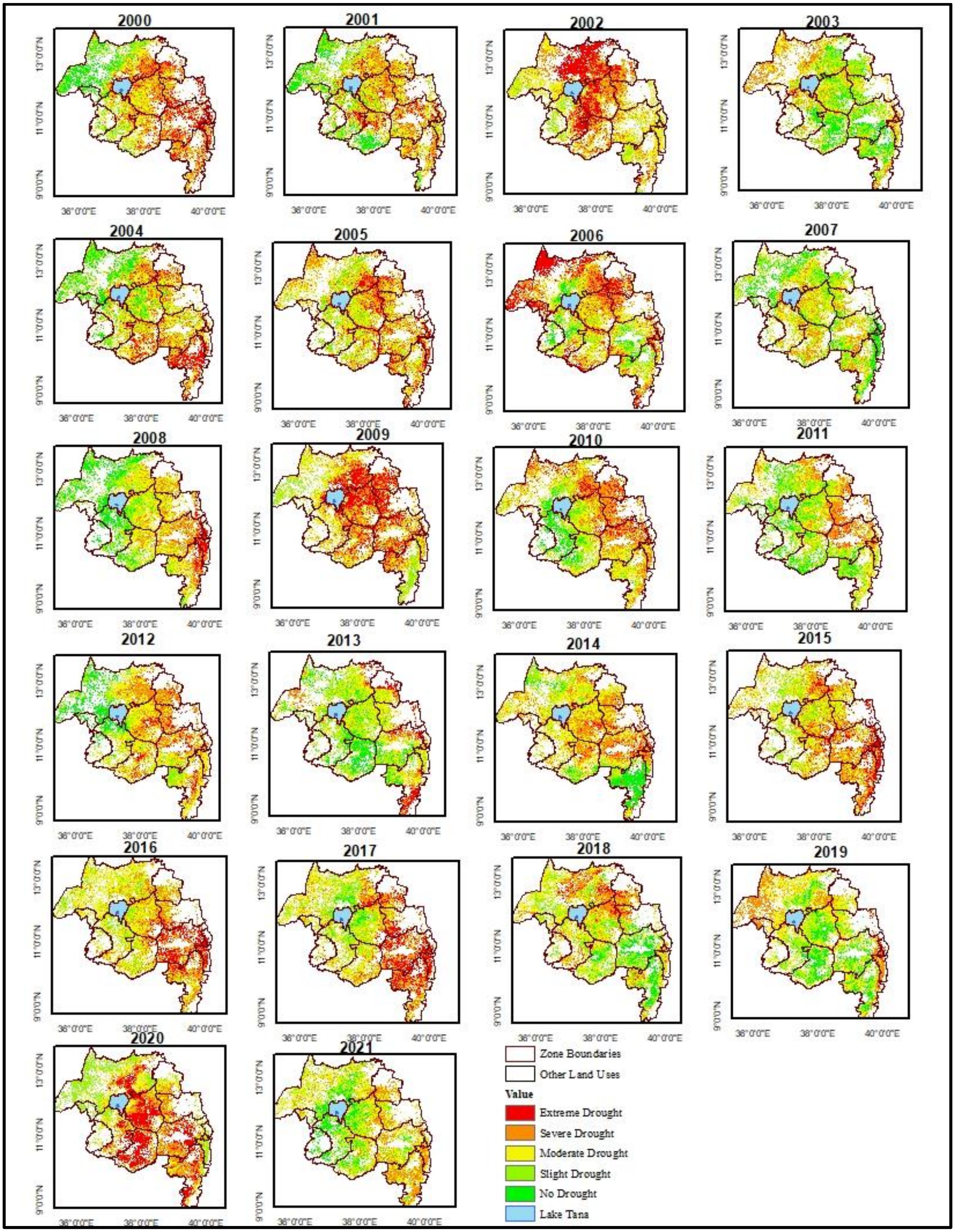

Figure 15: Spatial pattern of agricultural drought in Amhara Region using CADI in September

The table provided below displays the areal coverages and percentages of drought based on the CADI for each year from 2000 to 2021 in September. From the table, we can observe the variations in the extent of drought over the years. The fluctuations in these percentages indicate the dynamic nature of drought patterns.

Table 10: Drought-Affected Areas by Using CADI Severity Level in September

Year	Extreme Drought		Severe Drought		Moderate Drought		Slight Drought		No Drought	
	Area (km^2)	%	Area (km^2)	%	Area (km^2)	%	Area (km^2)	%	Area (km^2)	%
2000	15042.81	16.58	29681.56	32.72	21547.56	23.75	14047.13	15.48	10395.63	11.46
2001	9131.94	9.72	26146.56	27.83	25729.38	27.38	21703.81	23.10	11249.00	11.97
2002	12098.56	13.77	29086.94	33.10	31563.63	35.91	14933.63	16.99	202.38	0.23
2003	477.81	0.54	16897.13	18.98	26227.13	29.46	30054.25	33.76	15371.06	17.27
2004	11334.31	12.09	23259.25	24.82	27397.50	29.23	19071.06	20.35	12658.81	13.51
2005	11832.44	13.12	28845.50	31.99	32833.00	36.41	15971.44	17.71	681.13	0.76
2006	19439.88	19.93	29652.38	30.41	26513.63	27.19	16339.50	16.75	5577.00	5.72
2007	114.38	0.13	13433.69	15.14	28236.25	31.83	31473.19	35.48	15452.25	17.42
2008	4155.50	4.43	18319.31	19.51	29869.75	31.82	24904.56	26.53	16630.19	17.71
2009	22453.38	24.29	31492.31	34.06	26048.81	28.17	12409.81	13.42	52.69	0.06
2010	8439.19	8.85	30714.06	32.21	30066.38	31.53	17864.06	18.73	8282.81	8.69
2011	1329.56	1.48	18664.81	20.80	27844.63	31.03	29087.50	32.42	12807.25	14.27
2012	4533.75	5.09	27524.13	30.91	31251.31	35.10	14387.69	16.16	11336.31	12.73
2013	5343.69	6.08	9580.50	10.90	27678.81	31.50	31527.25	35.88	13737.00	15.63
2014	3193.25	3.54	26645.94	29.55	35126.50	38.96	16541.75	18.34	8663.31	9.61
2015	22609.44	24.93	28751.13	31.70	28533.13	31.46	10758.19	11.86	44.00	0.05
2016	11544.69	12.75	25562.13	28.22	37643.69	41.56	15737.38	17.38	84.06	0.09
2017	15095.13	16.54	24171.31	26.48	29133.44	31.92	20638.69	22.61	2226.69	2.44
2018	3801.50	4.06	21515.81	23.00	31858.56	34.06	26774.06	28.63	9578.00	10.24
2019	1054.19	1.15	17282.25	18.80	33642.81	36.60	27088.13	29.47	12851.50	13.98
2020	21676.06	24.35	28128.44	31.60	19675.44	22.10	19431.69	21.83	106.88	0.12
2021	143.94	0.16	19159.88	21.22	33061.06	36.62	26366.63	29.20	11553.31	12.80

In 2007, for example, the area under drought was 114.38, 13433.69, and 28236.25 areas for extreme, severe, and moderate drought, respectively, accounting for 0.13, 15.14, and 31.83 percent of the study area under extreme, severe, and moderate drought conditions.

While the slight drought and drought-free area were 31473.19 and 15452.25, representing 35.48 % and 17.42% of the whole region during this month and this specific year, respectively. This indicates that a significant portion of the region experienced drought conditions even during that wet year.

The proportions of areas experiencing drought and those not experiencing it vary from year to year. For instance, in 2015, the area under drought reached 22609.44, 28751.13, and 28533.13 for extreme, severe, and moderate drought conditions, respectively, accounting for 24.93, 31.70, and 31.46 percent of the area, respectively, while slight drought and drought-free areas were 10758.19 and 44.00, representing 11.86% and 0.05% of the total area only in this month. This suggests a severe drought situation during that particular year. Analyzing the areal coverages and percentages of drought over time can provide valuable information for drought monitoring, water resource management, and agricultural planning. It allows policymakers, researchers, and stakeholders to assess the impact of drought on vegetation and make informed decisions regarding water allocation, crop management, and mitigation strategies.

4.3. Spatial Variations of Agricultural Drought Status Using CADI for the Primary Drought Years

Drought episodes occurred in the entire study area in 2002, 2009, and 2015 in all months as well as during the summer season. During the study period, most eastern parts of the study area (North Wollo, South Wollo, Wag Himra, South Gonder, North Shewa, and Oromia Zones of Amhara regions, as well as some parts of East Gojam Zone) were identified as drought-prone zones of the study area; thus, Figure 18 clarifies this result that indicates the reduction in yield within the specified zones of the study area specifically by referring to the crop yield during 2015. This study confirmed the findings of Gebrehiwot et al. (2016), Randriamampianina et al. (2019), and Viste et al. (2013), who identified Ethiopia's central and northern highlands, particularly the Amhara and Tigray regions, as the most vulnerable agriculturally producing areas. The findings of this study also support the findings of Gebre et al. (2017), who have reported that crops have failed and hunger and malnutrition have risen sharply, affecting millions in the North Wollo zone.

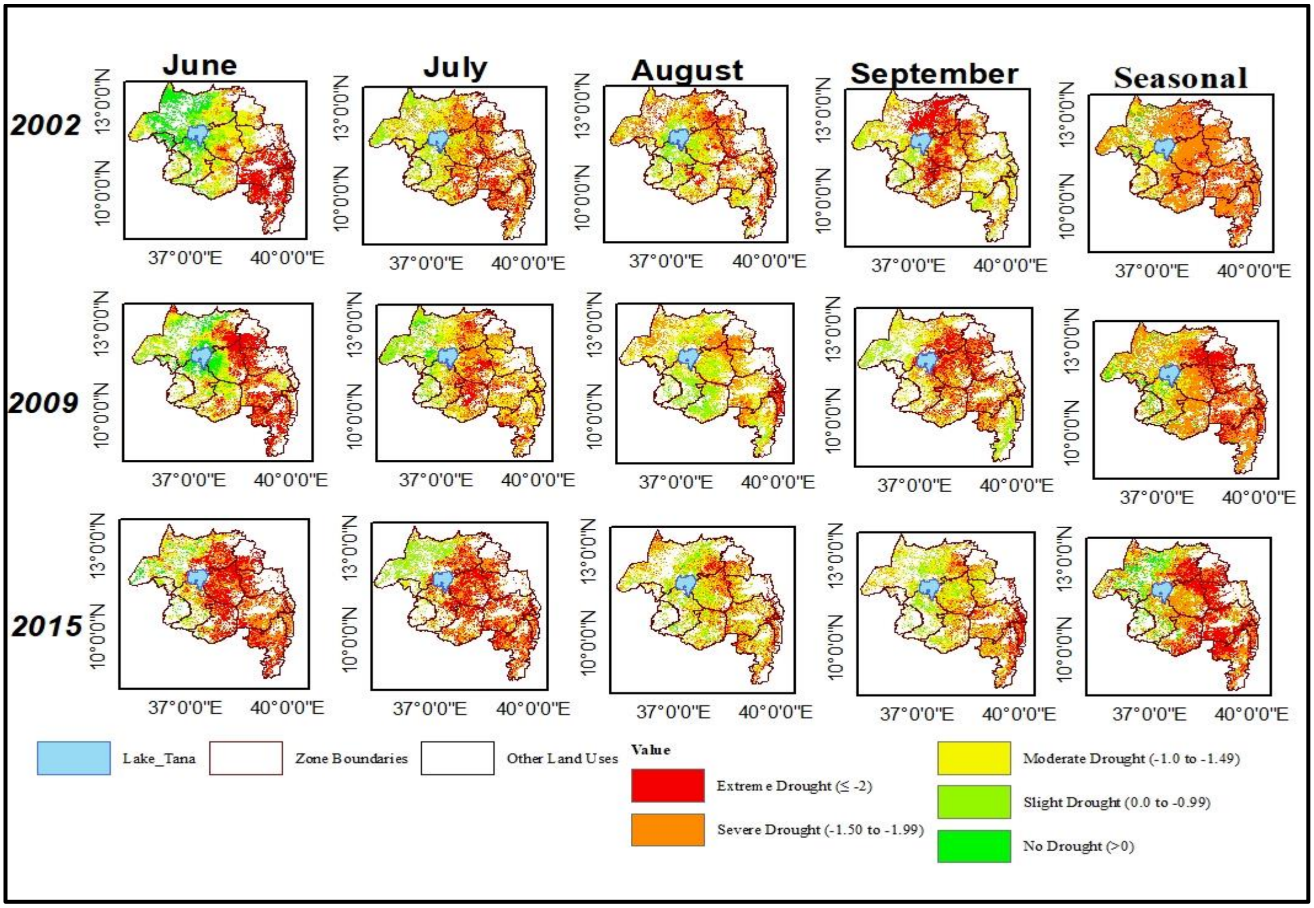

Figure 16: Spatial pattern of agricultural drought in the Amhara Region using CADI for the primary drought years

Furthermore, the historic drought years identified in this study are consistent with the results of previous studies' drought years (Moussa Kourouma et al., 2021); for example, they detected 2003, 2004, 2008, 2009, and 2015 as drought years in their remote sensing-based drought assessment from 2003 to 2017. Severe droughts were also observed during the Kiremt season in 2002-2004, 2009-2010, and 2014-2015 (Liou & Mulualem, 2019; Bayissa et al., 2019; and Chere et al., 2022) in their remote sensing-based vegetation condition index, combined drought index for Ethiopia (CDI-E), and vegetation health index (VHI) from 2001 to 2018, 2001 to 2015, and 2014 to 2018, respectively. In addition, the result of this study is in line with the results of interviews from the Amhara region agricultural offices and the region's Disaster Risk Management office. One of the interviewees from the region's Disaster Risk Management states that;

> Most eastern parts of the study area were the most agriculturally drought-prone areas, and the current political insecurity problems increase the risks to the community because it is difficult to take remedial action for these agriculturally prone parts of the study area. In addition, a lack of transport services also increases the impact of this problem, as it hinders the concerned body from traveling in freedom and taking action for the affected communities (August 03, 2024).

Upon examining the map from figure 16 above, it is evident that the eastern portion of the study area experienced a higher prevalence of drought and moisture stress. This finding suggests that this specific region faced more significant challenges in terms of water availability and vegetation health compared to other parts of the study area. The distribution of drought conditions depicted in the map can provide valuable insights for understanding the spatial patterns of drought occurrence and its potential impacts on agriculture. It helps to identify areas that require focused interventions and management strategies to mitigate the effects of agricultural drought and promote sustainable management strategies.

Table 11 provided below displays the areal coverages in percentages of drought-affected areas for the primary drought years, i.e., 2002, 2009, and 2015, in all summer months and for the summer season. From the table, we can observe the variations in the areal extent of drought over these years. The fluctuations in percentages indicate the dynamic nature of drought patterns. In June 2002, for example, the areas under drought recorded were 20.00, 14.98, 28.38, and 63.36 percent of areas for extreme, severe, moderate, and total drought-affected areas, respectively. In 2009 of this month, 32.42, 25.29, 18.76, and 76.47 percent of the area were affected by extreme, severe, moderate, and total affected areas, respectively. During 2015, 38.50, 37.25, and 13.86 percent of the area were affected by moderate to extreme conditions, and 89.61 percent was the total area affected in this year in June. In July 2002, the area under drought based on CADI recorded 15.91, 34.01, 34.67, and 84.6 percent of the total area experiencing extreme, severe, moderate, and total drought-affected areas, respectively. In 2009 of this month, 18.00, 36.99, 30.94, and 85.92 percent of the area were affected by extreme, severe, moderate, and total affected areas, respectively. During 2015, 36.27, 34.98, and 13.00 percent of the area were affected by moderate to extreme conditions, and 84.24 percent was the total area affected in this year in July.

In August 2002, the area under drought based on CADI recorded was 5.10, 33.59, 39.15, and 77.83 percent of areas for extreme, severe, moderate, and total drought-affected areas, respectively. In 2009 of this month,15.93, 37.65, 29.66, and 83.24 percent of the area were affected by extreme, severe, moderate, and total affected areas, respectively. During 2015, 31.63, 28.98, and 25.16 percent of the area were affected by moderate to extreme conditions, and 85.77 percent was the total area affected in this year in August.

Table 11: Drought-Affected Areas (Extreme to Moderate) for the Primary Drought Years

Year	Months	Extreme Drought	Severe Drought	Moderate Drought	Total area
2002	June	20.00	14.98	28.38	63.36
	July	15.91	34.01	34.67	84.6
	August	5.10	33.59	39.15	77.83
	Sept	13.77	33.10	35.91	82.78
	Seasonal	13.69	28.92	34.53	77.14
2009	June	32.42	25.29	18.76	76.47
	July	18.00	36.99	30.94	85.92
	August	15.93	37.65	29.66	83.24
	Sept	24.29	34.06	28.17	86.52
	Seasonal	22.65	33.49	26.88	83.04
2015	June	38.50	37.25	13.86	89.61
	July	36.27	34.98	13.00	84.24
	August	31.63	28.98	25.16	85.77
	Sept	24.93	31.70	31.46	88.09
	Seasonal	32.83	33.22643	20.87	86.93

The result of CADI for September 2002 showed that the percentage of areas impacted by extreme, severe, moderate, and overall drought was 13.77, 33.10, 35.91, and 82.78 percent, respectively. In 2009 of this month, 24.29, 34.06, 28.17, and 86.52 percent of the area were affected by extreme, severe, moderate, and total affected areas, respectively. During 2015, 24.93, 31.70, and 31.46

percent of the area were affected by moderate to extreme drought conditions, respectively, and 88.09 percent was the total area affected in this year in September.

Figure 17 below depicts the percentage of areas experiencing moderate to extreme drought conditions during these selected drought years in June, July, August, and September. For example, the total area affected by moderate to extreme drought in June was 63.36%, 76.47%, and 89.61 % of the total area affected in 2002, 2009, and 2015, respectively. In July, similar results of 84.6%, 85.92%, and 84.24% were observed in 2002, 2009, and 2015, respectively. Additionally, in August, 77.83 %, 83.24%, and 85.77% of the area were affected in 2002, 2009, and 2015, and in September, 82.78%, 86.52%, and 88.09% were affected in 2002, 2009, and 2015, respectively.

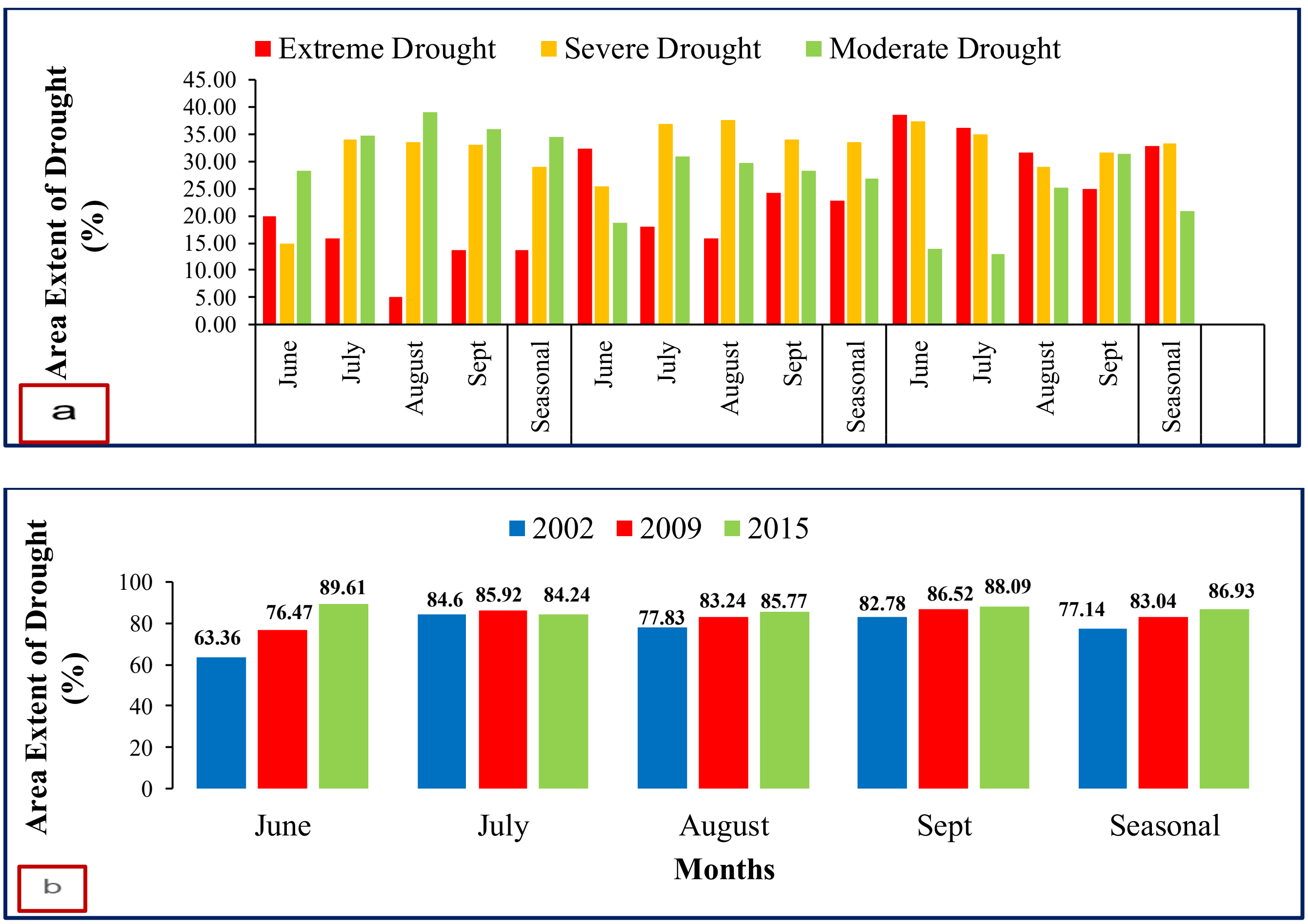

Figure 17: Percentage of drought-affected areas for the primary drought years (2002, 2009, and 2015, respectively) (moderate-extreme drought cases) (a) and percentage of total affected areas (b)

Based on the result of CADI in June, there have been droughts in each of the years under consideration. But in 2015, the study region experienced drought in the majority of its areas; that is, 89.61% of the total area was affected in this specified year. 2009 and 2002 were the years that came after. In addition, in July 2009, 85.92% of the total agricultural area had experienced drought; the years 2015 and 2002 were the years that came after this specified year. In August 2015, the study region experienced drought in the majority of its areas; that is, 85.77% of the total area was affected in this specified year. 2009 and 2002 were the years that came after. In September 2015, 88.09% of the area was affected. Seasonally, 77.14%, 83.04%, and 86% of the study area were the areas affected by extreme to moderate drought conditions in 2002, 2009, and 2015, respectively.

In 2002 and 2009, 84.6% and 85.92% of the total area, respectively, particularly in July, had moderate to extreme drought conditions, whereas in August, the percentage decreased to 77.83% and 83.24% during these specified years. The occurrence of considerable precipitation over the northern highlands of Ethiopia, according to Bayissa et al. (2019)**,** was the main reason why the drought area decreased in this month. In August 2009 and 2015, 83.24% and 85.77% of the area of the region, respectively, was affected by moderate to extreme drought conditions, whereas in September 2009 and 2015, 86.52% and 88.09% of the area, respectively, was affected. This happened as a result of a lack of precipitation towards the end of the growing season. Thus, the results are in line with those of Sohnesen (2020), who claimed that Ethiopia's northern regions experienced drought in 2015 and had a notable decrease in precipitation in North Ethiopia.

Based on figure 18 below and map 16 above, the level of drought condition at the zonal level, low CADI value (< 0), and reduction of crop yield in 2015 were observed in almost all eastern portions of the Amhara region, including North Wollo, Oromia, South Gonder, Wag Himra, North Shewa, South Wollo, and East Gojam Zones. In 2002, 2009, and 2015, almost all eastern parts of the study area and parts of the east Gojam zone experienced moderate to extreme drought conditions, as can be shown in map 16 and displayed in figure 18, as well as the reduction in crop yield in these parts of the study area, which proves it.

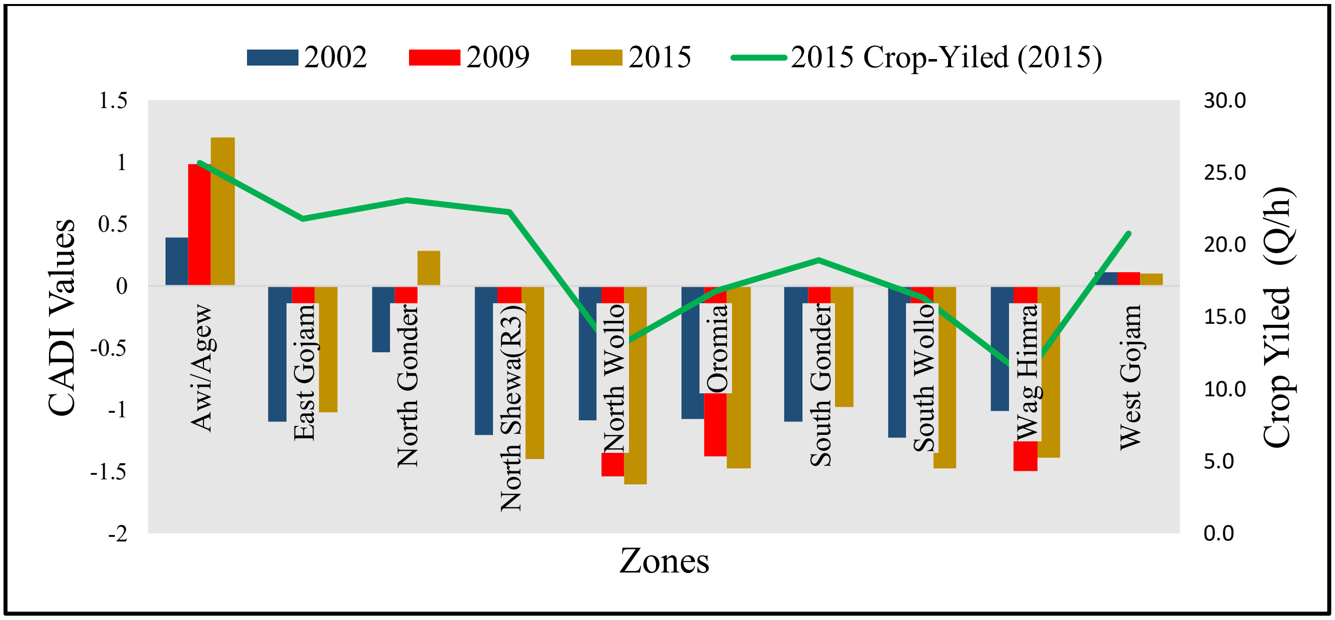

* Q = quintal; h = hectare

Figure 18: Comparison of primary drought years with crop yield during 2015 for different zones

4.3.1. Spatial Variations of Agricultural Drought Status Using CADI for the Most Drought Year, 2015, and for the Wettest Year, 2007

Figure 19 provided below displays the spatial patterns of drought-affected areas for the drought year 2015 and the normal year 2007. From the map, we can observe most eastern parts of the study areas have experienced drought during 2015, and even some eastern parts of the study area, such as Wag Himra, North Wollo, South Wollo, and Oromia zones of the study area, were affected by drought in the normal year (2007). During the entire study period, with the exception of July, the most severe drought event was seen during 2015.

Significant temporal and regional differences in drought intensity and extent are seen throughout the region when the Combined Agricultural Drought Index (CADI) for the drought year 2015 and the wet year 2007 is used to compare the agricultural drought situation. The CADI figures for 2015 show that there was a severe and pervasive agricultural drought. On the other hand, 2007 showed little effect from drought, with CADI scores primarily indicating good farming conditions. Nearly every region had sufficient rainfall. The regional variation between these two years highlights how

Crucial early warning and monitoring systems are required. The notable discrepancy demonstrates how CADI may accurately reflect the intensity of drought as well as agricultural recovery during rainy years. The result was aligned with the results of different studies; for instance, the most severe events in the last 30 years were the drought in 2015, which significantly impacted a substantial portion of the nation and worsened food insecurity (Chere & Debalke, 2024). This highlights the profound impact of drought on both the agricultural sector and the overall socioeconomic conditions in the study area. In addition, repercussions continued in 2015–16, affecting around 5 million people in Northern, Southern, and Eastern Ethiopia (Liou & Mulualem, 2019; Mera, 2018). Moreover, reports by Kassaye et al. (2021) estimate that a staggering 10.2 million people were affected by these events.

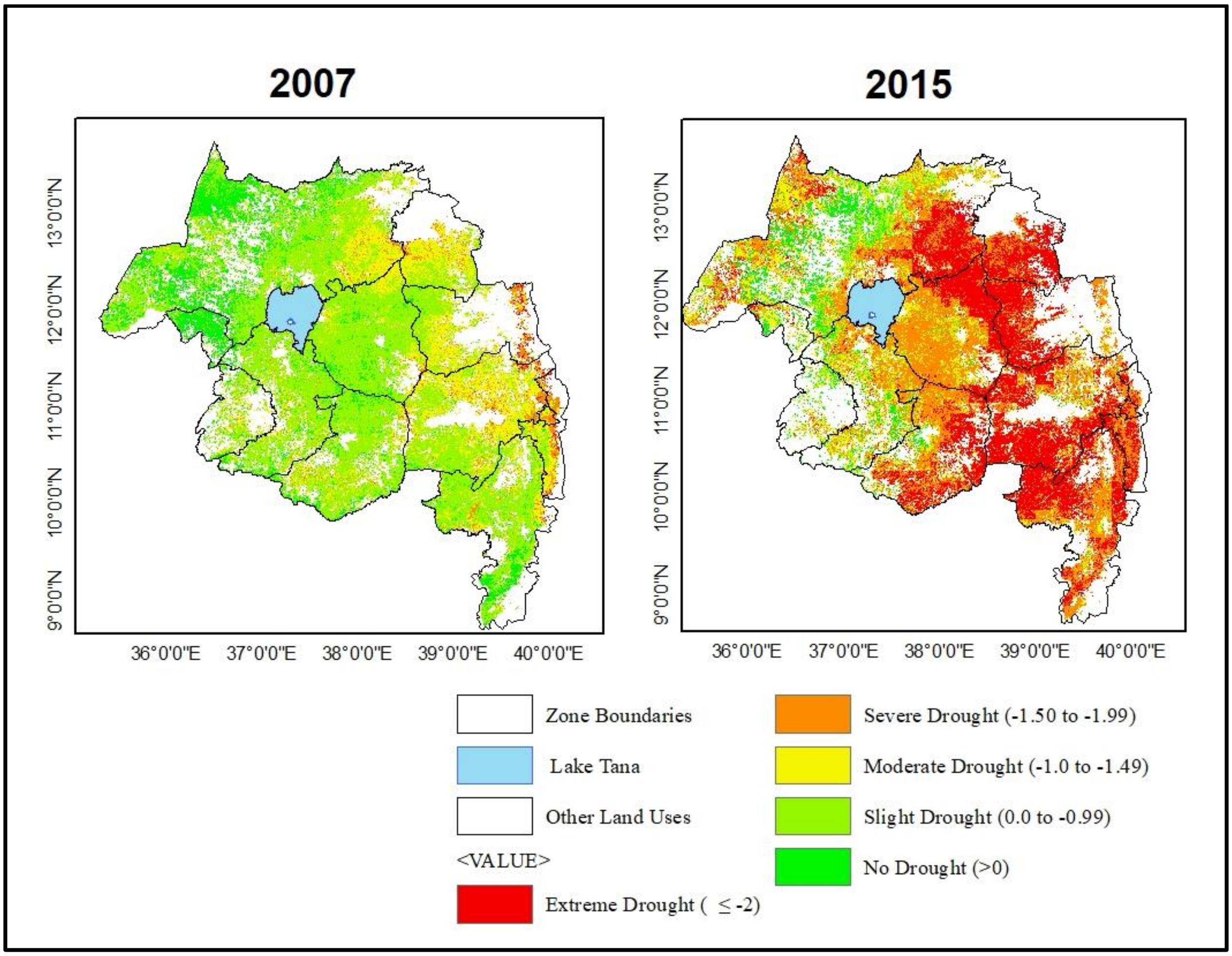

Figure 19: Comparison of the spatial distribution of agricultural drought for a wet year (2007) and for a drought year (2015) based on CADI seasonally

Figure 20 below illustrates the level of drought condition at the zonal level for the summer season. All eastern Amharan regions, including the Wag Himra Zone, North Shewa, North Wollo, Oromia, South Gonder, and South Wollo, have low CADI values (<0). During the most drought year, which was in 2015, almost all eastern parts of the study area and parts of East Gojam experienced moderate to extreme drought conditions. Even these parts of the study area experienced drought during a normal year, which was in 2007. This indicates that a significant portion of the region experienced drought conditions even during that wet year.

The result of this study was confirmed by the result obtained from key informant interviews with the region's disaster risk management experts; they stated that *"most eastern parts of the region experience drought frequently, and these parts are the most drought-affected parts of the region; they require food assistance and related support frequently."*

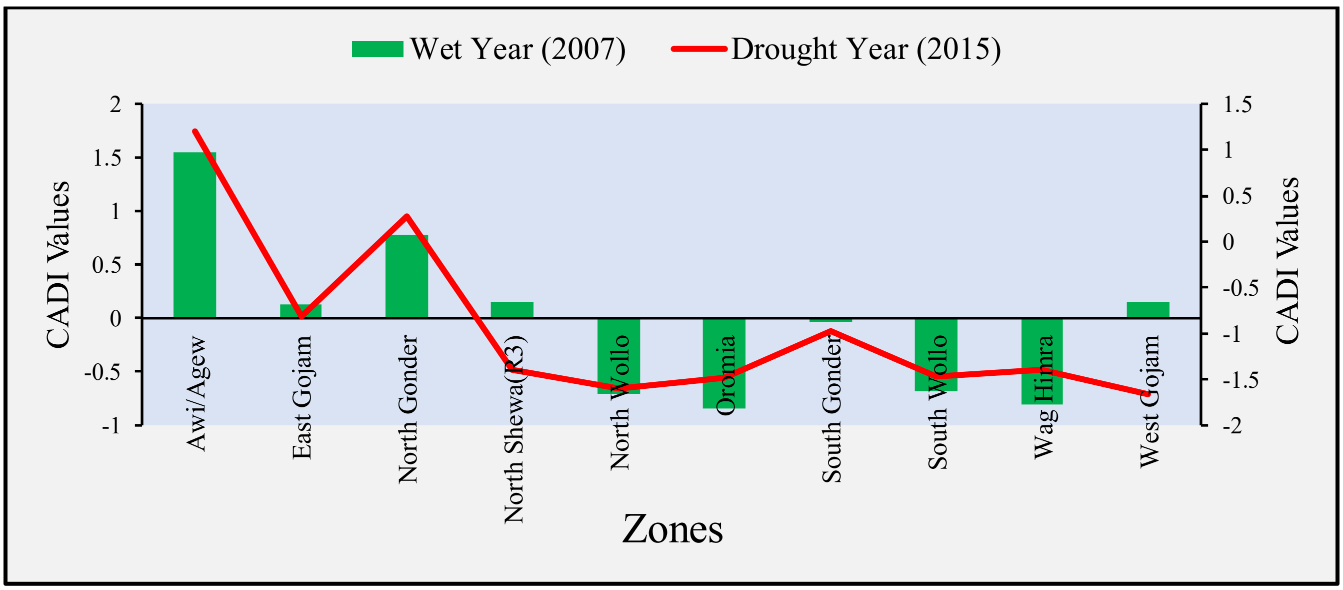

Figure 20: Comparison of a normal year (2007) and a drought year (2015) based on CADI for different zones

Furthermore, key informants' interviews in the Amhara region agricultural office and disaster risk management office confirmed that the drought in 2015 was very severe and the crop yield has reduced highly. The interviewee further stated that the rainfall did not fail early in the start of the growing season, which is in June, and it failed in September before the crop was mature.

The region's agricultural experts described this year as very critical for zones that are found in the eastern, southeastern, and portions of the central part of the study area.

4.4. Performance Evaluation of Combined Agricultural Drought Index (CADI)

4.4.1. Correlation Analysis between CADI and Crop Yield

The performance of CADI was evaluated using crop yield data; hence, drought variability and its spatio-temporal distribution are highly responsible for the fluctuations in crop productivity and overall agricultural conditions (Kulkarni et al., 2020). Detrending the crop yield records was done to exclude the influence of other factors, such as weather and climatic circumstances, scientific and technological advancements, and other factors that affect agricultural yields and productivity. A straightforward linear regression model that eliminates the crop yields' increasing linear trend (Lu et al., 2017) was used in this study. Finally, the capabilities of CADI for agricultural drought monitoring in the Amhara Region, Ethiopia, were evaluated through Pearson correlation methods. Pearson correlation was used to establish a relationship between the CADI time series and the annual production of the mean of major cereal crops.

The mean of the annual major cereal crop production was correlated with the mean of summer season CADI time series values. The results of Pearson correlation can be positive or negative. The relationship between CADI and detrended crop yield data is defined as strong, $r \geq 0.60$; moderate, $r = 0.40–0.59$; and weak, $r = -0.40$ to 0.40 (Evans, 1996). Several studies have found that severe to extreme drought events have a significant negative impact on crop yields in various parts of the world (Chere et al., 2022; Kulkarni et al., 2020). The current study sought to assess the spatiotemporal relationship between the mean of major crop yields (teff, maize, and wheat) and summer season CADI values of ten (10) crop-growing zones of the study area. Overall, the CADI and detrended crop yield agree well in the ten selected zones, with correlation coefficient values ranging from correlation coefficients $(r) = 0.51$ to $r = 0.95$. East Gojam had significantly higher correlation coefficients $(r = 0.95)$. Wag Himra, on the other hand, has a relatively lower correlation $(r = 0.51)$. Due to the 2015 drought, all crop-growing zones experienced significant crop yield reductions in 2015-2016.

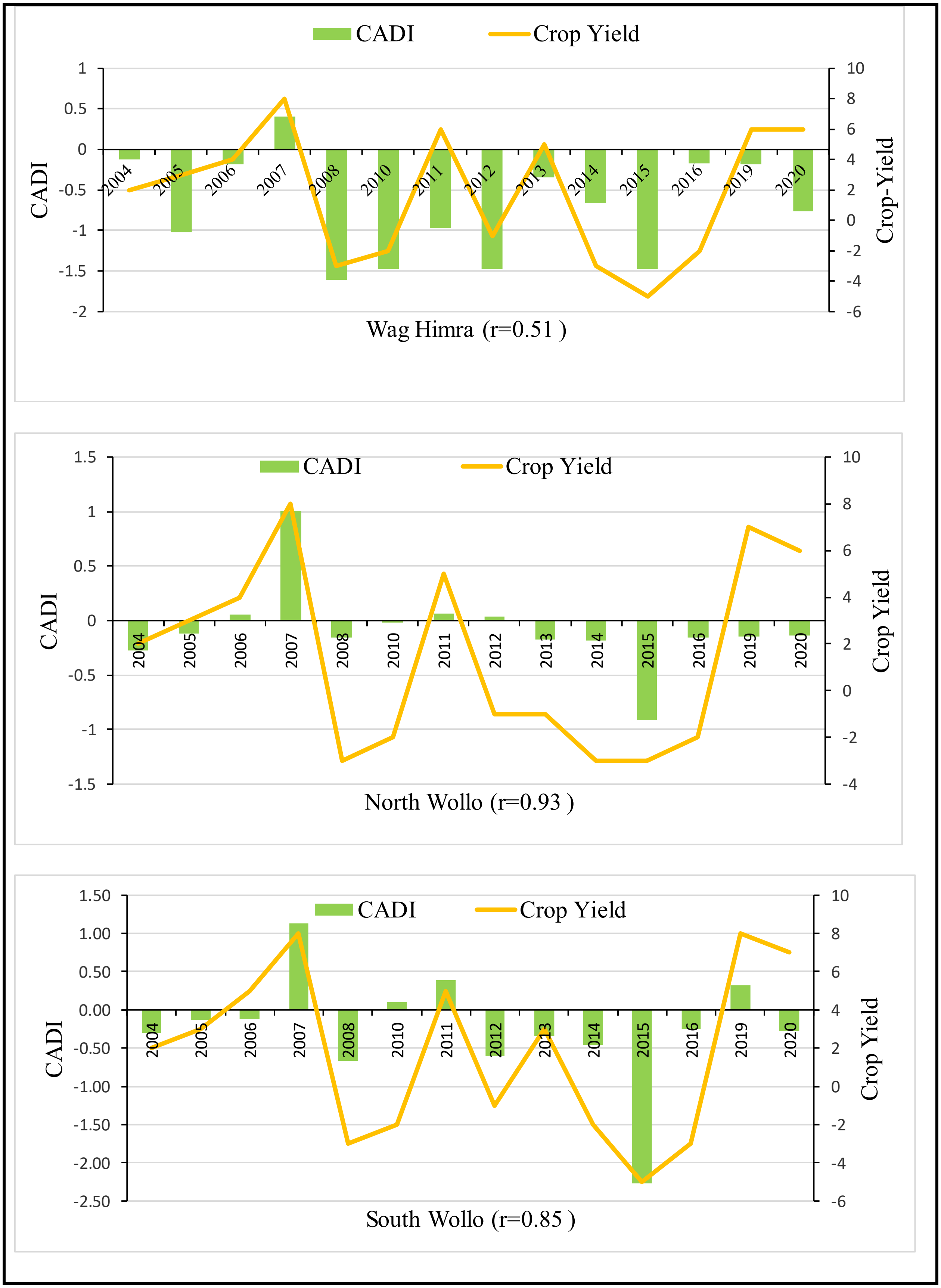
CADI
Crop Yield
1
0.5
0
-0.5
-1
-1.5
-2
10
8
6
4
2
0
-2
-4
-6
CADI
Crop-Yield
2004
2005
2006
2007
2008
2010
2011
2012
2013
2014
2015
2016
2019
2020
Wag Himra (r=0.51)
CADI
Crop Yield
1.5
1
0.5
0
-0.5
-1
-1.5
10
8
6
4
2
0
-2
-4
CADI
Crop Yield
2004
2005
2006
2007
2008
2010
2011
2012
2013
2014
2015
2016
2019
2020
North Wollo (r=0.93)
CADI
Crop Yield
1.50
1.00
0.50
0.00
-0.50
-1.00
-1.50
-2.00
-2.50
10
8
6
4
2
0
-2
-4
-6
CADI
Crop Yield
2004
2005
2006
2007
2008
2010
2011
2012
2013
2014
2015
2016
2019
2020
South Wollo (r=0.85)

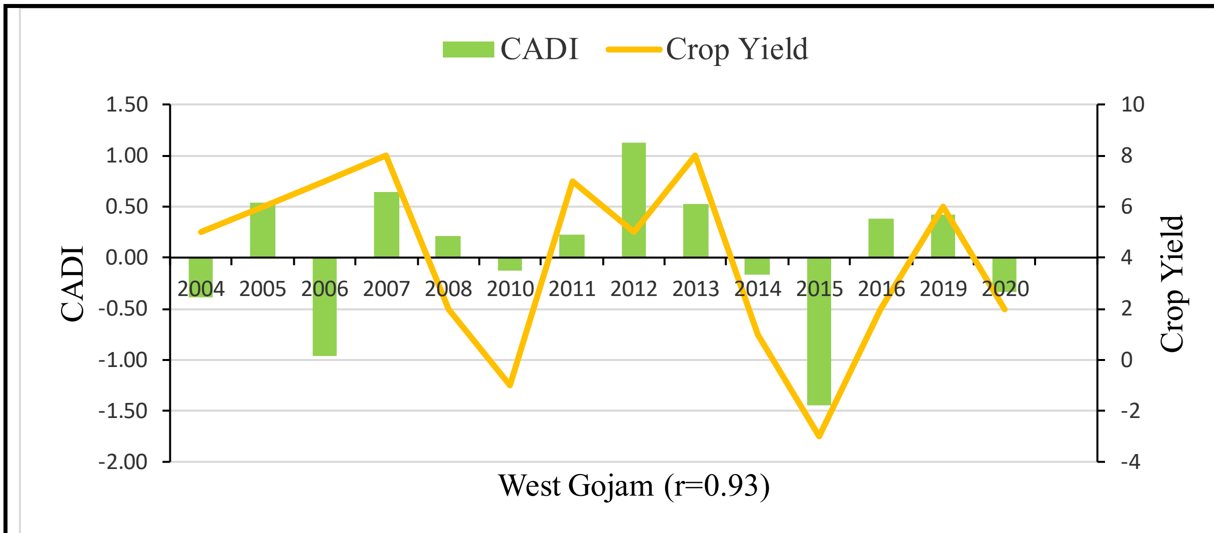
CADI
Crop Yield
CADI
Crop Yield
2004 2005 2006 2007 2008 2010 2011 2012 2013 2014 2015 2016 2019 2020
West Gojam (r=0.93)

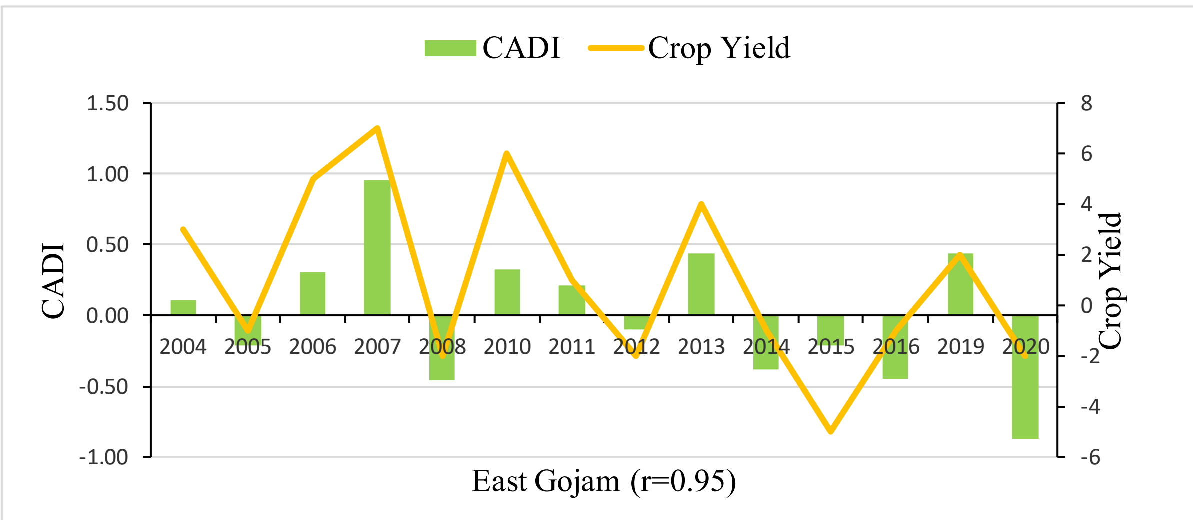
CADI
Crop Yield
CADI
Crop Yield
2004 2005 2006 2007 2008 2010 2011 2012 2013 2014 2015 2016 2019 2020
East Gojam (r=0.95)

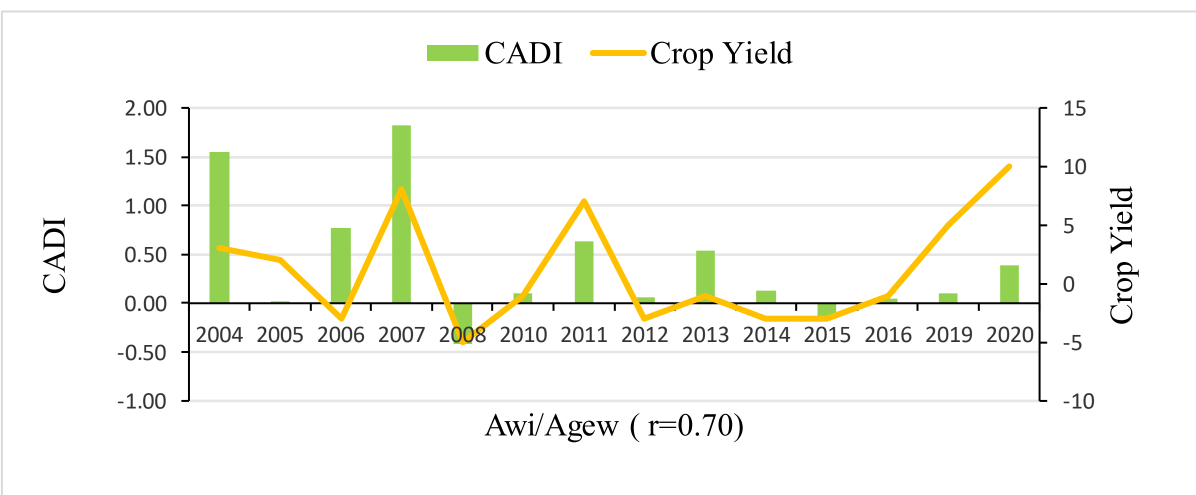
CADI
Crop Yield
CADI
Crop Yield
2004 2005 2006 2007 2008 2010 2011 2012 2013 2014 2015 2016 2019 2020
Awi/Agew (r=0.70)

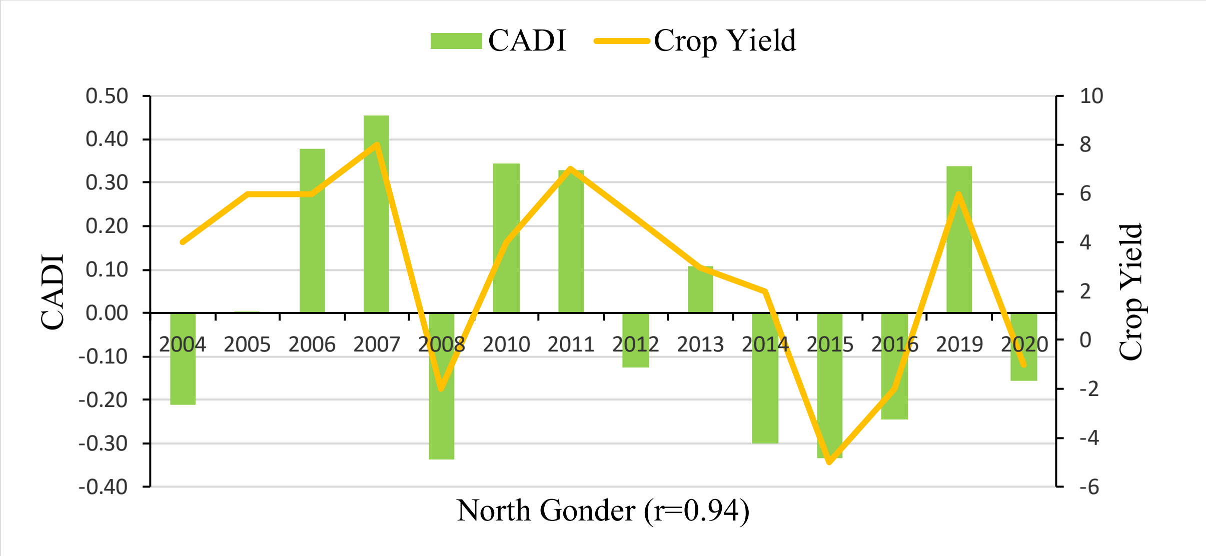
CADI
Crop Yield
North Gonder (r=0.94)

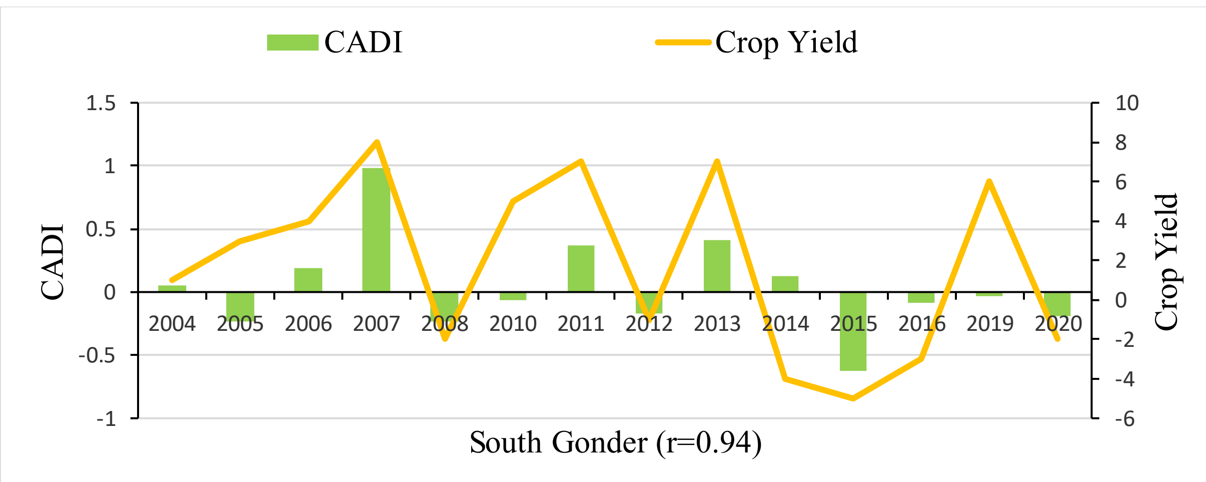
CADI
Crop Yield
South Gonder (r=0.94)

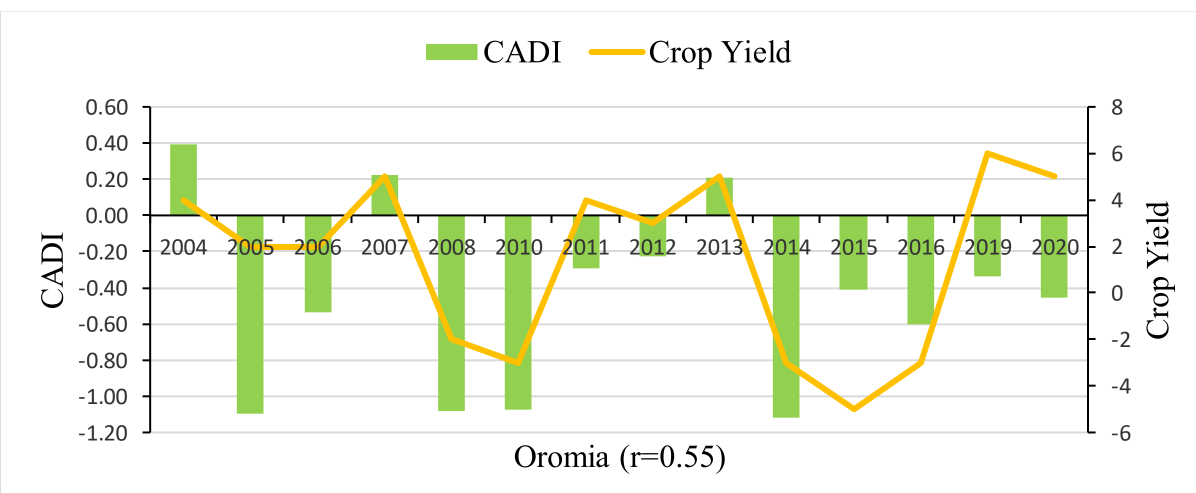
CADI
Crop Yield
Oromia (r=0.55)

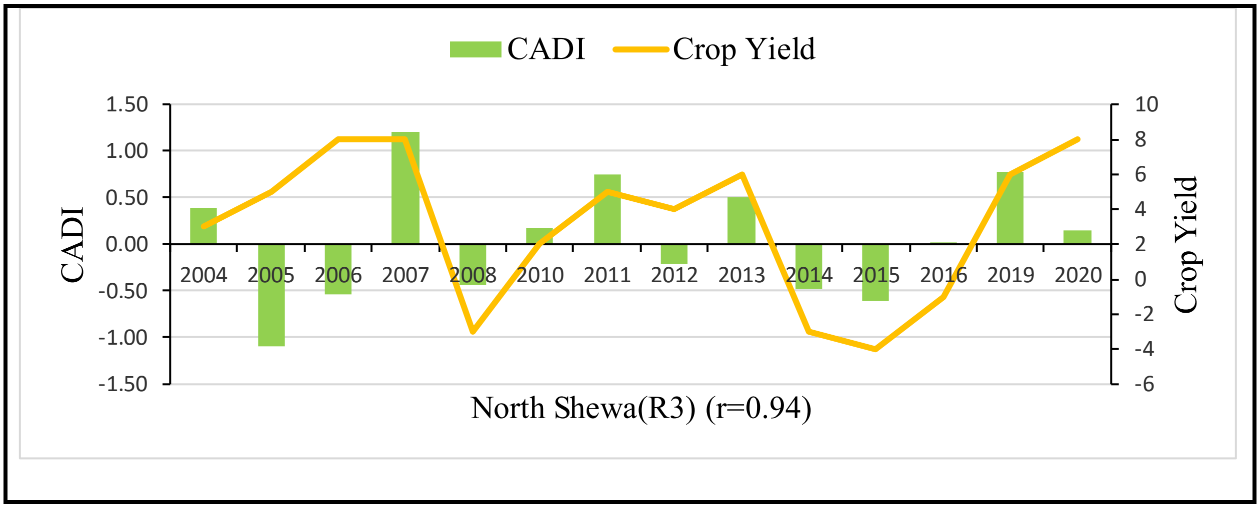

Figure 21: Performance evaluation of CADI with detrended crop yield (mean of major crop yields) (teff, maize, and wheat) with selected zones

According to a recent study by Liou and Mulualem (2019), the direct influence of El Niño on Ethiopian vegetation was visible, particularly during the El Niño years 2014-2015, when NDVI values gradually declined and remained marginally below average. This study's correlation analysis is consistent with Chere et al. (2022), Bayissa et al. (2019), and Tadesse et al. (2015), who used evapotranspiration products with cereal crop production and a combined drought indicator (CDI) to track agricultural drought in an attempt to evaluate the predictive power of VHI in Ethiopia's highlands. In these investigations, the detrended crop production and the created drought indicators showed a stronger association ($r > 0.5$) in the central and northern regions. Additional effort was made to validate the CADI using a different EM-DAT dataset. The drought years identified by this study correspond to EM-DAT reports. According to EM-DAT, the major drought years that affected a large number of people and animals in various parts of the country were 2003-2004, 2009-2010, 2014-2015, and 2021-2022 (EM-DAT, 2022).

The correlation analysis between CADI and crop yield revealed a significant relationship, indicating that lower CADI values, which denote more severe drought conditions, are generally associated with reduced crop yields. Crop type and area had different correlation strengths, underscoring the need for localized CADI calibration and validation. Overall, the findings confirm that CADI is a reliable indicator for assessing drought, and it can be a valuable tool for agricultural risk management and planning.

The correlation analysis between the Combined Agricultural Drought Index (CADI) and crop yield demonstrates a significant relationship, indicating that CADI effectively reflects the impact of drought conditions on agricultural productivity. Areas with lower CADI values, representing more severe drought stress, correspond to reduced crop yields, while higher CADI values align with better crop performance. This strong correlation validates CADI as a reliable tool for assessing agricultural drought and predicting crop yield variability, making it valuable for drought monitoring and decision-making in agricultural management.

Generally, the index showed strong correlation with historical drought events, crop yield data, and local drought reports, confirming its ability to capture both the severity and spatial extent of agricultural droughts across different climatic zones. CADI also performed well in distinguishing between drought and non-drought years, with higher sensitivity and spatial resolution than traditional drought indices.

Overall, the study confirms that CADI is a robust and adaptable index that enhances early warning capabilities and supports informed decision-making for drought risk management. Its application is especially valuable in regions like Ethiopia's Amhara region, where agriculture is highly climate-sensitive and timely drought information is critical for resilience planning.

CHAPTER FIVE

5. CONCLUSIONS AND RECOMMENDATIONS

5.1. Conclusions

As drought is one of the most devastating natural disasters in the world, affecting millions of people in various ways, better monitoring and assessment are essential. Decision-making is greatly aided by the creation of an agricultural drought monitoring index that combines several input factors into a single index. As a result, the goal of this research was to develop an Earth Observation Derived Combined Drought Index for Agricultural Drought Monitoring in the Amhara region, Ethiopia. The CADIs spanning from 2000 to 2021 were created using the Random Forest (RF) algorithm, a significant machine learning (ML) algorithm, by integrating eight input variables that represented various environmental variables, including soil moisture, precipitation condition index, normalized difference vegetation index, vegetation condition index, enhanced vegetation index, land surface temperature, temperature condition index, and evapotranspiration. In addition, three topographical factors (elevation, slope, and aspect) were considered in CADI development, and SPI data were calculated from selected fifty-one stations of the study area for each summer month. The RF model was trained and tested using the SPI values of each month; hence, 70% of the SPI value was used to train the RF algorithms, and the remaining 30% was used for testing.

Even though, the result of developed CADI precisely identified the historical drought years, from June to September of summer season months during 2000, 2002, 2004, 2008, 2009, 2012, 2013, 2014, 2015, 2016, 2018, 2019, 2020, and 2021 in June, during 2000, 2002, 2004, 2005, 2006, 2008, 2009, 2012, 2013, 2014, 2015, 2016, 2017, 2019, 2020, and 2021 in July, during 2000, 2002, 2006, 2008, 2009, 2012, 2013, 2014, 2015, 2016, 2019, and 2021 in August and during 2000, 2002, 2004, 2005, 2006, 2009, 2010, 2012, 2014, 2015, 2016, 2017, and 2020 in September, except the western portion of the study area specifically Awi/Agew zone, all parts particularly northern, northeastern and southeastern parts of the study area were affected by moderate to extreme drought levels, the years 2002, 2009, and 2015 were discovered the years of a primary drought occurrence (severe-to-extreme drought cases) in Amhara region, Ethiopia, and 2007 were the wettest year from the entire study period.

The effectiveness of CADI was evaluated using yield estimates for the mean of cereal crops (teff, wheat, and maize) during the main rainfall season (Kiremt) in Amhara's ten crop-growing zones. Overall, the selected crop-growing zones had a stronger relationship between CADI and detrended crop yields, with correlation coefficient values ranging from correlation coefficients (r) = 0.51 to r = 0.95. East Gojam had significantly higher correlation coefficients (r = 0.95). Wag Himra, on the other hand, has a relatively lower correlation (r = 0.51). Generally, the index showed strong correlation with historical drought events, crop yield data, and local drought reports, confirming its ability to capture both the severity and spatial extent of agricultural drought across different climatic zones. CADI also performed well in distinguishing between drought and non-drought years, with higher sensitivity and spatial resolution than traditional drought indices.

As a result, CADI can be used to help Amhara develop a drought forecasting model in order to better prepare for future agricultural droughts. Generally, the index showed strong correlation with historical drought events, crop yield data, and local drought reports, confirming its ability to capture both the severity and spatial extent of agricultural droughts across different climatic zones. CADI also performed well in distinguishing between drought and non-drought years, with higher sensitivity and spatial resolution than traditional drought indices.

The result of the study indicates that the combined index effectively captures the complex and multifaceted nature of agricultural drought, offering valuable insights for policymakers, resource managers, and agricultural stakeholders. By considering variables such as temperature, precipitation, soil moisture, and topographical factors (elevation, aspect, and slope), the index enables a more nuanced understanding of the severity and extent of drought events. Furthermore, the combined drought index emphasizes its role in enhancing drought preparedness and response strategies. The comprehensive nature of the index equips decision-makers with the information necessary to implement targeted mitigation measures and allocate resources effectively during drought periods. Overall, the combined drought index serves as a valuable tool in the assessment and monitoring of drought conditions, contributing to informed decision-making and adaptive strategies for managing the impacts of drought in the study area. Generally, the study confirms that CADI was a robust and adaptable index that enhances early warning capabilities and supports informed decision-making for drought risk management. Its application is especially valuable in regions like the Amhara region, where agriculture is highly climate-sensitive and timely drought information is critical for resilience planning.

5.2. Recommendations

The following suggestions were sent out in light of the study's findings.

- Based on the findings, most of the eastern, southeastern, and northeastern parts, some parts of central Amhara, and some portions of the east Gojam zone parts of the region were identified as the most vulnerable agricultural production areas. Therefore, effective drought risk management is urgently needed by the Amhara Region Disaster Risk Management offices and Amhara Region Agricultural offices cooperatively with other governmental and nongovernmental organizations as well as with volunteers and concerned bodies.
- According to the study's findings, in areas identified as extremely and severely affected by agricultural drought, proactive remedial actions should be implemented before drought occurs.
- National, regional, and local disaster risk management offices should provide continuous weather information and early warnings to the communities cooperatively with national meteorological agencies.
- The region's disaster risk management offices and the region's agricultural office should integrate this combined agricultural drought index with the existing disaster risk reduction frameworks and agricultural planning policies.
- Training should be conducted for local agencies on using Earth observation data for drought preparedness and responses.
- The Combined Agricultural Drought Index (CADI), which was created in this work, ought to be incorporated into regional drought monitoring systems in order to give farmers, development organizations, and decision-makers timely and geographically precise information.
- Especially in districts that are susceptible and often affected by drought, the CADI should be integrated into early warning systems to initiate proactive measures like targeted irrigation support, input subsidies, or food assistance.

- The region's Disaster Risk Management office and the region's Agricultural office should collaborate with Ethiopian universities to embed remote sensing and drought monitoring modules into academic programs.
- Initially, all of the input parameters for this study were available in a variety of spatial resolutions. Some datasets, such as soil moisture, LST, and rainfall, were only available in coarse resolution. Despite the fact that these coarse-resolution data still represented spatial variability, this study suggests that future research should use high-resolution input data.
- For this study, all croplands (excluding other land uses) were considered, ignoring other land uses such as forests and grasslands; future researchers should incorporate other land uses.

REFERENCES

Abdulkadir, B., Kassa, S., Desalegn, T., Tadesse, K., & Haileselassie, M. (2016). Soil Fertility Management Studies on Wheat in Ethiopia: A Review. *Ethiopian Journal of Natural Resources*, *16*(1), 1–23.

Adou, M., Almouctar, S., Wu, Y., Zhao, F., & Qin, C. (2024). Journal of Hydrology: Regional Studies Drought analysis using normalized difference vegetation index and land surface temperature over Niamey region, the southwestern of the Niger between 2013 and 2019. *Journal of: Regional Studies*, *52*(January),101689. https://doi.org/10.1016/j.ejrh.2024.101689

Aghakouchak, A., Farahmand, A., Melton, F. S., Teixeira, J., Anderson, M. C., Wardlow, B. D., & Hain, C. R. (2015). Reviews of geophysics remote sensing of drought: Progress, challenges. *Reviews of Geophysics*, *53*, 1–29. https://doi.org/10.1002/2014RG000456.Received

Alarifi, A., Al-Salman, A., Alsaleh, M., Alnafessah, A., Al-Hadhrami, S., Al-Ammar, M. A., & Al-Khalifa, H. S. (2016). Ultra-wideband indoor positioning technologies: Analysis and recent advances. *Sensors (Switzerland)*, *16*(5), 1–36. https://doi.org/10.3390/s16050707

Alemu, M. G., & Zimale, F. A. (2025). Integration of remote sensing and machine learning algorithm for agricultural drought early warning over Genale Dawa river basin, Ethiopia. *Environmental Monitoring and Assessment*, *197*(3), 243. https://doi.org/10.1007/s10661-025-13708-0

Allen, R. G., Pereira, L. S., Howell, T. A., & Jensen, M. E. (2011). Evapotranspiration information reporting: II. Recommended documentation. *Agricultural Water Management*, *98*(6), 921–929. https://doi.org/10.1016/j.agwat.2010.12.016

Amsalu, E. T., Akalu, T. Y., & Gelaye, K. A. (2019). Spatial distribution and determinants of acute respiratory infection among under-five children in Ethiopia: Ethiopian demographic Health Survey 2016. *PLoS ONE*, *14*(4), 1–14. https://doi.org/10.1371/journal.pone.0215572

Anderson, M. C., Norman, J. M., Diak, G. R., Kustas, W. P., & Mecikalski, J. R. (1997). A two-source time-integrated model for estimating surface fluxes using thermal infrared remote sensing. *Remote Sensing of Environment*, *60*(2), 195–216. https://doi.org/10.1016/S0034-4257(96)00215-5

Anderson, W., Taylor, C., McDermid, S., Ilboudo-Nébié, E., Seager, R., Schlenker, W., Cottier, F., de Sherbinin, A., Mendeloff, D., & Markey, K. (2021). Violent conflict exacerbated drought-related food insecurity between 2009 and 2019 in sub-Saharan Africa. *Nature Food*, *2*(8), 603–615. https://doi.org/10.1038/s43016-021-00327-4

Asaye, T. S., Amare, Z. Y., Geremew, B. B., & Abebe, M. G. (2025). Rainfall variability and trends in western Amhara: implication for sustainable water management and agricultural productivity. *Water Practice & Technology*, *20*(2), 449-467.

Avanzi, F., Munerol, F., Milelli, M., Gabellani, S., Massari, C., Girotto, M., Cremonese, E., Galvagno, M., Bruno, G., Morra, U., Rossi, L., Altamura, M., & Ferraris, L. (2024). *Winter snow deficit was a harbinger of summer 2022 socio-hydrologic drought in the Po Basin, Italy*. 1–12. https://doi.org/10.1038/s43247-024-01222-z

Bayissa, Y. A., Tadesse, T., Svoboda, M., Wardlow, B., Poulsen, C., Swigart, J., & Van Andel, S. J. (2019). Developing a satellite-based combined drought indicator to monitor agricultural drought: A case study for Ethiopia. *Geosciences & Remote Sensing*, *56*(5), 718-748.

Belal, A. A., El-Ramady, H. R., Mohamed, E. S., & Saleh, A. M. (2014). Drought risk assessment using remote sensing and GIS techniques. *Arabian Journal of Geosciences*, *7*(1), 35–53. https://doi.org/10.1007/s12517-012-0707-2

Beltman, M. R. (2019). *Defining drought: towards a functional definition of drought for the Vechtstromen water authority*.

Bewket, W., & Conway, D. (2007). A note on the temporal and spatial variability of rainfall in the drought-prone Amhara region of Ethiopia. *International Journal of Climatology*, *27*(11), 1467–1477. https://doi.org/10.1002/joc.1481

Bezabih, A. W. (2021). Evaluation of small hydropower plant at Ribb irrigation dam in Amhara regional state, Ethiopia. *Environmental Systems Research*, *10*(1). https://doi.org/10.1186/s40068-020-00196-z

Bogale, G. A., & Erena, Z. B. (2022). *Drought vulnerability and impacts of climate change on livestock production and productivity in different agro-Ecological zones of Ethiopia*. https://doi.org/10.1080/09712119.2022.2103563

Boken, V. K. (2009). Improving a drought early warning model for an arid region using a soil-moistureindex.*AppliedGeography*,*29*(3), 402408.https://doi.org/10.1016/j.apgeog.2008.12.06

Brocca, L., Hasenauer, S., Lacava, T., Melone, F., Moramarco, T., Wagner, W., Dorigo, W., Matgen, P., Martínez-Fernández, J., Llorens, P., Latron, J., Martin, C., & Bittelli, M. (2011). Soil moisture estimation through ASCAT and AMSR-E sensors: An intercomparison and validation study across Europe. *Remote Sensing of Environment*, *115*(12), 3390–3408. https://doi.org/10.1016/j.rse.2011.08.003

Cai, S., Zuo, D., Wang, H., Xu, Z., Wang, G., & Yang, H. (2023). Assessment of agricultural drought based on multi-source remote sensing data in a major grain producing area of Northwest China. *Agricultural Water Management*, *278*(October 2022), 108142. https://doi.org/10.1016/j.agwat.2023.108142

Carle, T., Potop-butucaru, D., Sorel, Y., Lesens, D., Carle, T., Potop-butucaru, D., Sorel, Y., Lesens, D., Dataflow, F., Carle, T., Potop-butucaru, D., & Sorel, Y. (2016). *From Dataflow Specification to Multiprocessor Partitioned Time-triggered Real-time Implementation * To* *cite this version: HAL Id: hal-01263994 From Dataflow Specification to Multiprocessor Partitioned Time-triggered Real-time*.

Castro, P., Marisa, A., Walter, A., & Filho, L. (n.d.). *Climate Change- Resilient Agriculture and Agroforestry Ecosystem Services and Sustainability*.

Cerveny, R. S., Bessemoulin, P., Burt, C. C., Cooper, M. A., Cunjie, Z., Dewan, A., Finch, J., Holle, R. L., Kalkstein, L., Kruger, A., Lee, T. C., Martínez, R., Mohapatra, M., Pattanaik, D. R., Peterson, T. C., Sheridan, S., Trewin, B., Tait, A., & Abdel Wahab, M. M. (2017). WMO assessment of weather and climate mortality extremes: Lightning, tropical cyclones, tornadoes,andhail.*Weather,Climate,andSociety*,*9*(3),487–497.https://doi.org/10.1175/WCAS-D-16-0120.1

Chere, Z., Abegaz, A., Tamene, L., & Abera, W. (2022). Modeling and mapping the spatiotemporal variation in agricultural drought based on a satellite-derived vegetation health index across the highlands of Ethiopia. *Modeling Earth Systems and Environment*, *8*(4), 4539–4552. https://doi.org/10.1007/s40808-022-01439-x

Chere, Z., & Debalke, D. B. (2024). Modeling agricultural drought based on the earth observation-derived standardized precipitation evapotranspiration index and vegetation health index in the northeastern highlands of Ethiopia. *Natural Hazards*, *120*(3), 3127-3151.

Coppin, P., Jonckheere, I., Nackaerts, K., Muys, B., & Lambin, E. (2004). Digital change detection methods in ecosystem monitoring: A review. *International Journal of Remote Sensing*, *25*(9), 1565–1596. https://doi.org/10.1080/0143116031000101675

Crocetti, L., Forkel, M., Fischer, M., Jurečka, F., Grlj, A., Salentinig, A., Trnka, M., Anderson, M., Ng, W. T., Kokalj, Ž., Bucur, A., & Dorigo, W. (2020). Earth Observation for agricultural drought monitoring in the Pannonian Basin (southeastern Europe): current state and future directions. *Regional Environmental Change*, *20*(4). https://doi.org/10.1007/s10113-020-01710-w

Dai, A. (2011). Drought under global warming: A review. *Wiley Interdisciplinary Reviews: Climate Change*, *2*(1), 45–65. https://doi.org/10.1002/wcc.81

Dalezios, N. R., Petropoulos, G. P., & Faraslis, I. N. (2020). Concepts and Methodologies of Environmental Hazards and Disasters. *Techniques for Disaster Risk Management and Mitigation*, *May 2021*, 1–22. https://doi.org/10.1002/9781119359203.ch1

Dash, P., Göttsche, F. M., Olesen, F. S., & Fischer, H. (2002). Land surface temperature and emissivity estimation from passive sensor data: Theory and practice-current trends. *InternationalJournalofRemoteSensing*,*23*(13),25632594.https://doi.org/10.1080/01431160110115041 de Paul Obade, V., Gaya, C. O., & Obade, P. T. (2023). Statistical diagnostics for sensing spatial residue cover. *Precision Agriculture*, *24*(5), 1932–1964. https://doi.org/10.1007/s11119-023-10024-w

Degefu, M. A., & Bewket, W. (2015). Trends and spatial patterns of drought incidence in the Omo-Ghibe River Basin, Ethiopia. *Geografiska Annaler, Series A: Physical Geography*, *97*(2), 395–414. https://doi.org/10.1111/geoa.12080

Demeku, M. A., Addisu, D. A., & Husen, M. A. (2015). The status of food availability in the face of climate change and variability in Choke Mountain Watersheds, Central Ethiopia. *Journal of Development and Agricultural Economics*, *7*(10), 358–372. https://doi.org/10.5897/jdae2015.0672

Demisse, G. B., & Suryabhagavan, K. V. (2016). *Evaluation of vegetation indices for agricultural drought monitoring in East Evaluation of Vegetation Indices for Agricultural Drought Monitoring*. *October*, 1–7.

Deressa, T. T., Ringler, C., & Hassan, R. M. (2010). Factors affecting the choices of coping strategies for climate extremes: The case of farmers in the Nile Basin of Ethiopia. *IFPRI Discussion Paper*, *1032*(November), 25.

Dietz, K. J., Zörb, C., & Geilfus, C. M. (2021). Drought and crop yield. *Plant Biology*, *23*(6), 881–893. https://doi.org/10.1111/plb.13304

Dikici, M., & Aksel, M. (2021). Evaluation of Two Vegetation Indices (NDVI and VCI) Over Asi Basin in Turkey. *Teknik Dergi/Technical Journal of Turkish Chamber of Civil Engineers*, *32*(4), 10995–11011. https://doi.org/10.18400/tekderg.590356

Dinku, T., Funk, C., Peterson, P., Maidment, R., Tadesse, T., Gadain, H., & Ceccato, P. (2018). Validation of the CHIRPS satellite rainfall estimates over eastern Africa. *Quarterly Journal of the Royal Meteorological Society*, *144*(November 2017), 292–312. https://doi.org/10.1002/qj.3244

Dutta, D., Kundu, A., Patel, N. R., Saha, S. K., & Siddiqui, A. R. (2015). Assessment of agricultural drought in Rajasthan (India) using remote sensing derived Vegetation Condition Index (VCI) and Standardized Precipitation Index (SPI). *Egyptian Journal of Remote Sensing and Space Science*, *18*(1), 53–63. https://doi.org/10.1016/j.ejrs.2015.03.006

En-Nagre, K., Aqnouy, M., Ouarka, A., Ali Asad Naqvi, S., Bouizrou, I., Eddine Stitou El Messari, J., Tariq, A., Soufan, W., Li, W., & El-Askary, H. (2024). Assessment and prediction of meteorological drought using machine learning algorithms and climate data. *Climate Risk Management*, *45*. https://doi.org/10.1016/j.crm.2024.100630

Enyew, F. B., Wassie, S. B., & Bekele, D. A. (2025). Monitoring agricultural drought using geospatial technologies: the case of Menna Watershed, northwestern Ethiopia. *Theoretical and Applied Climatology*, *156*(2), 81. https://doi.org/10.1007/s00704-024-05342-6

Evans, R. H. (1996). An analysis of criterion variable relimility in conjoint analysis. In *Perceptual and Motor Skills* (Vol. 82).

Feyisa, S. T. (2017). Climate Variability and Drought in the Past 30 Years in Central Rift Valley of Ethiopia. *Journal of Natural Sciences Research*, *7*(9), 18–26.

Ford, T. W., & Quiring, S. M. (2019). Comparison of Contemporary in Situ, Model, and Satellite Remote Sensing Soil Moisture with a Focus on Drought Monitoring. *Water Resources Research*, 1565–1582. https://doi.org/10.1029/2018WR024039

Gautam, D., & Pagay, V. (2020). A review of current and potential applications of remote sensing to study thewater status of horticultural crops. *Agronomy*, *10*(1). https://doi.org/10.3390/agronomy10010140

Gebre, E., Berhan, G., & Lelago, A. (2017). Application of Remote Sensing and GIS to Characterize Agricultural Drought Conditions in North Wollo Zone, Amhara Regional State, Ethiopia. *Journal of Natural Sciences Research Www.Iiste. Org ISSN*, *7*(17), 41–50.

Gebregziabher, S., Mouazen, A. M., Van Brussel, H., Ramon, H., Nyssen, J., Verplancke, H., Behailu, M., Deckers, J., & De Baerdemaeker, J. (2006). Animal drawn tillage, the Ethiopian ard plough, maresha: A review. *Soil and Tillage Research*, *89*(2), 129–143. https://doi.org/10.1016/j.still.2005.08.010

Gebrehiwot, T., van der Veen, A., & Maathuis, B. (2011). Spatial and temporal assessment of drought in the Northern highlands of Ethiopia. *International Journal of Applied Earth Observation and Geoinformation*, *13*(3), 309–321. https://doi.org/10.1016/j.jag.2010.12.002

Gebrehiwot, T., Van der Veen, A., & Maathuis, B. (2016). Governing agricultural drought: Monitoring using the vegetation condition index. *Ethiopian Journal of Environmental Studies and Management*, *9*(3), 354. https://doi.org/10.4314/ejesm.v9i3.9

Gebremeskel, G., Tang, Q., Sun, S., Huang, Z., Zhang, X., & Liu, X. (2019). Droughts in East Africa: Causes, impacts and resilience. *Earth-Science Reviews*, *193*, 146–161. https://doi.org/10.1016/j.earscirev.2019.04.015

Gelata, F. T., Jiqin, H., Gemeda, S. C., & Asefa, B. W. (2023). Application of GIS using NDVI and LST estimation to measure climate variability-induced drought risk assessment in Ethiopia. *JournalofWaterandClimate Change*, *14*(7), 2479–2489. https://doi.org/10.2166/wcc.2023.154

Gerland, P., Software, C., & Information, S. (1996). Socio-economic data and GIS: datasets, databases, indicators and data integration issues. *Development*, *1980*(28), 1–29.

Goyet, C. D. V. De, Leader, T., Hoogendoorn, A., Teklu, A. A., & Koriche, S. A. (2012). *"Evaluation of DG ECHO' s actions in Ethiopia." July*.

Haile, G. G., Tang, Q., Li, W., Liu, X., & Zhang, X. (2020). Drought: Progress in broadening its understanding. *Wiley Interdisciplinary Reviews: Water*, *7*(2), 1–25. https://doi.org/10.1002/WAT2.1407

He, C., Valayamkunnath, P., Barlage, M., Chen, F., Gochis, D., Cabell, R., Schneider, T., Rasmussen, R., Niu, G.-Y., Yang, Z.-L., Niyogi, D., & Ek, M. (2023). *Modernizing the open-source community Noah-MP land surface model (version 5.0) with enhanced modularity, interoperability, and applicability*. https://doi.org/10.5194/egusphere-2023-675

Hirko, A., Mergia, G., Nigussie, A., & Dandesa, T. (2021). Seasonal and Annual Meteorological Drought Frequency: Case Study East Hararge Province (Zone). *International Journal of Research in Environmental Science*, *7*(1), 11–19. https://doi.org/10.20431/2454-9444.0701002

Huijgevoort, M. Van, Lanen, H. Van, Teuling, R., Wanders, N., & Uijlenhoet, R. (2013). *Influence of climate change on drought occurrence in catchments across the globe*. *15*, 8955.

Huryna, H., & Pokorný, J. (2016). The role of water and vegetation in the distribution of solar energy and local climate: a review. *Folia Geobotanica*, *51*(3), 191–208. https://doi.org/10.1007/s12224-016-9261-0

Immerzeel, W. W., Lutz, A. F., Andrade, M., Bahl, A., Biemans, H., Bolch, T., Hyde, S., Brumby, S., Davies, B. J., Elmore, A. C., Emmer, A., Feng, M., Fernández, A., Haritashya, U., Kargel, J. S., Koppes, M., Kraaijenbrink, P. D. A., Kulkarni, A. V., Mayewski, P. A., … Baillie, J. E. M. (2020). Importance and vulnerability of the world's water towers. *Nature*, *577*(7790), 364–369. https://doi.org/10.1038/s41586-019-1822-y

Ji, L., & Peters, A. J. (2003). Assessing vegetation response to drought in the northern Great Plains using vegetation and drought indices. *Remote Sensing of Environment*, *87*(1), 85–98. https://doi.org/10.1016/S0034-4257(03)00174-3

Jiang, Z., Huete, A. R., Didan, K., & Miura, T. (2008). Development of a two-band enhanced vegetation index without a blue band. *Remote Sensing of Environment*, *112*(10), 3833–3845. https://doi.org/10.1016/j.rse.2008.06.006

Kane, S. N., Mishra, A., & Dutta, A. K. (2016). Preface: International Conference on Recent Trends in Physics (ICRTP 2016). *Journal of Physics: Conference Series*, *755*(1). https://doi.org/10.1088/1742-6596/755/1/011001

Karimi, M., Shahedi, K., Raziei, T., & Miryaghoubzadeh, M. (2022). Meteorological and agricultural drought monitoring in Southwest of Iran using a remote sensing-based combined drought index. *Stochastic Environmental Research and Risk Assessment*, *36*(11), 3707–3724. https://doi.org/10.1007/s00477-022-02220-3

Kassaye, A. Y., Shao, G., Wang, X., Shifaw, E., & Wu, S. (2021). Impact of climate change on the staple food crops yield in Ethiopia: implications for food security. *Theoretical and Applied Climatology*, *145*(1–2), 327–343. https://doi.org/10.1007/s00704-021-03635-8

Kassaye, A. Y., Shao, G., Wang, X., & Wu, S. (2021). Quantification of drought severity change in Ethiopia during 1952–2017. *Environment, Development and Sustainability*, *23*(4), 5096–5121. https://doi.org/10.1007/s10668-020-00805-y

Kebede, A., Raju, U. J. P., Korecha, D., & Nigussie, M. (2020). Developing new drought indices with and without climate signal information over the Upper Blue Nile. *Modeling Earth Systems and Environment*, *6*(1), 151–161. https://doi.org/10.1007/s40808-019-00667-y

Khampeera, A., Yongchalermchai, C., & Techato, K. (2018). Drought monitoring using drought indices and gis techniques in kuan kreng peat swamp, Southern Thailand. *Walailak Journal of Science and Technology*, *15*(5), 357–370. https://doi.org/10.48048/wjst.2018.2723

Kikstra, J. S., Nicholls, Z. R. J., Smith, C. J., Lewis, J., Lamboll, R. D., Byers, E., Sandstad, M., Meinshausen, M., Gidden, M. J., Rogelj, J., Kriegler, E., Peters, G. P., Fuglestvedt, J. S., Skeie, R. B., Samset, B. H., Wienpahl, L., Van Vuuren, D. P., Van Der Wijst, K. I., Al Khourdajie, A., … Riahi, K. (2022). The IPCC Sixth Assessment Report WGIII climate assessment of mitigation pathways: from emissions to global temperatures. *Geoscientific Model Development*, *15*(24), 9075–9109. https://doi.org/10.5194/gmd-15-9075-2022

Kogan, F., & Guo, W. (2016). Early twenty-first-century droughts during the warmest climate. *Geomatics, Natural Hazards and Risk*, *7*(1), 127–137. https://doi.org/10.1080/19475705.2013.878399

Kogan, F., Guo, W., & Yang, W. (2019). Drought and food security prediction from NOAA new generation of operational satellites. *Geomatics, Natural Hazards and Risk*, *10*(1), 651–666. https://doi.org/10.1080/19475705.2018.1541257

Kogan, F. N. (1997). Global Drought Watch from Space. *Bulletin of the American Meteorological Society*, *78*(4), 621–636. https://doi.org/10.1175/1520-0477(1997)078<0621: GDWFS>2.0.CO;2

Kogan, F. N. (2001). Operational space technology for global vegetation assessment. *Bulletin of the American Meteorological Society*, *82*(9), 1949–1964. https://doi.org/10.1175/1520-0477(2001)082<1949: OSTFGV>2.3.CO;2

Kulkarni, S. S., Wardlow, B. D., Bayissa, Y. A., Tadesse, T., Svoboda, M. D., & Gedam, S. S. (2020). Developing a remote sensing-based combined drought indicator approach for agricultural drought monitoring over Marathwada, India. *Remote Sensing*, *12*(13). https://doi.org/10.3390/rs12132091

Latocha, A., & Migon, P. (2006). Geomorphology of medium-high mountains Geomorphology of medium-high mountains under changing human impact, from managed slopes to nature restoration: a study from the Sudetes, SW Poland. *Earth Surf. Process. Landforms*, *31*, 1657–1673. https://doi.org/10.1002/esp

Lee, S., Kim, N., & Lee, Y. (2021). *Development of Integrated Crop Drought Index by Combining Rainfall, Land Surface Temperature, Evapotranspiration, Drought Monitoring*.

Li, F.-B., Guang-De, L. U., Xi-Yue, Z., Hui-Xiang, N. I., Xu, C.-C., Chao, Y., Xiu-Mei, Y., Feng, J.-F., & Fang, F.-P. (2015). *ScienceDirect Elevation and Land Use Types Have Significant Impacts on Spatial Variability of Soil Organic Matter Content in Hani Terraced Field of Yuanyang County, China*. https://doi.org/10.1016/S1672-6308(14)60282-1

Li, Q., Jiao, L., Xue, R., Chen, X., Zhang, P., Wang, X., & Yuan, X. (2023). *Season and depth differences of soil moisture use for tree growth across wet and dry gradients in the Tibetan Plateau*. https://doi.org/10.21203/rs.3.rs-3236892/v1

Li, X., Jia, H., & Wang, L. (2023). Remote Sensing Monitoring of Drought in Southwest China Using Random Forest and eXtreme Gradient Boosting Methods. *Remote Sensing*, *15*(19). https://doi.org/10.3390/rs15194840

Lilienthal, G., Ahmad, N., Awoke, S., & Elfakharani, A. M. A. (2023). Tulane Environmental Law Journal the Blue Nile and its Watercourse Through Ethiopia into Sudan and Egypt. *Law Journal*, *36*(1), 7–42. https://doi.org/10.2307/27250867

Liou, Y. A., & Mulualem, G. M. (2019). Spatio-temporal assessment of drought in Ethiopia and the impact of recent intense droughts. *Remote Sensing*, *11*(15), 1–19. https://doi.org/10.3390/rs11151828

Liu, X., Zhu, X., Pan, Y., Li, S., Liu, Y., & Ma, Y. (2016). Agricultural drought monitoring: Progress, challenges, and prospects. *Journal of Geographical Sciences*, *26*(6), 750–767. https://doi.org/10.1007/s11442-016-1297-9

Lu, J., Carbone, G. J., & Gao, P. (2017). *Detrending crop yield data for spatial visualization of drought impacts in the United States, 1895–2014*.

Lyon, B. (2014). Seasonal drought in the Greater Horn of Africa and its recent increase during the March-May long rains. *Journal of Climate*, *27*(21), 7953–7975. https://doi.org/10.1175/JCLI-D-13-00459.1

Malhi, Y., Franklin, J., Seddon, N., Solan, M., Turner, M. G., Field, C. B., & Knowlton, N. (2020). Climate change and ecosystems: Threats, opportunities and solutions. *Philosophical*

Transactions of the Royal Society B: Biological Sciences, *375*(1794). https://doi.org/10.1098/rstb.2019.0104

Marshall, M. T., Funk, C., & Michaelsen, J. (2012). Agricultural drought monitoring in kenya using evapotranspiration derived from remote sensing and reanalysis data. *Remote Sensing of Drought: Innovative Monitoring Approaches*, *June*, 169–193. https://doi.org/10.1201/b11863

Marthews, T. R., Otto, F. E. L., Mitchell, D., Dadson, S. J., & Jones, R. G. (2015). The 2014 drought in the horn of Africa: Attribution of meteorological drivers. *Bulletin of the American Meteorological Society*, *96*(12), S83–S88. https://doi.org/10.1175/BAMS-D-15-00115.1

Martínez-Fernández, J., González-Zamora, A., Sánchez, N., Gumuzzio, A., & Herrero-Jiménez, C. M. (2016). Satellite soil moisture for agricultural drought monitoring: Assessment of the SMOS derived Soil Water Deficit Index. *Remote Sensing of Environment*, *177*, 277–286. https://doi.org/10.1016/j.rse.2016.02.064

Maselli, F., Angeli, L., Battista, P., Fibbi, L., Gardin, L., Magno, R., Rapi, B., & Chiesi, M. (2020). Evaluation of Terra/Aqua MODIS and Sentinel-2 MSI NDVI data for predicting actual evapotranspiration in Mediterranean regions. *International Journal of Remote Sensing*, *41*(14), 5186–5205. https://doi.org/10.1080/01431161.2020.1731000

Masih, I., Maskey, S., Mussá, F. E. F., & Trambauer, P. (2014). A review of droughts on the African continent: A geospatial and long-term perspective. *Hydrology and Earth System Sciences*, *18*(9), 3635–3649. https://doi.org/10.5194/hess-18-3635-2014

Matsumura, E. M., Prakash, R., & Vera-Muñoz, S. C. (2014). Firm-value effects of carbon emissions and carbon disclosures. *Accounting Review*, *89*(2), 695–724. https://doi.org/10.2308/accr-50629

Mekonen, A. A., Berlie, A. B., & Ferede, M. B. (2020). Spatial and temporal drought incidence analysis in the northeastern highlands of Ethiopia. *Geoenvironmental Disasters*, *7*(1). https://doi.org/10.1186/s40677-020-0146-4

Mera, G. A. (2018). Drought and its impacts in Ethiopia. *Weather and Climate Extremes*, *22*(September), 24–35. https://doi.org/10.1016/j.wace.2018.10.002

Merga, B., & Ahmed, A. (2019). A Review on Agricultural Problems and Their Management in Ethiopia. *Turkish Journal of Agriculture - Food Science and Technology*, *7*(8), 1189–1202. https://doi.org/10.24925/turjaf.v7i8.1189-1202.2626

Meze-Hausken, E. (2000). Migration caused by climate change in northern Ethiopia. *Mitigation and Adaptation Strategies for Global Change*, *5*, 379–406.

Mohammed, U. D., Legesse, S. A., Berlie, A. B., & Ehsan, M. A. (2022). Climate Change Repercussions on Meteorological Drought Frequency and Intensity in South Wollo, Ethiopia. *Earth Systems and Environment*, *6*(3), 645–655. https://doi.org/10.1007/s41748-022-00293-2

Moussa Kourouma, J., Eze, E., Negash, E., Phiri, D., Vinya, R., Girma, A., & Zenebe, A. (2021). Assessing the spatio-temporal variability of NDVI and VCI as indices of crops productivity in Ethiopia: a remote sensing approach. *Geomatics, Natural Hazards and Risk*, *12*(1), 2880–2903. https://doi.org/10.1080/19475705.2021.1976849

Mukherjee, S., Mishra, A., & Trenberth, K. E. (2018). Climate Change and Drought: a Perspective on Drought Indices. *Current Climate Change Reports*, *4*(2), 145–163. https://doi.org/10.1007/s40641-018-0098-x

Mutsotso, R. B., Sichangi, A. W., & Makokha, G. O. (2018). Spatio-Temporal Drought Characterization in Kenya from 1987 to 2016. *Advances in Remote Sensing*, *07*(02), 125–143. https://doi.org/10.4236/ars.2018.72009

Narasimhan, B., & Srinivasan, R. (2005). Development and evaluation of Soil Moisture Deficit Index (SMDI) and Evapotranspiration Deficit Index (ETDI) for agricultural drought monitoring. *Agricultural and Forest Meteorology*, *133*(1–4), 69–88. https://doi.org/10.1016/j.agrformet.2005.07.012

Nema, P. (2012). *An overview of global climate changing in current scenario and mitigation action*. *May*. https://doi.org/10.1016/j.rser.2012.01.044

Nut, N., Mihara, M., Jeong, J., Ngo, B., Sigua, G., Prasad, P. V. V., & Reyes, M. R. (2021). Land use and land cover changes and its impact on soil erosion in stung sangkae catchment of cambodia. *Sustainability (Switzerland)*, *13*(16). https://doi.org/10.3390/su13169276

O'Connor, D., Boyle, P., Ilcan, S., & Oliver, M. (2017). Living with insecurity: Food security, resilience, and the world food programme (WFP). *Global Social Policy*, *17*(1), 3–20. https://doi.org/10.1177/1468018116658776

Parviz, L. (2016). Determination of Effective Indices in the Drought Monitoring Through Analysis of Satellite Images. *The Journal "Agriculture and Forestry," 62*(1), 305–324. https://doi.org/10.17707/agricultforest.62.1.34

Patel, N. R., Chopra, P., & Dadhwal, V. K. (2007). Analyzing spatial patterns of meteorological drought using standardized precipitation index. *Meteorological Applications*, *14*(4), 329–336. https://doi.org/10.1002/met.33

Pei, F., Wu, C., Liu, X., Li, X., Yang, K., Zhou, Y., Wang, K., Xu, L., & Xia, G. (2018). Monitoring the vegetation activity in China using vegetation health indices. *Agricultural and Forest Meteorology*, *248*(101), 215–227. https://doi.org/10.1016/j.agrformet.2017.10.001

Peng, J., Dadson, S., Hirpa, F., Dyer, E., Lees, T., Miralles, D. G., & Funk, C. (2019). *A pan - African high - resolution drought index dataset*. *2016*(October).

Rahman, M. T. (2016). Land use and Land cover changes and urban sprawl in Riyadh, Saudi Arabia: An analysis using multi-temporal Landsat data and Shannon's Entropy index.

International Archives of the Photogrammetry, Remote Sensing and Spatial Information Sciences - ISPRS Archives, *41*(July), 1017–1021. https://doi.org/10.5194/isprsarchives-XLI-B8-1017-2016

Rahmati, O., Falah, F., Dayal, K. S., Deo, R. C., Mohammadi, F., Biggs, T., Moghaddam, D. D., Naghibi, S. A., & Bui, D. T. (2020). Machine learning approaches for spatial modeling of agricultural droughts in the south-east region of Queensland Australia. *Science of the Total Environment*, *699*. https://doi.org/10.1016/j.scitotenv.2019.134230

Raleigh, C., & Urdal, H. (2007). Climate change, environmental degradation and armed conflict. *Political Geography*, *26*(6), 674–694. https://doi.org/10.1016/j.polgeo.2007.06.005

Randriamampianina, R., Schyberg, H., & Mile, M. (2019). Observing system experiments with an Arctic mesoscale numericalweather prediction model. *Remote Sensing*, *11*(8). https://doi.org/10.3390/rs11080902

Reiners, P., Sobrino, J., & Kuenzer, C. (2023). Satellite-Derived Land Surface Temperature Dynamics in the Context of Global Change—A Review. In *Remote Sensing* (Vol. 15, Issue 7). MDPI. https://doi.org/10.3390/rs15071857

Rockström, J. (2003). Resilience building and water demand management for drought mitigation. *Physics and Chemistry of the Earth*, *28*(20–27), 869–877. https://doi.org/10.1016/j.pce.2003.08.009

Rosegrant, M. W., Ringler, C., & Zhu, T. (2009). Water for agriculture: Maintaining food security under growing scarcity. *Annual Review of Environment and Resources*, *34*, 205–222. https://doi.org/10.1146/annurev.environ.030308.090351

Rosenzweig, C., Elliott, J., Deryng, D., Ruane, A. C., Müller, C., Arneth, A., Boote, K. J., Folberth, C., Glotter, M., Khabarov, N., Neumann, K., Piontek, F., Pugh, T. A. M., Schmid, E., Stehfest, E., Yang, H., & Jones, J. W. (2014). Assessing agricultural risks of climate change in the 21st century in a global gridded crop model intercomparison. *Proceedings of the National Academy of Sciences of the United States of America*, *111*(9), 3268–3273. https://doi.org/10.1073/pnas.1222463110

Running, S.W., Mu, Q., Zhao, M., & Moreno, A. (2019). *MODIS Global Terrestrial Evapotranspiration (ET) Product (NASA MOD16A2/A3) Algorithm Theoretical Basis Document Collection 6*. *March*, 1–40.

Sanjerehei, M. M. (2017). *Spectral vegetation indices for estimating vegetation cover*. *October*.

Schreiner, B. G., Mungatana, E. D., & Baleta, H. (2018). *Impacts of Drought Induced Water Shortages in South Africa: Economic Analysis Report to the Water Research Commission* (Issue 2604).

Schuldt, B., Buras, A., Arend, M., Vitasse, Y., Beierkuhnlein, C., Damm, A., Gharun, M., Grams, T. E. E., Hauck, M., Hajek, P., Hartmann, H., Hiltbrunner, E., Hoch, G., Holloway-Phillips, M., Körner, C., Larysch, E., Lübbe, T., Nelson, D. B., Rammig, A., … Kahmen, A. (2020). A first assessment of the impact of the extreme 2018 summer drought on Central European forests. *Basic and Applied Ecology*, *45*, 86–103. https://doi.org/10.1016/j.baae.2020.04.003

Seasonal and Annual Meteorological Drought Frequency: Case Study East Hararge Province (Zone). (2021). *International Journal of Research in Environmental Science*, *7*(1). https://doi.org/10.20431/2454-9444.0701002

Senamaw, A., Addisu, S., & Suryabhagavan, K. V. (2021). Mapping the spatial and temporal variation of agricultural and meteorological drought using geospatial techniques, Ethiopia. *Environmental Systems Research*, *10*(1). https://doi.org/10.1186/s40068-020-00204-2

Senay, G. B. (2018). Satellite psychrometric formulation of the operational simplified surface energy balance (ssebop) model for. *Applied Engineering in Agriculture*, *34*(3), 555–566. https://doi.org/10.13031/aea.12614

Senay, G. B., Velpuri, N. M., Bohms, S., Budde, M., Young, C., Rowland, J., & Verdin, J. P. (2014). Drought Monitoring and Assessment: Remote Sensing and Modeling Approaches for the Famine Early Warning Systems Network. Remote Sensing and Modeling Approaches for the Famine Early Warning Systems Network. In *Hydro-Meteorological Hazards, Risks, and Disasters*. https://doi.org/10.1016/B978-0-12-394846-5.00009-6

Kebede, A. S. (2019). *Remote Sensing and GIS-based Agricultural Drought Assessment: The Case of Waghimra Zone, Amhara Regional State, Ethiopia*.

Shahzaman, M., Zhu, W., Ullah, I., Mustafa, F., Bilal, M., Ishfaq, S., Nisar, S., Arshad, M., Iqbal, R., & Aslam, R. W. (2021). Comparison of multi-year reanalysis, models, and satellite remote sensing products for agricultural drought monitoring over south asian countries. *Remote Sensing*, *13*(16). https://doi.org/10.3390/rs13163294

Shalishe, A., Bhowmick, A., & Elias, K. (2022). Meteorological Drought Monitoring Based on Satellite CHIRPS Product over Gamo Zone, Southern Ethiopia. *Advances in Meteorology*, *2022*. https://doi.org/10.1155/2022/9323263

Shao, M., Wang, Y., Xia, Y., & Jia, X. (2018). Soil Drought and Water Carrying Capacity for Vegetation in the Critical Zone of the Loess Plateau: A Review. *Vadose Zone Journal*, *17*(1), 1–8. https://doi.org/10.2136/vzj2017.04.0077

Shawul, A. A., & Chakma, S. (2020). Trend of extreme precipitation indices and analysis of long-term climate variability in the Upper Awash basin, Ethiopia. *Theoretical and Applied Climatology*, *140*(1–2), 635–652. https://doi.org/10.1007/s00704-020-03112-8

Shumuye, M. Y. (2015). The Role of Developmental State in Development: The Case of Ethiopia. *International Journal of African and Asian Studies*, *14*, 96–110.

Sikhwari, T. (2019). *Variability and long-term trends of climate extremes over the Limpopo, South Africa*.

Siname, B., Beyene, H., Deressa, W., Kumie, A., Berhane, K., & Samet, J. (2016). CLIMATE CHANGE RISK PROFILE: Ethiopia. *Fact Sheet*, *30*, 1–23.

Singh, S. (2018). Understanding the role of slope aspect in shaping the vegetation attributes and soil properties in Montane ecosystems. *Tropical Ecology*, *59*(3), 417–430. www.tropecol.com

Sivakumar, M. (2010). Agricultural Drought indices Proceedings of an expert meeting. *Agricultural Drought Indices Proceedings of an Expert Meeting*, *June*, 205.

Slette, I. J., Post, A. K., Awad, M., Even, T., Punzalan, A., Williams, S., Smith, M. D., & Knapp, A. K. (2019). How ecologists define drought, and why we should do better. *Global Change Biology*, *25*(10), 3193–3200. https://doi.org/10.1111/gcb.14747

Sohnesen, T. P. (2020). Two Sides to Same Drought: Measurement and Impact of Ethiopia's 2015 Historical Drought. *Economics of Disasters and Climate Change*, *4*(1), 83–101. https://doi.org/10.1007/s41885-019-00048-w

Stamford, J. D., Vialet-Chabrand, S., Cameron, I., & Lawson, T. (2023). Development of an accurate low cost NDVI imaging system for assessing plant health. *Plant Methods*, *19*(1). https://doi.org/10.1186/s13007-023-00981-8

Tadesse, T. (2018). Strategic Framework for Drought Risk Management and Enhancing Resilience in Africa. *Nebraska, University of Nebraska-Lincoln*, 15–19.

Tadesse, T., Senay, G. B., Berhan, G., Regassa, T., & Beyene, S. (2015). Evaluating a satellite-based seasonal evapotranspiration product and identifying its relationship with other satellite-derived products and crop yield: A case study for Ethiopia. *International Journal of Applied Earth Observation and Geoinformation*, *40*, 39–54. https://doi.org/10.1016/j.jag.2015.03.006

Tallaksen, L. M., & van Lanen, H. A. J. (2023). Hydrological Drought: Processes and Estimation Methods for Streamflow and Groundwater, Second Edition. *Hydrological Drought: Processes and Estimation Methods for Streamflow and Groundwater, Second Edition*, 1–684. https://doi.org/10.1016/C2017-0-03464-X

Tela, Y. T., Wassie, S. B., & Ferede, M. B. (2024). Assessment of meteorological and socioeconomic drought conditions in the Tekeze watershed, northern Ethiopia. *Frontiers in Environmental Science*, *12*. https://doi.org/10.3389/fenvs.2024.1506883

Temam, D., Uddameri, V., Mohammadi, G., Hernandez, E. A., & Ekwaro-Osire, S. (2019). Long-term drought trends in Ethiopia with implications for dryland agriculture. *Water (Switzerland)*, *11*(12), 1–22. https://doi.org/10.3390/w11122571

Thenkabail, P. S., Smith, R. B., & De Pauw, E. (2002). Evaluation of narrowband and broadband vegetation indices for determining optimal hyperspectral wavebands for agricultural crop characterization. *Photogrammetric Engineering and Remote Sensing*, *68*(6), 607–621.

Tierney, J. E., Smerdon, J. E., Anchukaitis, K. J., & Seager, R. (2013). Multidecadal variability in East African hydroclimate controlled by the Indian Ocean. *Nature*, *493*(7432), 389–392. https://doi.org/10.1038/nature11785

Tijdeman, E., Blauhut, V., Stoelzle, M., Menzel, L., & Stahl, K. (2022). Different drought types and the spatial variability in their hazard, impact, and propagation characteristics. *Natural Hazards and Earth System Sciences*, *22*(6), 2099–2116. https://doi.org/10.5194/nhess-22-2099-2022

Tran, H. T., Campbell, J. B., Tran, T. D., & Tran, H. T. (2017). Monitoring drought vulnerability using multispectral indices observed from sequential remote sensing (Case Study: Tuy Phong, Binh Thuan, Vietnam). *GIScience and Remote Sensing*, *54*(2), 167–184. https://doi.org/10.1080/15481603.2017.1287838

Trenberth, K. E., Dai, A., Van Der Schrier, G., Jones, P. D., Barichivich, J., Briffa, K. R., & Sheffield, J. (2014). Global warming and changes in drought. *Nature Climate Change*, *4*(1), 17–22. https://doi.org/10.1038/nclimate2067

Tsatsaris, A., Kalogeropoulos, K., Stathopoulos, N., Louka, P., Tsanakas, K., Tsesmelis, D. E., Krassanakis, V., Petropoulos, G. P., Pappas, V., & Chalkias, C. (2021). Geoinformation technologies in support of environmental hazards monitoring under climate change: An extensive review. *ISPRS International Journal of Geo-Information*, *10*(2). https://doi.org/10.3390/ijgi10020094

Tsige, M. (2019). Who Benefits from Production Outcomes? Gendered Production Relations among Climate-Smart Agriculture Technology Users in Rural Ethiopia. *Rural Sociology*, *84*(4), 799–825. https://doi.org/10.1111/ruso.12263

Uddameri, V., Singaraju, S., & Hernandez, E. A. (2019). Is Standardized Precipitation Index (SPI) a Useful Indicator to Forecast Groundwater Droughts? — Insights from a Karst Aquifer. *Journal of the American Water Resources Association*, *55*(1), 70–88. https://doi.org/10.1111/1752-1688.12698

Usman, M., Liedl, R., Shahid, M. A., & Abbas, A. (2015). Land use/land cover classification and its change detection using multi-temporal MODIS NDVI data. *Journal of Geographical Sciences*, *25*(12), 1479–1506. https://doi.org/10.1007/s11442-015-1247-y van Aalst, M. K., Cannon, T., & Burton, I. (2008). Community level adaptation to climate change: The potential role of participatory community risk assessment. *Global Environmental Change*, *18*(1), 165–179. https://doi.org/10.1016/j.gloenvcha.2007.06.002

van Ginkel, M., & Biradar, C. (2021). Drought early warning in agri-food systems. *Climate*, *9*(9). https://doi.org/10.3390/cli9090134

Van Loon, A. F. (2015). Hydrological drought explained. *Wiley Interdisciplinary Reviews: Water*, *2*(4), 359–392. https://doi.org/10.1002/WAT2.1085

Velpuri, N. M., Senay, G. B., Singh, R. K., Bohms, S., & Verdin, J. P. (2013). A comprehensive evaluation of two MODIS evapotranspiration products over the conterminous United States: Using point and gridded FLUXNET and water balance ET. *Remote Sensing of Environment*, *139*, 35–49. https://doi.org/10.1016/j.rse.2013.07.013

Viste, E., Korecha, D., & Sorteberg, A. (2013). Recent drought and precipitation tendencies in Ethiopia. *Theoretical and Applied Climatology*, *112*(3–4), 535–551. https://doi.org/10.1007/s00704-012-0746-3

Wang, Q., Zhao, L., Wang, M., Wu, J., Zhou, W., Zhang, Q., & Deng, M. (2022). A Random Forest Model for Drought: Monitoring and Validation for Grassland Drought Based on Multi-Source Remote Sensing Data. *Remote Sensing*, *14*(19). https://doi.org/10.3390/rs14194981

Wardlow, B. D., Egbert, S. L., & Kastens, J. H. (2007). Analysis of time-series MODIS 250 m vegetation index data for crop classification in the U.S. Central Great Plains. *Remote Sensing of Environment*, *108*(3), 290–310. https://doi.org/10.1016/j.rse.2006.11.021

Wassie, S. B., Mengistu, D. A., & Berlie, A. B. (2022). Trends and spatiotemporal patterns of meteorological drought incidence in North Wollo, northeastern highlands of Ethiopia. *Arabian Journal of Geosciences*, *15*(12). https://doi.org/10.1007/s12517-022-10423-9

Wassie, S. B., Mengistu, D. A., & Birlie, A. B. (2022). Agricultural drought assessment and monitoring using MODIS-based multiple indices: the case of North Wollo, Ethiopia. *Environmental Monitoring and Assessment*, *194*(10). https://doi.org/10.1007/s10661-022-10455-4

Wei, W., Zhang, J., Zhou, L., Xie, B., Zhou, J., & Li, C. (2021). Comparative evaluation of drought indices for monitoring drought based on remote sensing data. *Environmental Science and Pollution Research*, *28*(16), 20408–20425. https://doi.org/10.1007/s11356-020-12120-0

Weldlul, A. (2016). Analysis of smallholder farmers' perceptions of climate change and adaptation strategies to climate change: the case of Western Amhara Region, Ethiopia. *Ethiopia Doctoral Thesis University of South Africa*, *May*.

Wen, J., Wan, C., Ye, Q., Yan, J., & Li, W. (2023). Disaster Risk Reduction, Climate Change Adaptation and Their Linkages with Sustainable Development over the Past 30 Years: A

Review. *International Journal of Disaster Risk Science*, *14*(1), 1–13. https://doi.org/10.1007/s13753-023-00472-3

Wilhite, D. A. (1993). Chapter 1 Drought. *Drought Assessment, Management, and Planning: Theory and Case Studies*, 3–15.

Wilhite, D. A., & Glantz, M. H. (1985). Glantz,1987. *Understanding the Drought Phenomenon: The Role of Definitions*.

Wilhite, D., & Vanyarkho, O. (2000). Chapter 18 Drought: Pervasive Impacts of a Creeping Phenomenon. *Drought Mitigation Center Faculty Publications*, 71.

Winker, D. M., Vaughan, M. A., Omar, A., Hu, Y., Powell, K. A., Liu, Z., Hunt, W. H., & Young, S. A. (2009). Overview of the CALIPSO mission and CALIOP data processing algorithms. *Journal of Atmospheric and Oceanic Technology*, *26*(11), 2310–2323. https://doi.org/10.1175/2009JTECHA1281.1

Wolka, K., Uma, T., & Tofu, D. A. (2023). The role of integrated watershed management in climate change adaptation for small-scale farmers in Southwest Ethiopia. *Environmental and Sustainability Indicators*, *19*(May), 100260. https://doi.org/10.1016/j.indic.2023.100260

Xu, T., Guo, Z., Xia, Y., Ferreira, V. G., Liu, S., Wang, K., Yao, Y., Zhang, X., & Zhao, C. (2019). *Evaluation of Twelve Evapotranspiration Products from Machine Learning, Remote Sensing and Land Surface Models over Conterminous United States*.

Yozgatligil, C., Aslan, S., Iyigun, C., & Batmaz, I. (2013). Comparison of missing value imputation methods in time series: The case of Turkish meteorological data. *Theoretical and Applied Climatology*, *112*(1–2), 143–167. https://doi.org/10.1007/s00704-012-0723-x

Zargar, A., Sadiq, R., Naser, B., & Khan, F. I. (2011). A review of drought indices. *Environmental Reviews*, *19*(1), 333–349. https://doi.org/10.1139/a11-013

Zegeye, H. (2018). Climate change in Ethiopia: impacts, mitigation and adaptation. *International Journal of Research in Environmental Studies*, *5*(1), 18-35.

Zeleke, T. T., Giorgi, F., Diro, G. T., & Zaitchik, B. F. (2017). Trend and periodicity of drought over Ethiopia. *International Journal of Climatology*, *37*(13), 4733–4748. https://doi.org/10.1002/joc.5122

Zhang, L., Yu, X., Zhou, T., Zhang, W., Hu, S., & Clark, R. (2023). Understanding and Attribution of Extreme Heat and Drought Events in 2022: Current Situation and Future Challenges. *Advances in Atmospheric Sciences*, *40*(11), 1941–1951. https://doi.org/10.1007/s00376-023-3171-x

Zhao, Q., Li, D., Zhuo, M., Guo, T., Liao, Y., & Xie, Z. (2015). Effects of rainfall intensity and slope gradient on erosion characteristics of the red soil slope. *Stochastic Environmental Research and Risk Assessment*, *29*(2), 609–621. https://doi.org/10.1007/s00477-014-0896-1

APPENDICES

APPENDIX 1: Samples to download some Input Variables to develop CADI

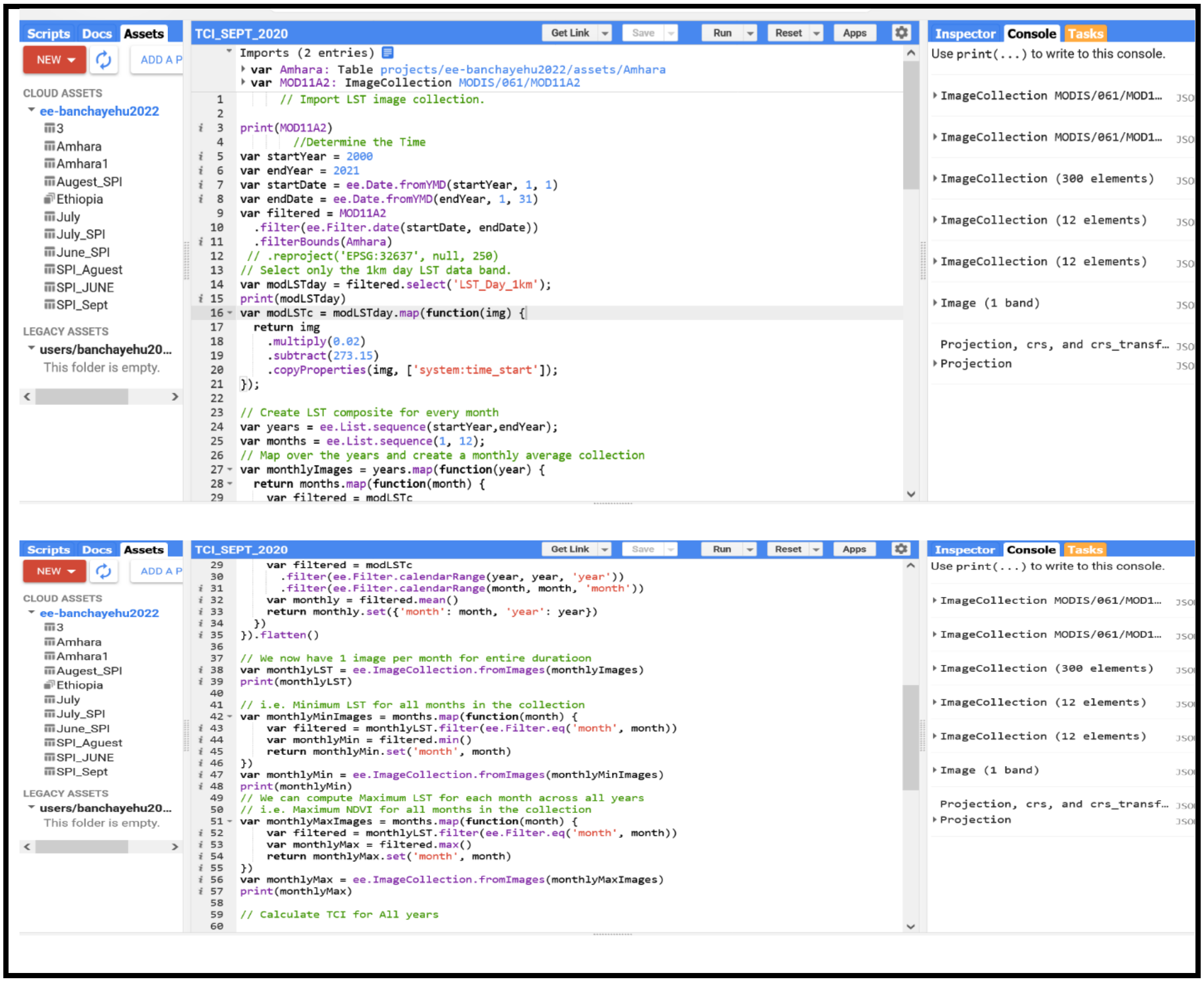

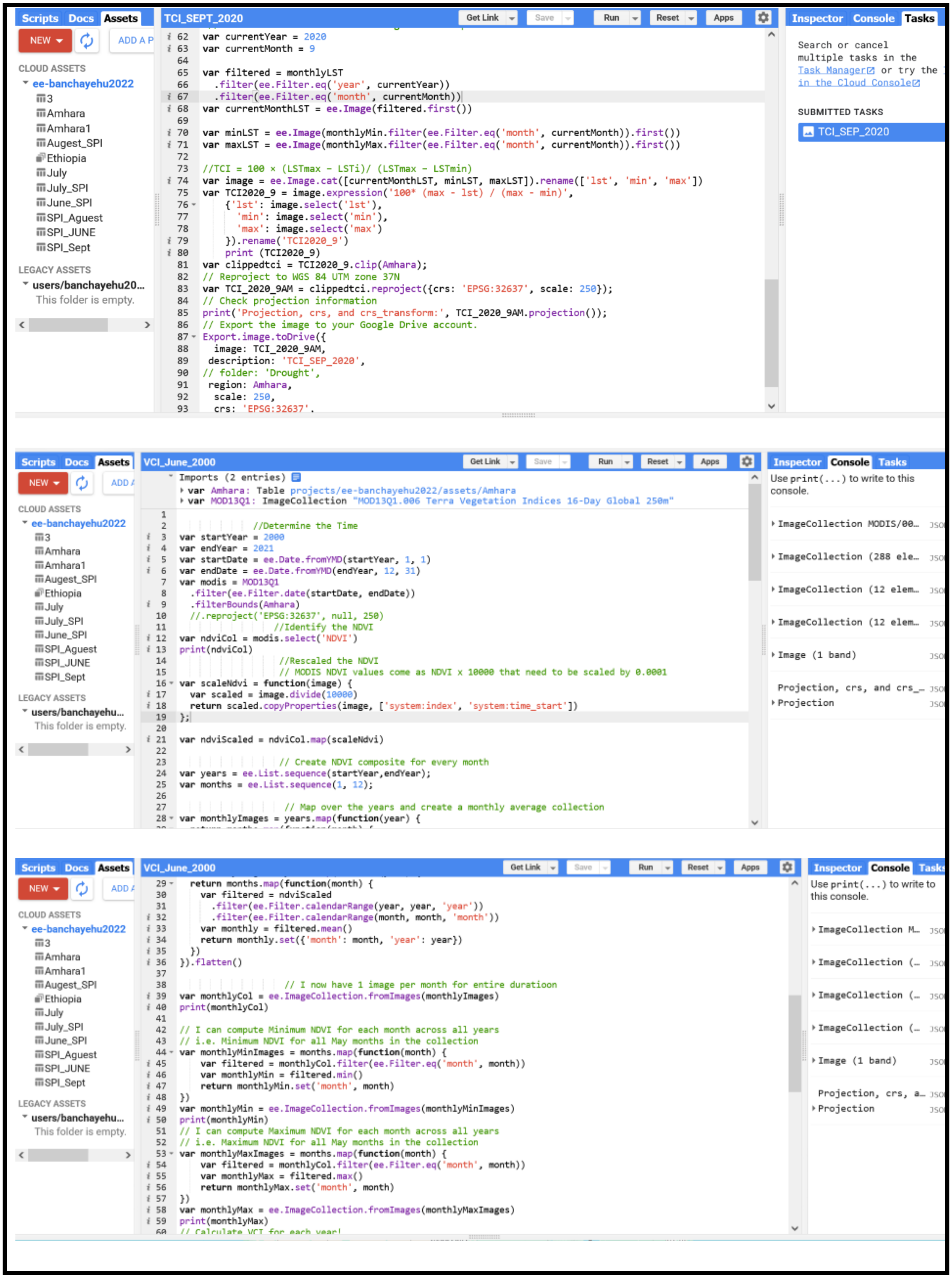
Scripts Docs Assets
NEW
CLOUD ASSETS
ee-banchayehu2022
3
Amhara
Amhara1
Augest_SPI
Ethiopia
July
July_SPI
June_SPI
SPI_Aguest
SPI_JUNE
SPI_Sept
LEGACY ASSETS
users/banchayehu20...
This folder is empty.
TCI_SEPT_2020
Get Link
Save
Run
Reset
Apps
var currentYear = 2020
var currentMonth = 9
var filtered = monthlyLST
.filter(ee.Filter.eq('year', currentYear))
.filter(ee.Filter.eq('month', currentMonth))
var currentMonthLST = ee.Image(filtered.first())
var minLST = ee.Image(monthlyMin.filter(ee.Filter.eq('month', currentMonth)).first())
var maxLST = ee.Image(monthlyMax.filter(ee.Filter.eq('month', currentMonth)).first())
//TCI = 100 x (LSTmax - LSTi)/ (LSTmax - LSTmin)
var image = ee.Image.cat([currentMonthLST, minLST, maxLST]).rename(['lst', 'min', 'max'])
var TCI2020_9 = image.expression('100* (max - lst) / (max - min)',
{'lst': image.select('lst'),
'min': image.select('min'),
'max': image.select('max')
}).rename('TCI2020_9')
print (TCI2020_9)
var clippedtci = TCI2020_9.clip(Amhara);
// Reproject to WGS 84 UTM zone 37N
var TCI_2020_9AM = clippedtci.reproject({crs: 'EPSG:32637', scale: 250});
// Check projection information
print('Projection, crs, and crs_transform:', TCI_2020_9AM.projection());
// Export the image to your Google Drive account.
Export.image.toDrive({
image: TCI_2020_9AM,
description: 'TCI_SEP_2020',
// folder: 'Drought',
region: Amhara,
scale: 250,
crs: 'EPSG:32637',
Inspector Console Tasks
Search or cancel multiple tasks in the Task Manager or try the in the Cloud Console
SUBMITTED TASKS
TCI_SEP_2020
VCI_June_2000
Imports (2 entries)
var Amhara: Table projects/ee-banchayehu2022/assets/Amhara
var MOD13Q1: ImageCollection "MOD13Q1.006 Terra Vegetation Indices 16-Day Global 250m"
//Determine the Time
var startYear = 2000
var endYear = 2021
var startDate = ee.Date.fromYMD(startYear, 1, 1)
var endDate = ee.Date.fromYMD(endYear, 12, 31)
var modis = MOD13Q1
.filter(ee.Filter.date(startDate, endDate))
.filterBounds(Amhara)
//.reproject('EPSG:32637', null, 250)
//Identify the NDVI
var ndviCol = modis.select('NDVI')
print(ndviCol)
//Rescaled the NDVI
// MODIS NDVI values come as NDVI x 10000 that need to be scaled by 0.0001
var scaleNdvi = function(image) {
var scaled = image.divide(10000)
return scaled.copyProperties(image, ['system:index', 'system:time_start'])
};
var ndviScaled = ndviCol.map(scaleNdvi)
// Create NDVI composite for every month
var years = ee.List.sequence(startYear,endYear);
var months = ee.List.sequence(1, 12);
// Map over the years and create a monthly average collection
var monthlyImages = years.map(function(year) {
Use print(...) to write to this console.
ImageCollection MODIS/00...
ImageCollection (288 ele...
ImageCollection (12 elem...
ImageCollection (12 elem...
Image (1 band)
Projection, crs, and crs_...
Projection
return months.map(function(month) {
var filtered = ndviScaled
.filter(ee.Filter.calendarRange(year, year, 'year'))
.filter(ee.Filter.calendarRange(month, month, 'month'))
var monthly = filtered.mean()
return monthly.set({'month': month, 'year': year})
})
}).flatten()
// I now have 1 image per month for entire durationn
var monthlyCol = ee.ImageCollection.fromImages(monthlyImages)
print(monthlyCol)
// I can compute Minimum NDVI for each month across all years
// i.e. Minimum NDVI for all May months in the collection
var monthlyMinImages = months.map(function(month) {
var filtered = monthlyCol.filter(ee.Filter.eq('month', month))
var monthlyMin = filtered.min()
return monthlyMin.set('month', month)
})
var monthlyMin = ee.ImageCollection.fromImages(monthlyMinImages)
print(monthlyMin)
// I can compute Maximum NDVI for each month across all years
// i.e. Maximum NDVI for all May months in the collection
var monthlyMaxImages = months.map(function(month) {
var filtered = monthlyCol.filter(ee.Filter.eq('month', month))
var monthlyMax = filtered.max()
return monthlyMax.set('month', month)
})
var monthlyMax = ee.ImageCollection.fromImages(monthlyMaxImages)
print(monthlyMax)
// Calculate VCI for each year!


Scripts Docs Assets
VCI_June_2000
Get Link Save Run Reset Apps
Inspector Console Tasks
NEW
CLOUD ASSETS
ee-banchayehu2022
3
Amhara
Amhara1
Augest_SPI
Ethiopia
July
July_SPI
June_SPI
SPI_Aguest
SPI_JUNE
SPI_Sept
LEGACY ASSETS
users/banchayehu...
This folder is empty.
// I are interested in calculating VCI for a particular month
var currentYear = 2000
var currentMonth = 6
var filtered = monthlyCol
.filter(ee.Filter.eq('year', currentYear))
.filter(ee.Filter.eq('month', currentMonth))
var currentMonthNdvi = ee.Image(filtered.first())
var minNdvi = ee.Image(monthlyMin.filter(ee.Filter.eq('month', currentMonth)).first())
var maxNdvi = ee.Image(monthlyMax.filter(ee.Filter.eq('month', currentMonth)).first())
// VCI = (NDVI - min) / (max - min)
var image = ee.Image.cat([currentMonthNdvi, minNdvi, maxNdvi]).rename(['ndvi', 'min', 'max'])
var vci2000_6 = image.expression('100 * (ndvi - min) / (max - min)',
{'ndvi': image.select('ndvi'),
'min': image.select('min'),
'max': image.select('max')
}).rename('vci2000_6')
print(vci2000_6)
var clippedvci = vci2000_6.clip(Amhara);
// Reproject to WGS 84 UTM zone 37N
var VCI_2000_6AM = clippedvci.reproject({crs: 'EPSG:32637', scale: 250});
// Check projection information
print('Projection, crs, and crs_transform:', VCI_2000_6AM.projection());
// Export the image to your Google Drive account.
Export.image.toDrive({
image: VCI_2000_6AM,
description: 'VCI_2000_June',
// folder: 'Drought',
region: Amhara,
Use print(...) to write to this console.
ImageCollection M...
ImageCollection (...
ImageCollection (...
ImageCollection (...
Image (1 band)
Projection, crs, a...
Projection

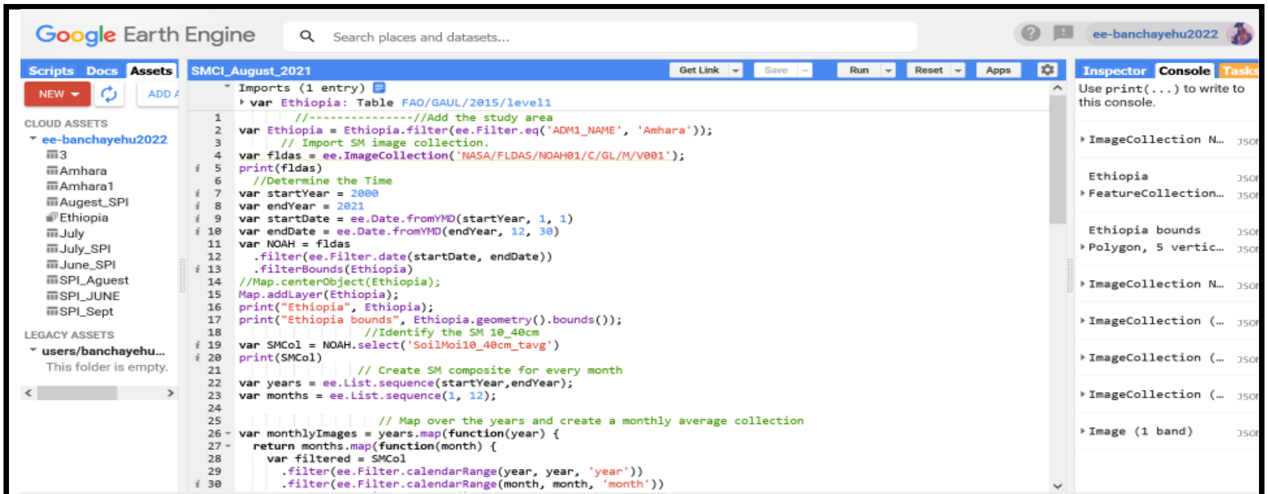
Google Earth Engine
Search places and datasets...
ee-banchayehu2022
Scripts Docs Assets
SMCI_August_2021
Get Link Save Run Reset Apps
Inspector Console Tasks
Imports (1 entry)
var Ethiopia: Table FAO/GAUL/2015/level1
//---------------//Add the study area
var Ethiopia = Ethiopia.filter(ee.Filter.eq('ADM1_NAME', 'Amhara'));
// Import SM image collection.
var fldas = ee.ImageCollection('NASA/FLDAS/NOAH01/C/GL/M/V001');
print(fldas)
//Determine the Time
var startYear = 2000
var endYear = 2021
var startDate = ee.Date.fromYMD(startYear, 1, 1)
var endDate = ee.Date.fromYMD(endYear, 12, 30)
var NOAH = fldas
.filter(ee.Filter.date(startDate, endDate))
.filterBounds(Ethiopia)
//Map.centerObject(Ethiopia);
Map.addLayer(Ethiopia);
print("Ethiopia", Ethiopia);
print("Ethiopia bounds", Ethiopia.geometry().bounds());
//Identify the SM 10_40cm
var SMCol = NOAH.select('SoilMoi10_40cm_tavg')
print(SMCol)
// Create SM composite for every month
var years = ee.List.sequence(startYear,endYear);
var months = ee.List.sequence(1, 12);
// Map over the years and create a monthly average collection
var monthlyImages = years.map(function(year) {
return months.map(function(month) {
var filtered = SMCol
.filter(ee.Filter.calendarRange(year, year, 'year'))
.filter(ee.Filter.calendarRange(month, month, 'month'))
Use print(...) to write to this console.
ImageCollection N...
Ethiopia
FeatureCollection...
Ethiopia bounds
Polygon, 5 vertic...
ImageCollection N...
ImageCollection (...
ImageCollection (...
ImageCollection (...
Image (1 band)

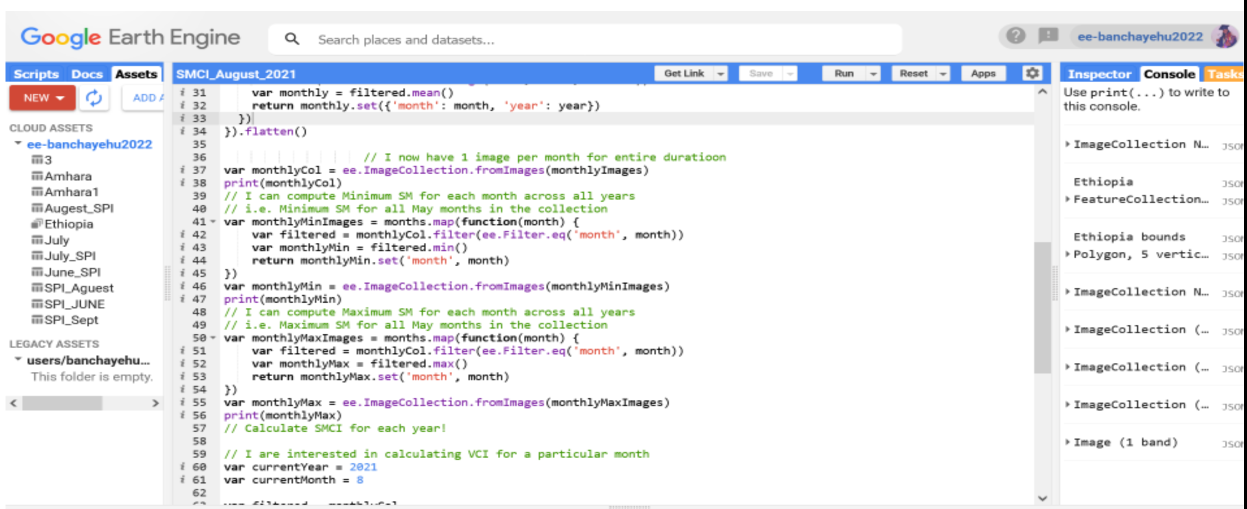
Google Earth Engine
Search places and datasets...
ee-banchayehu2022
Scripts Docs Assets
SMCI_August_2021
Get Link Save Run Reset Apps
Inspector Console Tasks
var monthly = filtered.mean()
return monthly.set({'month': month, 'year': year})
})
}).flatten()
// I now have 1 image per month for entire duratioon
var monthlyCol = ee.ImageCollection.fromImages(monthlyImages)
print(monthlyCol)
// I can compute Minimum SM for each month across all years
// i.e. Minimum SM for all May months in the collection
var monthlyMinImages = months.map(function(month) {
var filtered = monthlyCol.filter(ee.Filter.eq('month', month))
var monthlyMin = filtered.min()
return monthlyMin.set('month', month)
})
var monthlyMin = ee.ImageCollection.fromImages(monthlyMinImages)
print(monthlyMin)
// I can compute Maximum SM for each month across all years
// i.e. Maximum SM for all May months in the collection
var monthlyMaxImages = months.map(function(month) {
var filtered = monthlyCol.filter(ee.Filter.eq('month', month))
var monthlyMax = filtered.max()
return monthlyMax.set('month', month)
})
var monthlyMax = ee.ImageCollection.fromImages(monthlyMaxImages)
print(monthlyMax)
// Calculate SMCI for each year!
// I are interested in calculating VCI for a particular month
var currentYear = 2021
var currentMonth = 8
Use print(...) to write to this console.
ImageCollection N...
Ethiopia
FeatureCollection...
Ethiopia bounds
Polygon, 5 vertic...
ImageCollection N...
ImageCollection (...
ImageCollection (...
ImageCollection (...
Image (1 band)

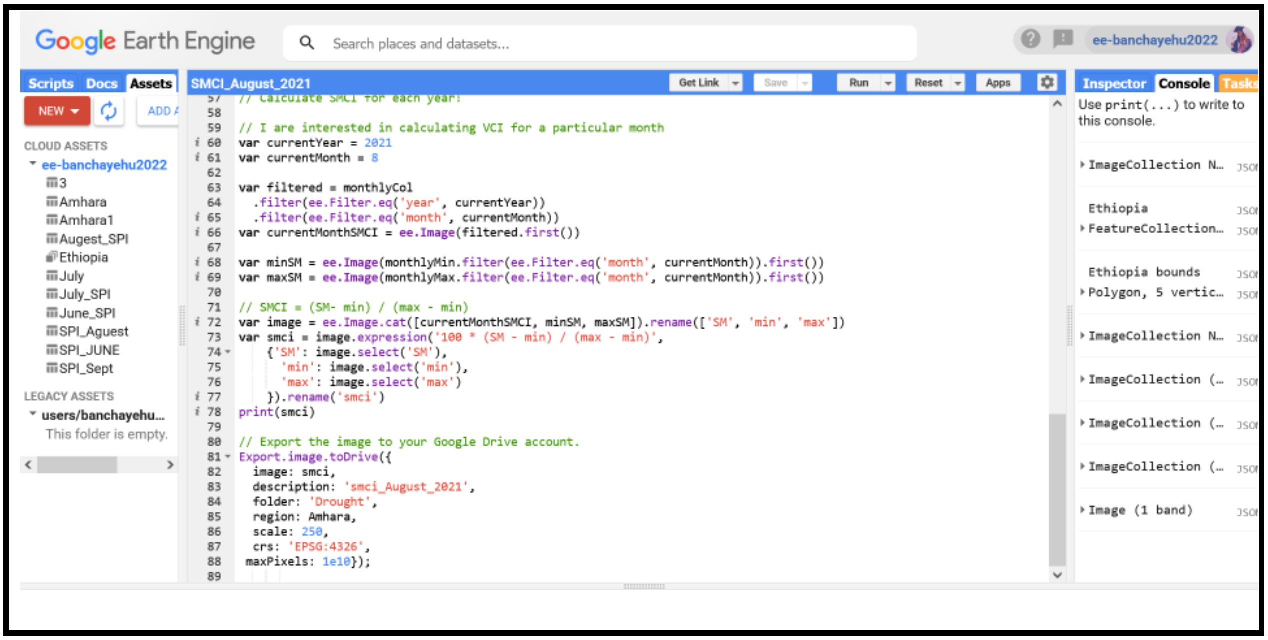
Google Earth Engine
Search places and datasets...
ee-banchayehu2022
Scripts Docs Assets
NEW
ADD A
CLOUD ASSETS
ee-banchayehu2022
3
Amhara
Amhara1
Augest_SPI
Ethiopia
July
July_SPI
June_SPI
SPI_Aguest
SPI_JUNE
SPI_Sept
LEGACY ASSETS
users/banchayehu...
This folder is empty.
SMCI_August_2021
Get Link
Save
Run
Reset
Apps
// Calculate SMCI for each year!
// I are interested in calculating VCI for a particular month
var currentYear = 2021
var currentMonth = 8
var filtered = monthlyCol
.filter(ee.Filter.eq('year', currentYear))
.filter(ee.Filter.eq('month', currentMonth))
var currentMonthSMCI = ee.Image(filtered.first())
var minSM = ee.Image(monthlyMin.filter(ee.Filter.eq('month', currentMonth)).first())
var maxSM = ee.Image(monthlyMax.filter(ee.Filter.eq('month', currentMonth)).first())
// SMCI = (SM- min) / (max - min)
var image = ee.Image.cat([currentMonthSMCI, minSM, maxSM]).rename(['SM', 'min', 'max'])
var smci = image.expression('100 * (SM - min) / (max - min)',
{'SM': image.select('SM'),
'min': image.select('min'),
'max': image.select('max')
}).rename('smci')
print(smci)
// Export the image to your Google Drive account.
Export.image.toDrive({
image: smci,
description: 'smci_August_2021',
folder: 'Drought',
region: Amhara,
scale: 250,
crs: 'EPSG:4326',
maxPixels: 1e10});
Inspector Console Tasks
Use print(...) to write to this console.
ImageCollection N...
Ethiopia
FeatureCollection...
Ethiopia bounds
Polygon, 5 vertic...
ImageCollection N...
ImageCollection (...
ImageCollection (...
ImageCollection (...
Image (1 band)

APPENDIX 2: Sample for the process of CADI Construction

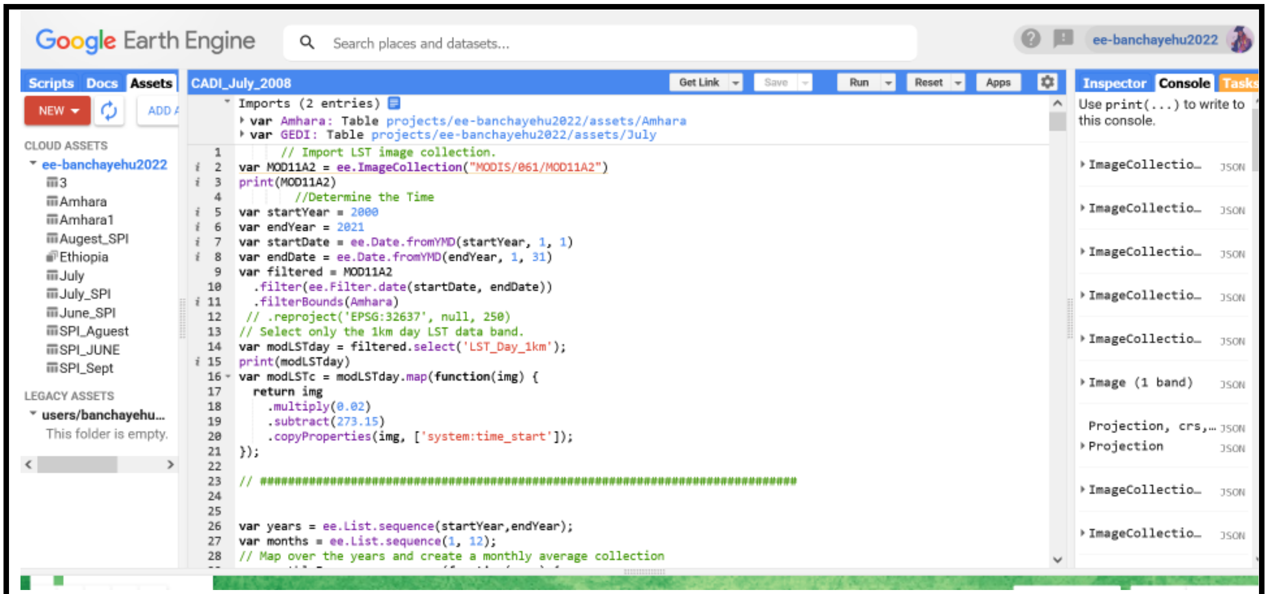

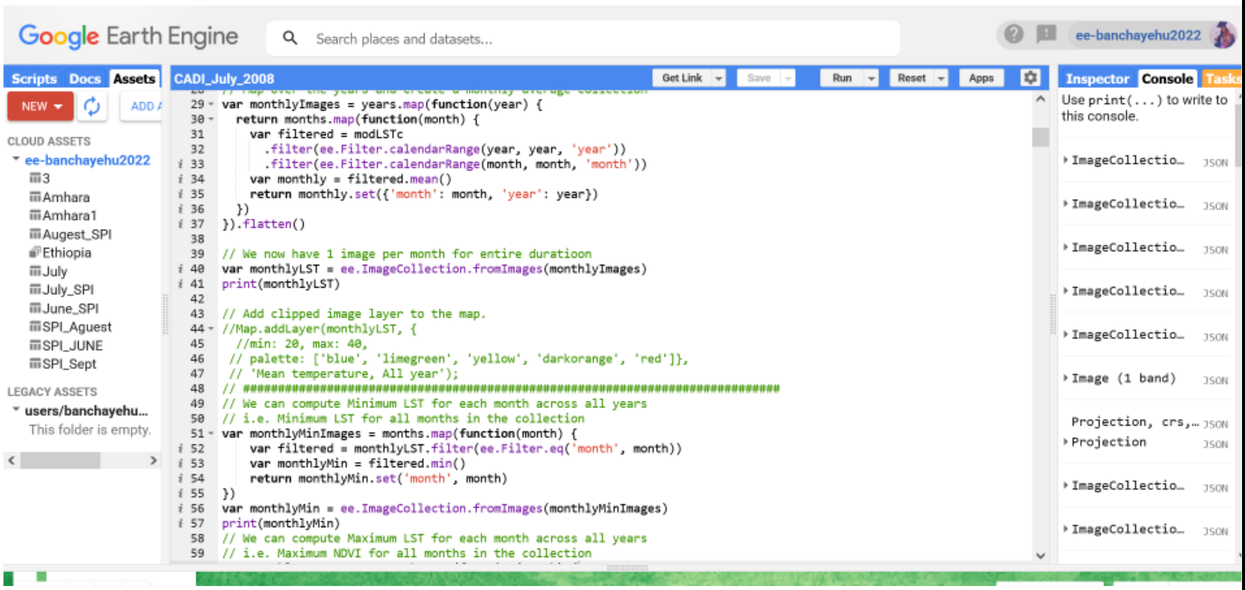

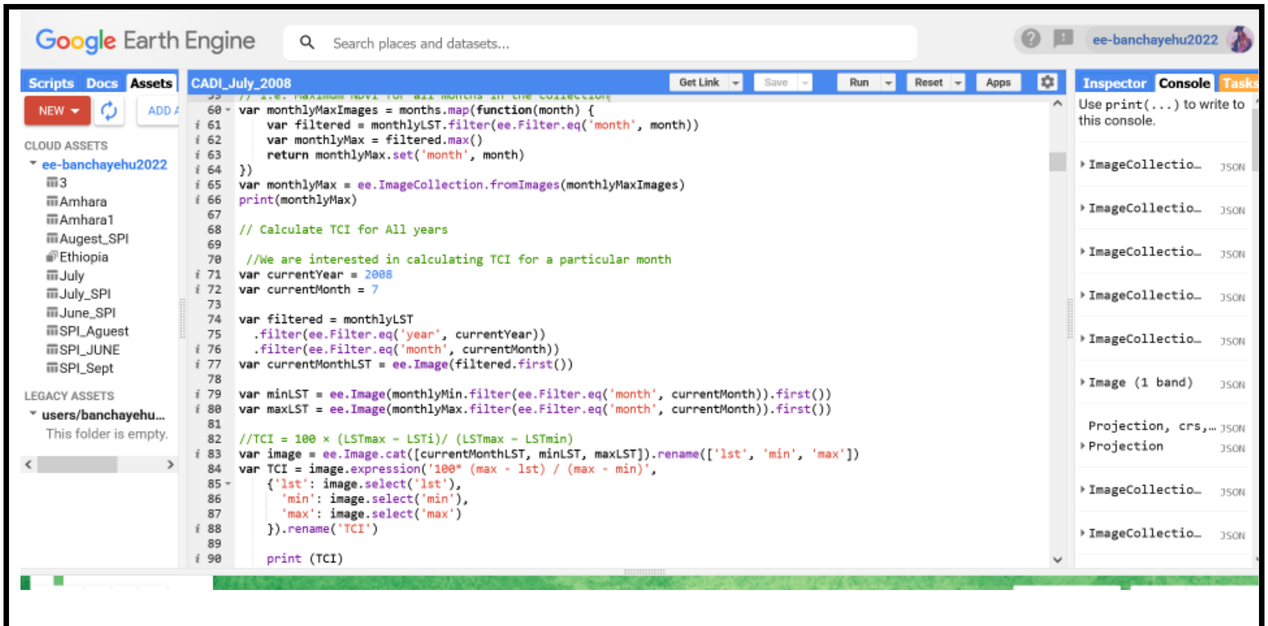
Google Earth Engine
Search places and datasets...
ee-banchayehu2022
Scripts Docs Assets
CADI_July_2008
Get Link Save Run Reset Apps
Inspector Console Tasks
NEW
CLOUD ASSETS
ee-banchayehu2022
3
Amhara
Amhara1
Augest_SPI
Ethiopia
July
July_SPI
June_SPI
SPI_Aguest
SPI_JUNE
SPI_Sept
LEGACY ASSETS
users/banchayehu...
This folder is empty.
var monthlyMaxImages = months.map(function(month) {
var filtered = monthlyLST.filter(ee.Filter.eq('month', month))
var monthlyMax = filtered.max()
return monthlyMax.set('month', month)
})
var monthlyMax = ee.ImageCollection.fromImages(monthlyMaxImages)
print(monthlyMax)
// Calculate TCI for All years
//We are interested in calculating TCI for a particular month
var currentYear = 2008
var currentMonth = 7
var filtered = monthlyLST
.filter(ee.Filter.eq('year', currentYear))
.filter(ee.Filter.eq('month', currentMonth))
var currentMonthLST = ee.Image(filtered.first())
var minLST = ee.Image(monthlyMin.filter(ee.Filter.eq('month', currentMonth)).first())
var maxLST = ee.Image(monthlyMax.filter(ee.Filter.eq('month', currentMonth)).first())
//TCI = 100 × (LSTmax − LSTi)/ (LSTmax − LSTmin)
var image = ee.Image.cat([currentMonthLST, minLST, maxLST]).rename(['lst', 'min', 'max'])
var TCI = image.expression('100* (max - lst) / (max - min)',
{'lst': image.select('lst'),
'min': image.select('min'),
'max': image.select('max')
}).rename('TCI')
print (TCI)
Use print(...) to write to this console.
ImageCollectio… JSON
ImageCollectio… JSON
ImageCollectio… JSON
ImageCollectio… JSON
ImageCollectio… JSON
Image (1 band) JSON
Projection, crs,… JSON
Projection JSON
ImageCollectio… JSON
ImageCollectio… JSON

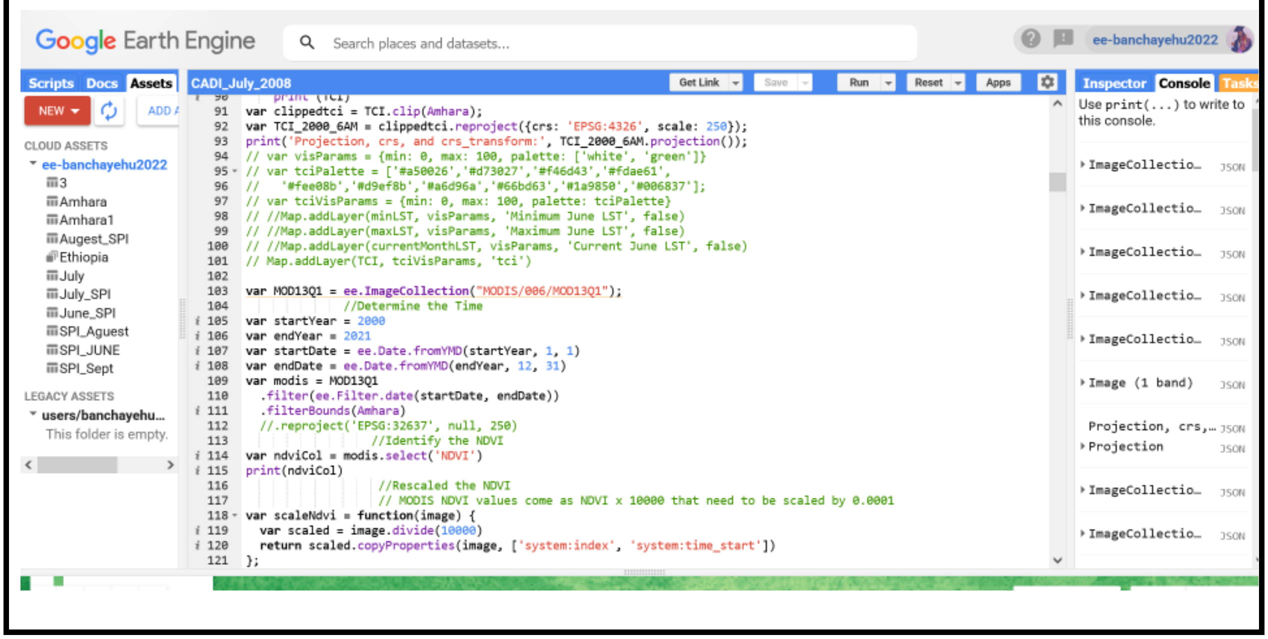
Google Earth Engine
Search places and datasets...
ee-banchayehu2022
Scripts Docs Assets
CADI_July_2008
Get Link Save Run Reset Apps
Inspector Console Tasks
NEW
CLOUD ASSETS
ee-banchayehu2022
3
Amhara
Amhara1
Augest_SPI
Ethiopia
July
July_SPI
June_SPI
SPI_Aguest
SPI_JUNE
SPI_Sept
LEGACY ASSETS
users/banchayehu...
This folder is empty.
var clippedtci = TCI.clip(Amhara);
var TCI_2000_6AM = clippedtci.reproject({crs: 'EPSG:4326', scale: 250});
print('Projection, crs, and crs_transform:', TCI_2000_6AM.projection());
// var visParams = {min: 0, max: 100, palette: ['white', 'green']}
// var tciPalette = ['#a50026','#d73027','#f46d43','#fdae61',
// '#fee08b','#d9ef8b','#a6d96a','#66bd63','#1a9850','#006837'];
// var tciVisParams = {min: 0, max: 100, palette: tciPalette}
// //Map.addLayer(minLST, visParams, 'Minimum June LST', false)
// //Map.addLayer(maxLST, visParams, 'Maximum June LST', false)
// //Map.addLayer(currentMonthLST, visParams, 'Current June LST', false)
// Map.addLayer(TCI, tciVisParams, 'tci')
var MOD13Q1 = ee.ImageCollection("MODIS/006/MOD13Q1");
//Determine the Time
var startYear = 2000
var endYear = 2021
var startDate = ee.Date.fromYMD(startYear, 1, 1)
var endDate = ee.Date.fromYMD(endYear, 12, 31)
var modis = MOD13Q1
.filter(ee.Filter.date(startDate, endDate))
.filterBounds(Amhara)
//.reproject('EPSG:32637', null, 250)
//Identify the NDVI
var ndviCol = modis.select('NDVI')
print(ndviCol)
//Rescaled the NDVI
// MODIS NDVI values come as NDVI x 10000 that need to be scaled by 0.0001
var scaleNdvi = function(image) {
var scaled = image.divide(10000)
return scaled.copyProperties(image, ['system:index', 'system:time_start'])
};
Use print(...) to write to this console.
ImageCollectio… JSON
ImageCollectio… JSON
ImageCollectio… JSON
ImageCollectio… JSON
ImageCollectio… JSON
Image (1 band) JSON
Projection, crs,… JSON
Projection JSON
ImageCollectio… JSON
ImageCollectio… JSON

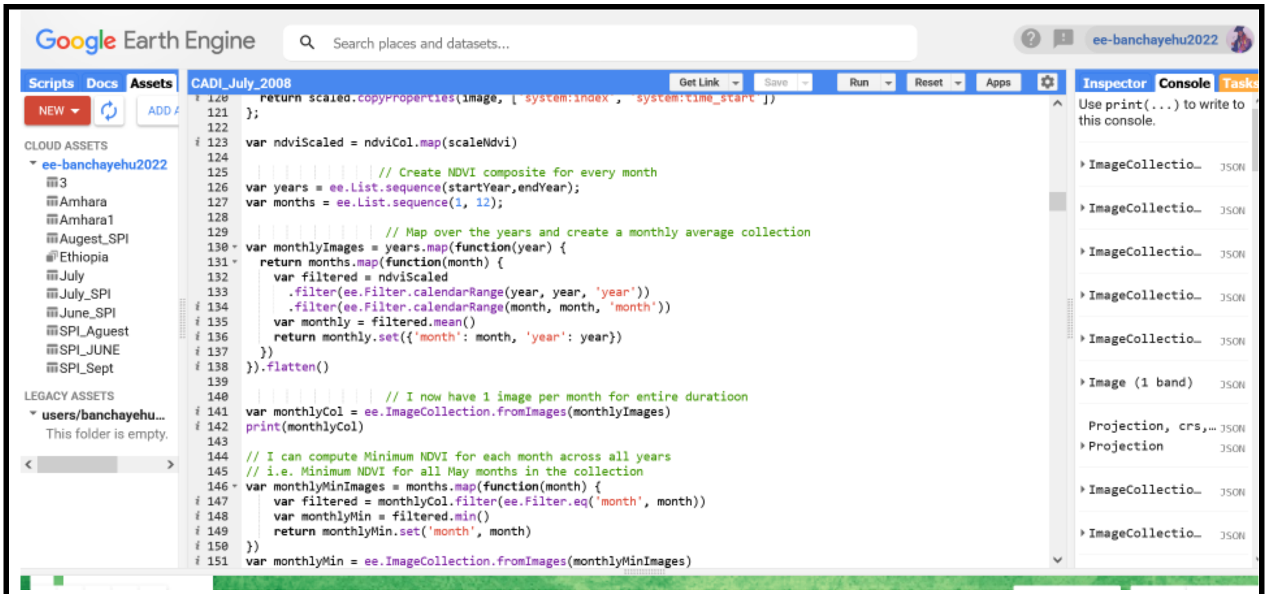
Google Earth Engine
Search places and datasets...
ee-banchayehu2022
Scripts Docs Assets
CADI_July_2008
Get Link Save Run Reset Apps
Inspector Console Tasks
NEW
CLOUD ASSETS
ee-banchayehu2022
3
Amhara
Amhara1
Augest_SPI
Ethiopia
July
July_SPI
June_SPI
SPI_Aguest
SPI_JUNE
SPI_Sept
LEGACY ASSETS
users/banchayehu...
This folder is empty.
return scaled.copyProperties(image, ['system:index', 'system:time_start'])
};
var ndviScaled = ndviCol.map(scaleNdvi)
// Create NDVI composite for every month
var years = ee.List.sequence(startYear,endYear);
var months = ee.List.sequence(1, 12);
// Map over the years and create a monthly average collection
var monthlyImages = years.map(function(year) {
return months.map(function(month) {
var filtered = ndviScaled
.filter(ee.Filter.calendarRange(year, year, 'year'))
.filter(ee.Filter.calendarRange(month, month, 'month'))
var monthly = filtered.mean()
return monthly.set({'month': month, 'year': year})
})
}).flatten()
// I now have 1 image per month for entire duratioon
var monthlyCol = ee.ImageCollection.fromImages(monthlyImages)
print(monthlyCol)
// I can compute Minimum NDVI for each month across all years
// i.e. Minimum NDVI for all May months in the collection
var monthlyMinImages = months.map(function(month) {
var filtered = monthlyCol.filter(ee.Filter.eq('month', month))
var monthlyMin = filtered.min()
return monthlyMin.set('month', month)
})
var monthlyMin = ee.ImageCollection.fromImages(monthlyMinImages)
Use print(...) to write to this console.
ImageCollectio... JSON
ImageCollectio... JSON
ImageCollectio... JSON
ImageCollectio... JSON
ImageCollectio... JSON
Image (1 band) JSON
Projection, crs,... JSON
Projection JSON
ImageCollectio... JSON
ImageCollectio... JSON

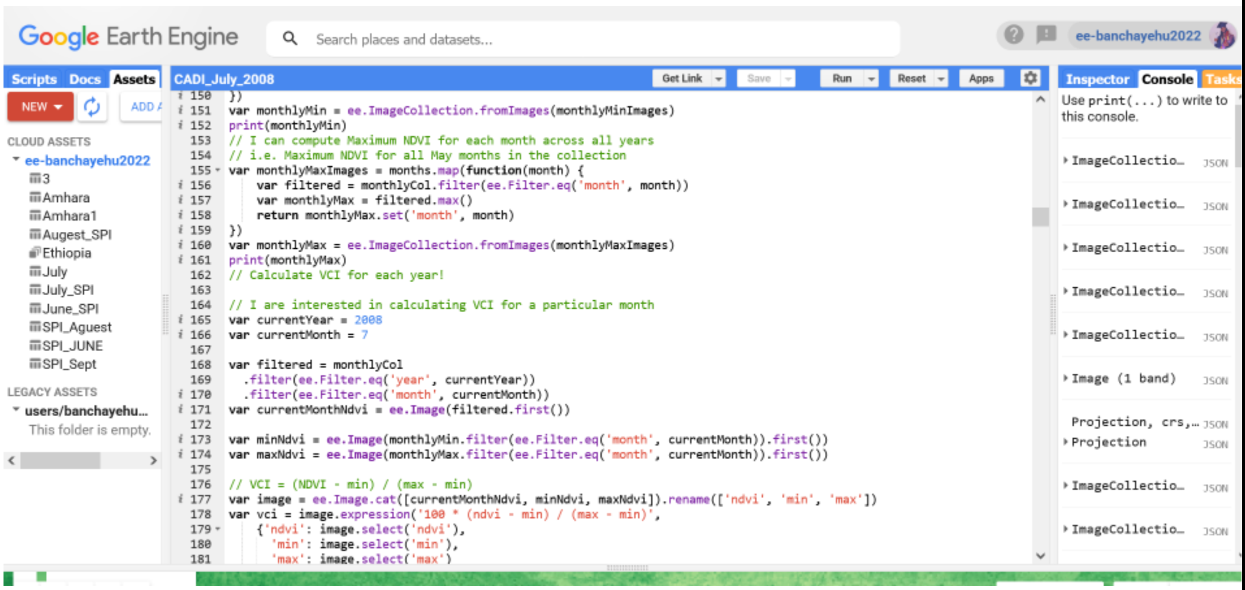
Google Earth Engine
Search places and datasets...
ee-banchayehu2022
Scripts Docs Assets
CADI_July_2008
Get Link Save Run Reset Apps
Inspector Console Tasks
NEW
CLOUD ASSETS
ee-banchayehu2022
3
Amhara
Amhara1
Augest_SPI
Ethiopia
July
July_SPI
June_SPI
SPI_Aguest
SPI_JUNE
SPI_Sept
LEGACY ASSETS
users/banchayehu...
This folder is empty.
})
var monthlyMin = ee.ImageCollection.fromImages(monthlyMinImages)
print(monthlyMin)
// I can compute Maximum NDVI for each month across all years
// i.e. Maximum NDVI for all May months in the collection
var monthlyMaxImages = months.map(function(month) {
var filtered = monthlyCol.filter(ee.Filter.eq('month', month))
var monthlyMax = filtered.max()
return monthlyMax.set('month', month)
})
var monthlyMax = ee.ImageCollection.fromImages(monthlyMaxImages)
print(monthlyMax)
// Calculate VCI for each year!
// I are interested in calculating VCI for a particular month
var currentYear = 2008
var currentMonth = 7
var filtered = monthlyCol
.filter(ee.Filter.eq('year', currentYear))
.filter(ee.Filter.eq('month', currentMonth))
var currentMonthNdvi = ee.Image(filtered.first())
var minNdvi = ee.Image(monthlyMin.filter(ee.Filter.eq('month', currentMonth)).first())
var maxNdvi = ee.Image(monthlyMax.filter(ee.Filter.eq('month', currentMonth)).first())
// VCI = (NDVI - min) / (max - min)
var image = ee.Image.cat([currentMonthNdvi, minNdvi, maxNdvi]).rename(['ndvi', 'min', 'max'])
var vci = image.expression('100 * (ndvi - min) / (max - min)',
{'ndvi': image.select('ndvi'),
'min': image.select('min'),
'max': image.select('max')
Use print(...) to write to this console.
ImageCollectio... JSON
ImageCollectio... JSON
ImageCollectio... JSON
ImageCollectio... JSON
ImageCollectio... JSON
Image (1 band) JSON
Projection, crs,... JSON
Projection JSON
ImageCollectio... JSON
ImageCollectio... JSON

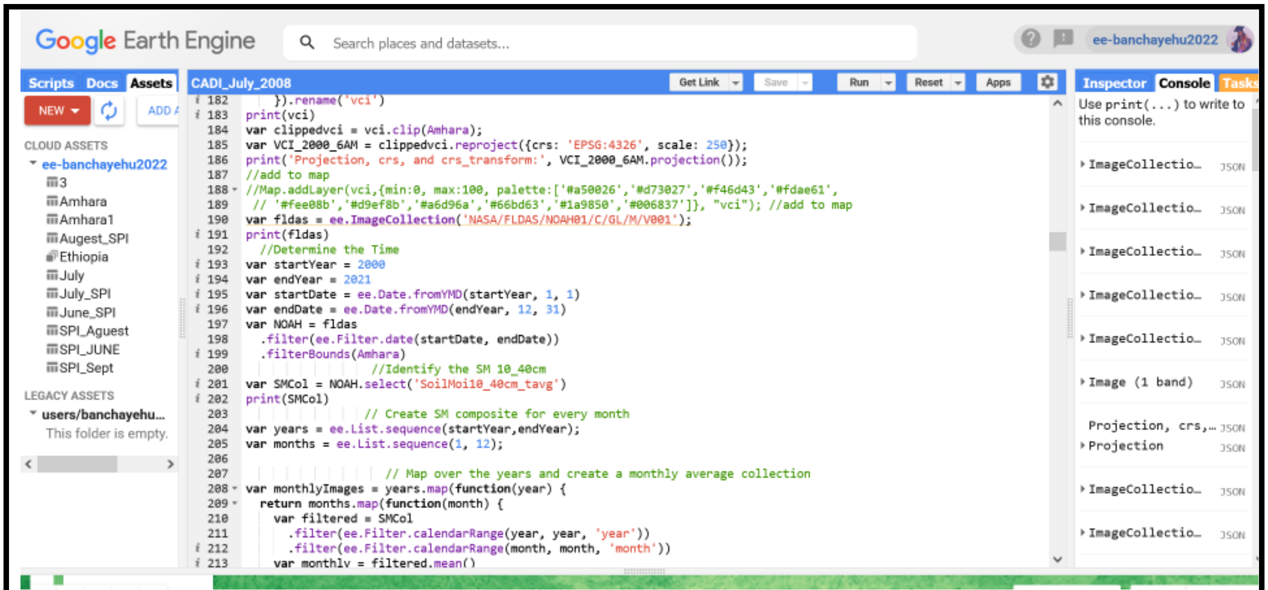
Google Earth Engine
Search places and datasets...
ee-banchayehu2022
Scripts Docs Assets
NEW
CLOUD ASSETS
ee-banchayehu2022
3
Amhara
Amhara1
Augest_SPI
Ethiopia
July
July_SPI
June_SPI
SPI_Aguest
SPI_JUNE
SPI_Sept
LEGACY ASSETS
users/banchayehu...
This folder is empty.
CADI_July_2008
Get Link
Save
Run
Reset
Apps
}).rename('vci')
print(vci)
var clippedvci = vci.clip(Amhara);
var VCI_2000_6AM = clippedvci.reproject({crs: 'EPSG:4326', scale: 250});
print('Projection, crs, and crs_transform:', VCI_2000_6AM.projection());
//add to map
//Map.addLayer(vci,{min:0, max:100, palette:['#a50026','#d73027','#f46d43','#fdae61',
// '#fee08b','#d9ef8b','#a6d96a','#66bd63','#1a9850','#006837']}, "vci"); //add to map
var fldas = ee.ImageCollection('NASA/FLDAS/NOAH01/C/GL/M/V001');
print(fldas)
//Determine the Time
var startYear = 2000
var endYear = 2021
var startDate = ee.Date.fromYMD(startYear, 1, 1)
var endDate = ee.Date.fromYMD(endYear, 12, 31)
var NOAH = fldas
.filter(ee.Filter.date(startDate, endDate))
.filterBounds(Amhara)
//Identify the SM 10_40cm
var SMCol = NOAH.select('SoilMoi10_40cm_tavg')
print(SMCol)
// Create SM composite for every month
var years = ee.List.sequence(startYear,endYear);
var months = ee.List.sequence(1, 12);
// Map over the years and create a monthly average collection
var monthlyImages = years.map(function(year) {
return months.map(function(month) {
var filtered = SMCol
.filter(ee.Filter.calendarRange(year, year, 'year'))
.filter(ee.Filter.calendarRange(month, month, 'month'))
var monthly = filtered.mean()
Inspector Console Tasks
Use print(...) to write to this console.
ImageCollectio… JSON
ImageCollectio… JSON
ImageCollectio… JSON
ImageCollectio… JSON
ImageCollectio… JSON
Image (1 band) JSON
Projection, crs,… JSON
Projection JSON
ImageCollectio… JSON
ImageCollectio… JSON

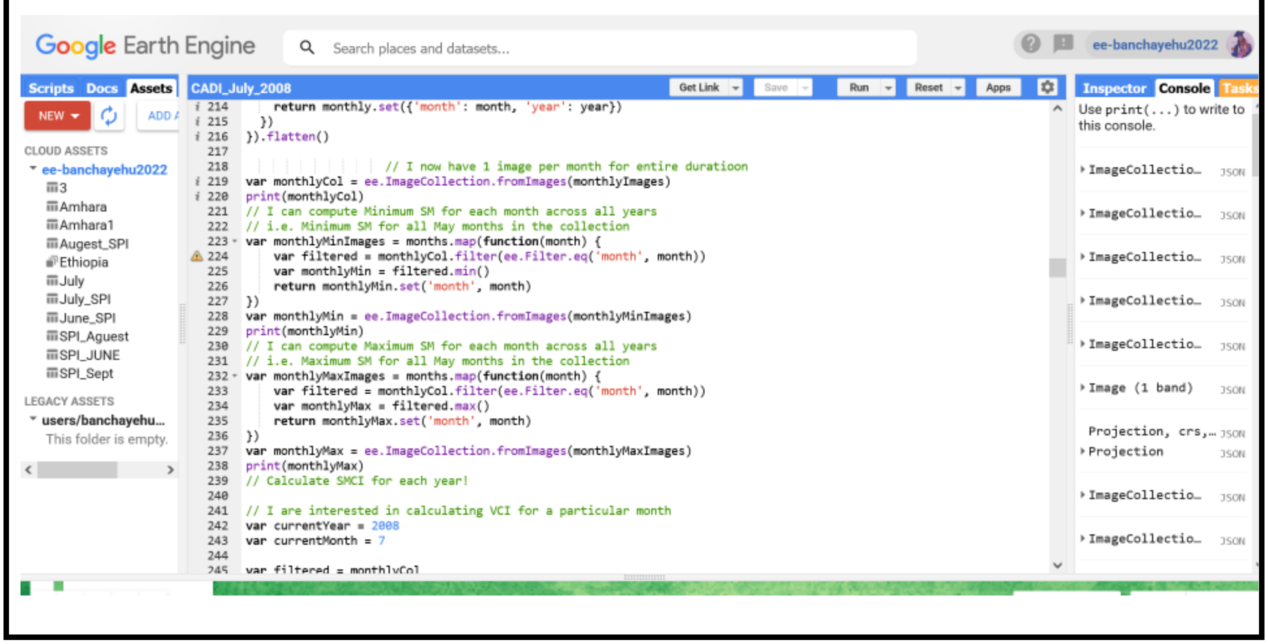
Google Earth Engine
Search places and datasets...
ee-banchayehu2022
Scripts Docs Assets
NEW
CLOUD ASSETS
ee-banchayehu2022
3
Amhara
Amhara1
Augest_SPI
Ethiopia
July
July_SPI
June_SPI
SPI_Aguest
SPI_JUNE
SPI_Sept
LEGACY ASSETS
users/banchayehu...
This folder is empty.
CADI_July_2008
Get Link
Save
Run
Reset
Apps
return monthly.set({'month': month, 'year': year})
})
}).flatten()
// I now have 1 image per month for entire durationn
var monthlyCol = ee.ImageCollection.fromImages(monthlyImages)
print(monthlyCol)
// I can compute Minimum SM for each month across all years
// i.e. Minimum SM for all May months in the collection
var monthlyMinImages = months.map(function(month) {
var filtered = monthlyCol.filter(ee.Filter.eq('month', month))
var monthlyMin = filtered.min()
return monthlyMin.set('month', month)
})
var monthlyMin = ee.ImageCollection.fromImages(monthlyMinImages)
print(monthlyMin)
// I can compute Maximum SM for each month across all years
// i.e. Maximum SM for all May months in the collection
var monthlyMaxImages = months.map(function(month) {
var filtered = monthlyCol.filter(ee.Filter.eq('month', month))
var monthlyMax = filtered.max()
return monthlyMax.set('month', month)
})
var monthlyMax = ee.ImageCollection.fromImages(monthlyMaxImages)
print(monthlyMax)
// Calculate SMCI for each year!
// I are interested in calculating VCI for a particular month
var currentYear = 2008
var currentMonth = 7
var filtered = monthlyCol
Inspector Console Tasks
Use print(...) to write to this console.
ImageCollectio… JSON
ImageCollectio… JSON
ImageCollectio… JSON
ImageCollectio… JSON
ImageCollectio… JSON
Image (1 band) JSON
Projection, crs,… JSON
Projection JSON
ImageCollectio… JSON
ImageCollectio… JSON

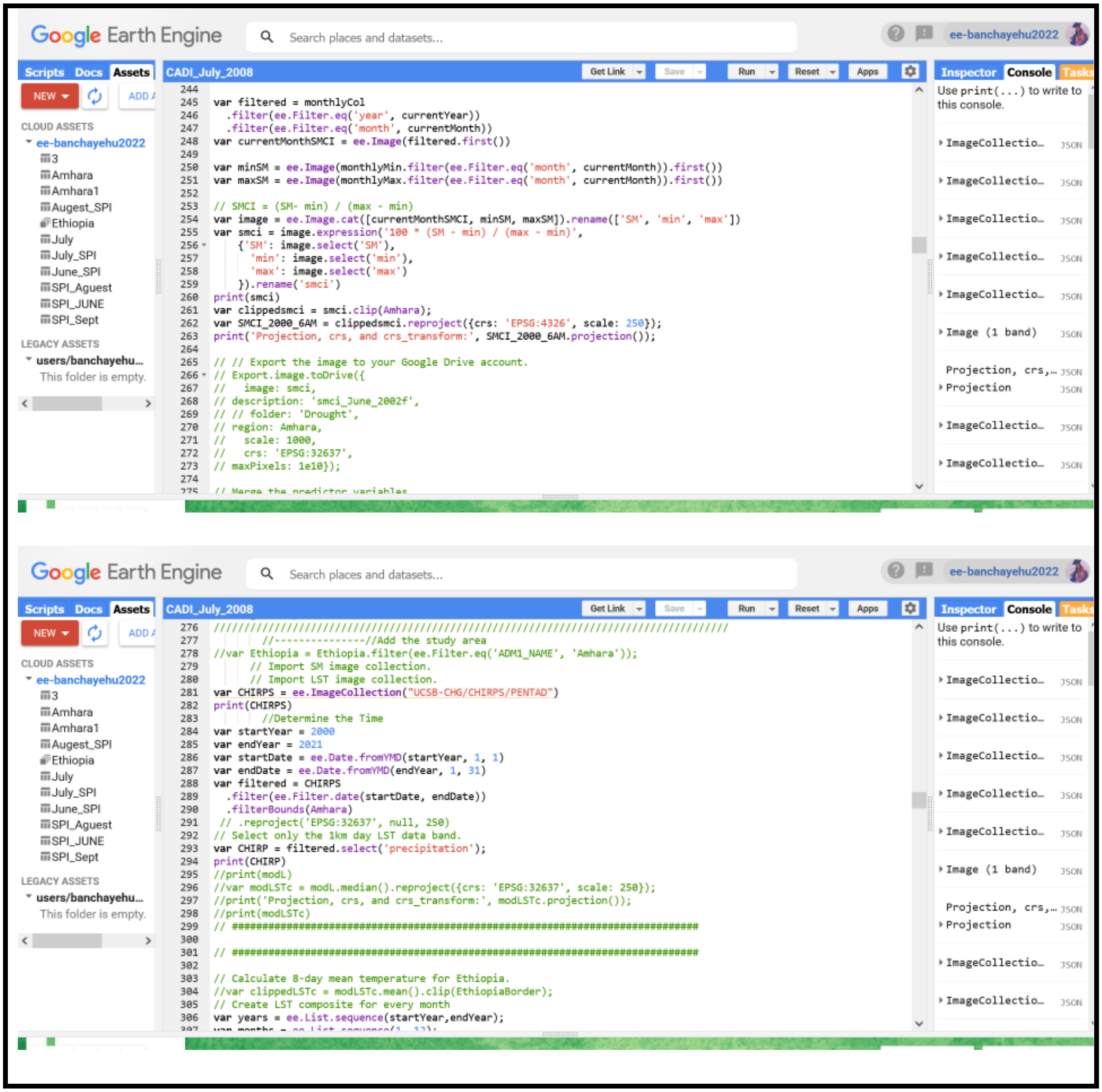
Google Earth Engine
Search places and datasets...
ee-banchayehu2022
Scripts Docs Assets
CADI_July_2008
Get Link Save Run Reset Apps
Inspector Console Tasks
NEW
ADD
CLOUD ASSETS
ee-banchayehu2022
3
Amhara
Amhara1
Augest_SPI
Ethiopia
July
July_SPI
June_SPI
SPI_Aguest
SPI_JUNE
SPI_Sept
LEGACY ASSETS
users/banchayehu...
This folder is empty.
var filtered = monthlyCol
.filter(ee.Filter.eq('year', currentYear))
.filter(ee.Filter.eq('month', currentMonth))
var currentMonthSMCI = ee.Image(filtered.first())
var minSM = ee.Image(monthlyMin.filter(ee.Filter.eq('month', currentMonth)).first())
var maxSM = ee.Image(monthlyMax.filter(ee.Filter.eq('month', currentMonth)).first())
// SMCI = (SM- min) / (max - min)
var image = ee.Image.cat([currentMonthSMCI, minSM, maxSM]).rename(['SM', 'min', 'max'])
var smci = image.expression('100 * (SM - min) / (max - min)',
{'SM': image.select('SM'),
'min': image.select('min'),
'max': image.select('max')
}).rename('smci')
print(smci)
var clippedsmci = smci.clip(Amhara);
var SMCI_2000_6AM = clippedsmci.reproject({crs: 'EPSG:4326', scale: 250});
print('Projection, crs, and crs_transform:', SMCI_2000_6AM.projection());
// // Export the image to your Google Drive account.
// Export.image.toDrive({
// image: smci,
// description: 'smci_June_2002f',
// // folder: 'Drought',
// region: Amhara,
// scale: 1000,
// crs: 'EPSG:32637',
// maxPixels: 1e10});
// Merge the predictor variables
Use print(...) to write to this console.
ImageCollectio... JSON
Image (1 band) JSON
Projection, crs,... JSON
Projection JSON
//
//---------------//Add the study area
//var Ethiopia = Ethiopia.filter(ee.Filter.eq('ADM1_NAME', 'Amhara'));
// Import SM image collection.
// Import LST image collection.
var CHIRPS = ee.ImageCollection("UCSB-CHG/CHIRPS/PENTAD")
print(CHIRPS)
//Determine the Time
var startYear = 2000
var endYear = 2021
var startDate = ee.Date.fromYMD(startYear, 1, 1)
var endDate = ee.Date.fromYMD(endYear, 1, 31)
var filtered = CHIRPS
.filter(ee.Filter.date(startDate, endDate))
.filterBounds(Amhara)
// .reproject('EPSG:32637', null, 250)
// Select only the 1km day LST data band.
var CHIRP = filtered.select('precipitation');
print(CHIRP)
//print(modL)
//var modLSTc = modL.median().reproject({crs: 'EPSG:32637', scale: 250});
//print('Projection, crs, and crs_transform:', modLSTc.projection());
//print(modLSTc)
// ###
// ###
// Calculate 8-day mean temperature for Ethiopia.
//var clippedLSTc = modLSTc.mean().clip(EthiopiaBorder);
// Create LST composite for every month
var years = ee.List.sequence(startYear,endYear);

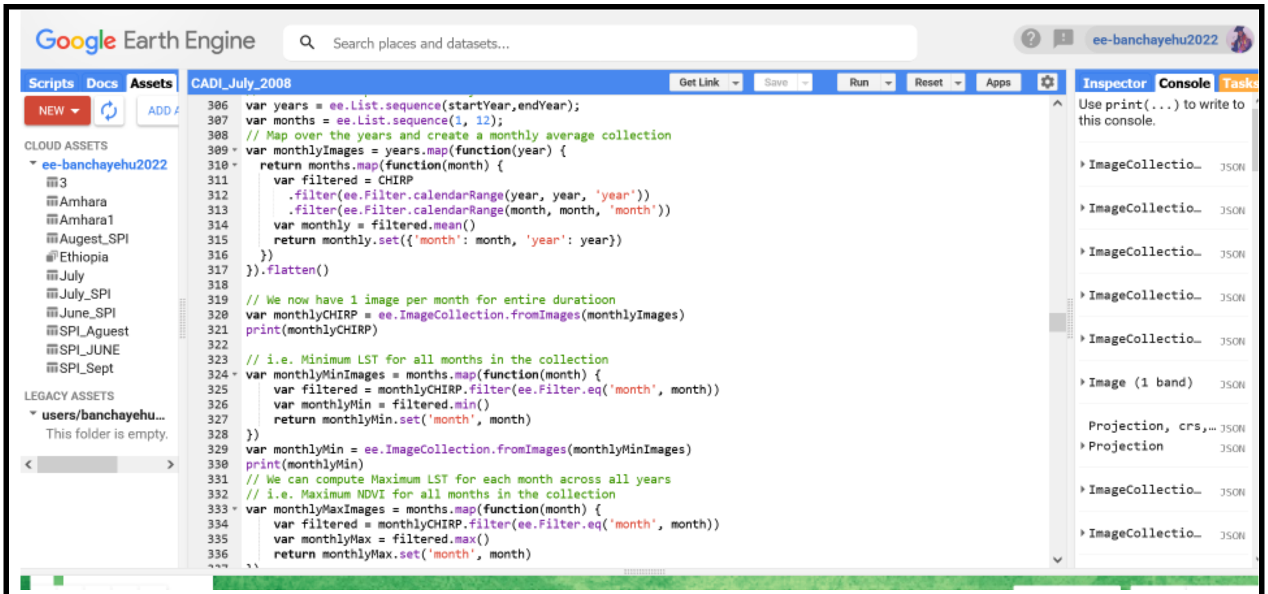
Google Earth Engine
CADI_July_2008
var years = ee.List.sequence(startYear,endYear);
var months = ee.List.sequence(1, 12);
// Map over the years and create a monthly average collection
var monthlyImages = years.map(function(year) {
return months.map(function(month) {
var filtered = CHIRP
.filter(ee.Filter.calendarRange(year, year, 'year'))
.filter(ee.Filter.calendarRange(month, month, 'month'))
var monthly = filtered.mean()
return monthly.set({'month': month, 'year': year})
})
}).flatten()
// We now have 1 image per month for entire duratioon
var monthlyCHIRP = ee.ImageCollection.fromImages(monthlyImages)
print(monthlyCHIRP)
// i.e. Minimum LST for all months in the collection
var monthlyMinImages = months.map(function(month) {
var filtered = monthlyCHIRP.filter(ee.Filter.eq('month', month))
var monthlyMin = filtered.min()
return monthlyMin.set('month', month)
})
var monthlyMin = ee.ImageCollection.fromImages(monthlyMinImages)
print(monthlyMin)
// We can compute Maximum LST for each month across all years
// i.e. Maximum NDVI for all months in the collection
var monthlyMaxImages = months.map(function(month) {
var filtered = monthlyCHIRP.filter(ee.Filter.eq('month', month))
var monthlyMax = filtered.max()
return monthlyMax.set('month', month)

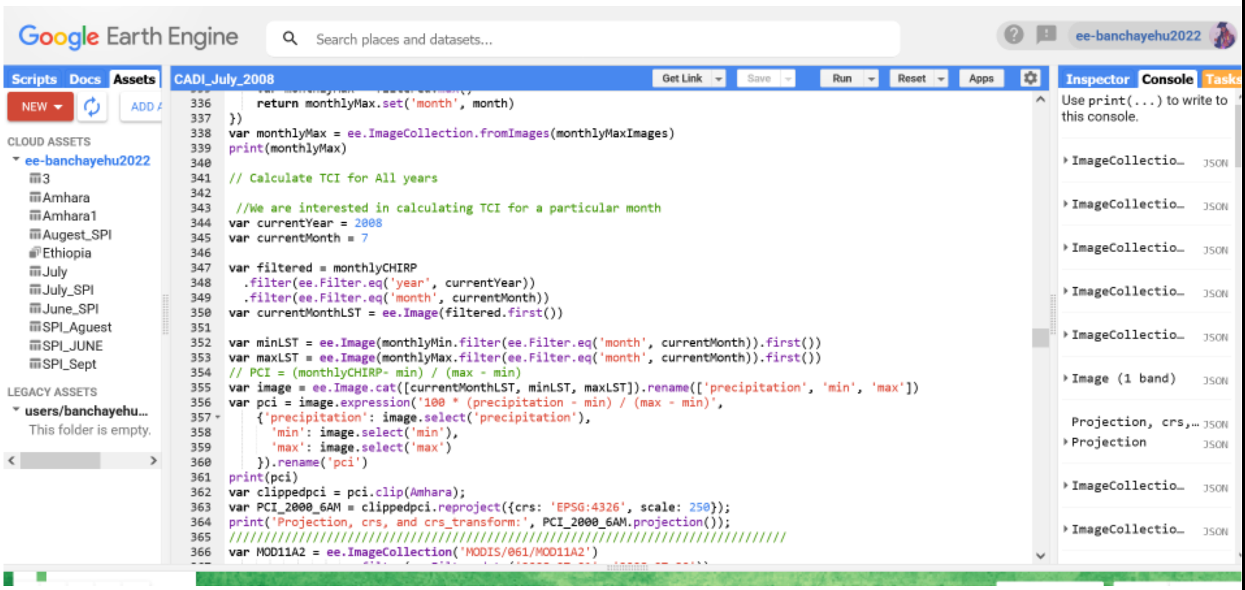
Google Earth Engine
CADI_July_2008
return monthlyMax.set('month', month)
})
var monthlyMax = ee.ImageCollection.fromImages(monthlyMaxImages)
print(monthlyMax)
// Calculate TCI for All years
//We are interested in calculating TCI for a particular month
var currentYear = 2008
var currentMonth = 7
var filtered = monthlyCHIRP
.filter(ee.Filter.eq('year', currentYear))
.filter(ee.Filter.eq('month', currentMonth))
var currentMonthLST = ee.Image(filtered.first())
var minLST = ee.Image(monthlyMin.filter(ee.Filter.eq('month', currentMonth)).first())
var maxLST = ee.Image(monthlyMax.filter(ee.Filter.eq('month', currentMonth)).first())
// PCI = (monthlyCHIRP- min) / (max - min)
var image = ee.Image.cat([currentMonthLST, minLST, maxLST]).rename(['precipitation', 'min', 'max'])
var pci = image.expression('100 * (precipitation - min) / (max - min)',
{'precipitation': image.select('precipitation'),
'min': image.select('min'),
'max': image.select('max')
}).rename('pci')
print(pci)
var clippedpci = pci.clip(Amhara);
var PCI_2000_6AM = clippedpci.reproject({crs: 'EPSG:4326', scale: 250});
print('Projection, crs, and crs_transform:', PCI_2000_6AM.projection());
var MOD11A2 = ee.ImageCollection('MODIS/061/MOD11A2')

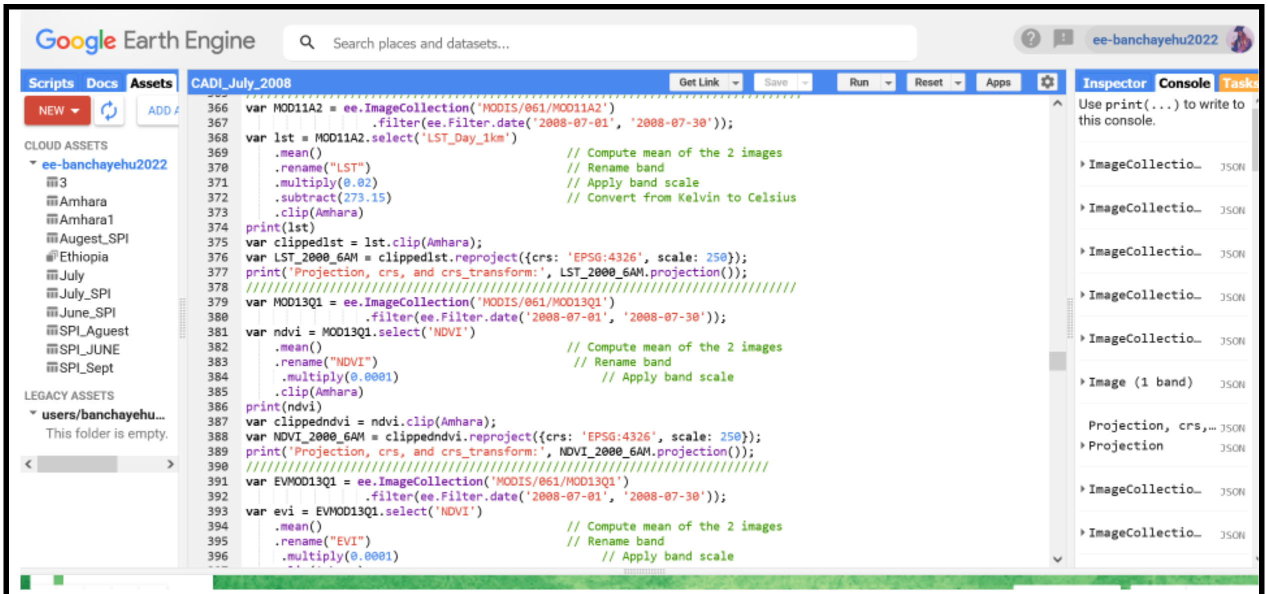
Google Earth Engine
Search places and datasets...
ee-banchayehu2022
Scripts Docs Assets
NEW
ADD
CLOUD ASSETS
ee-banchayehu2022
3
Amhara
Amhara1
Augest_SPI
Ethiopia
July
July_SPI
June_SPI
SPI_Aguest
SPI_JUNE
SPI_Sept
LEGACY ASSETS
users/banchayehu...
This folder is empty.
CADI_July_2008
Get Link
Save
Run
Reset
Apps
var MOD11A2 = ee.ImageCollection('MODIS/061/MOD11A2')
.filter(ee.Filter.date('2008-07-01', '2008-07-30'));
var lst = MOD11A2.select('LST_Day_1km')
.mean() // Compute mean of the 2 images
.rename("LST") // Rename band
.multiply(0.02) // Apply band scale
.subtract(273.15) // Convert from Kelvin to Celsius
.clip(Amhara)
print(lst)
var clippedlst = lst.clip(Amhara);
var LST_2008_6AM = clippedlst.reproject({crs: 'EPSG:4326', scale: 250});
print('Projection, crs, and crs_transform:', LST_2008_6AM.projection());
var MOD13Q1 = ee.ImageCollection('MODIS/061/MOD13Q1')
.filter(ee.Filter.date('2008-07-01', '2008-07-30'));
var ndvi = MOD13Q1.select('NDVI')
.mean() // Compute mean of the 2 images
.rename("NDVI") // Rename band
.multiply(0.0001) // Apply band scale
.clip(Amhara)
print(ndvi)
var clippedndvi = ndvi.clip(Amhara);
var NDVI_2008_6AM = clippedndvi.reproject({crs: 'EPSG:4326', scale: 250});
print('Projection, crs, and crs_transform:', NDVI_2008_6AM.projection());
var EVMOD13Q1 = ee.ImageCollection('MODIS/061/MOD13Q1')
.filter(ee.Filter.date('2008-07-01', '2008-07-30'));
var evi = EVMOD13Q1.select('NDVI')
.mean() // Compute mean of the 2 images
.rename("EVI") // Rename band
.multiply(0.0001) // Apply band scale
Inspector Console Tasks
Use print(...) to write to this console.
ImageCollectio… JSON
ImageCollectio… JSON
ImageCollectio… JSON
ImageCollectio… JSON
ImageCollectio… JSON
Image (1 band) JSON
Projection, crs,… JSON
Projection JSON
ImageCollectio… JSON
ImageCollectio… JSON

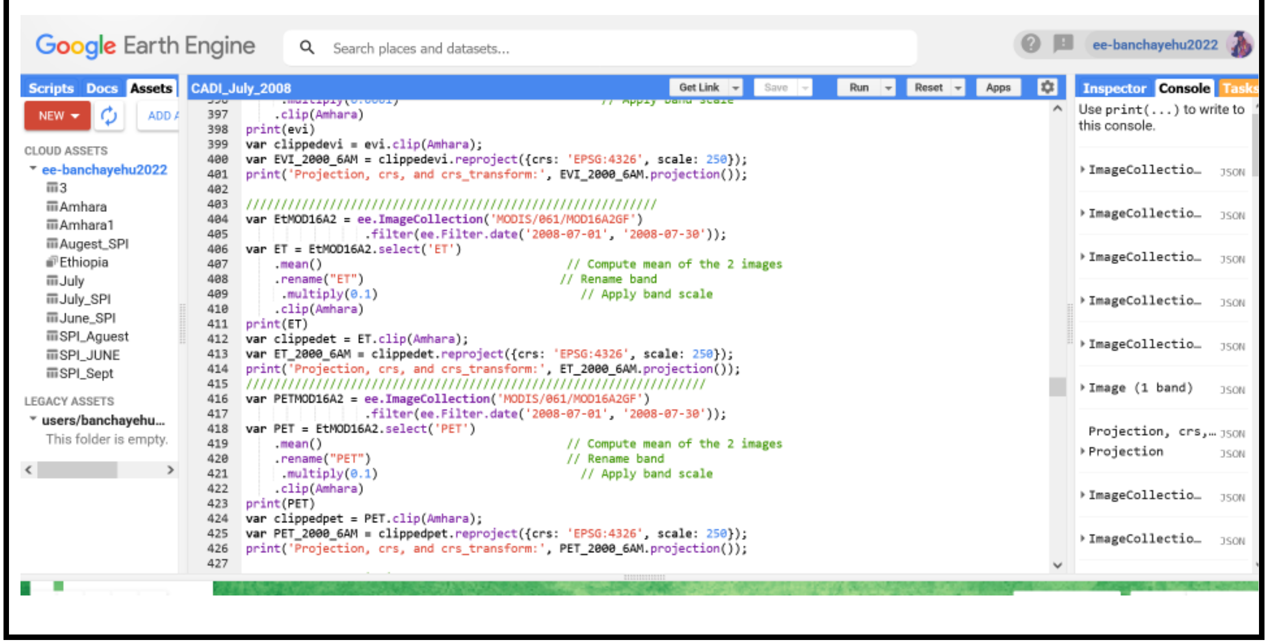
Google Earth Engine
Search places and datasets...
ee-banchayehu2022
Scripts Docs Assets
NEW
ADD
CLOUD ASSETS
ee-banchayehu2022
3
Amhara
Amhara1
Augest_SPI
Ethiopia
July
July_SPI
June_SPI
SPI_Aguest
SPI_JUNE
SPI_Sept
LEGACY ASSETS
users/banchayehu...
This folder is empty.
CADI_July_2008
Get Link
Save
Run
Reset
Apps
.clip(Amhara)
print(evi)
var clippedevi = evi.clip(Amhara);
var EVI_2008_6AM = clippedevi.reproject({crs: 'EPSG:4326', scale: 250});
print('Projection, crs, and crs_transform:', EVI_2008_6AM.projection());
var EtMOD16A2 = ee.ImageCollection('MODIS/061/MOD16A2GF')
.filter(ee.Filter.date('2008-07-01', '2008-07-30'));
var ET = EtMOD16A2.select('ET')
.mean() // Compute mean of the 2 images
.rename("ET") // Rename band
.multiply(0.1) // Apply band scale
.clip(Amhara)
print(ET)
var clippedet = ET.clip(Amhara);
var ET_2008_6AM = clippedet.reproject({crs: 'EPSG:4326', scale: 250});
print('Projection, crs, and crs_transform:', ET_2008_6AM.projection());
var PETMOD16A2 = ee.ImageCollection('MODIS/061/MOD16A2GF')
.filter(ee.Filter.date('2008-07-01', '2008-07-30'));
var PET = EtMOD16A2.select('PET')
.mean() // Compute mean of the 2 images
.rename("PET") // Rename band
.multiply(0.1) // Apply band scale
.clip(Amhara)
print(PET)
var clippedpet = PET.clip(Amhara);
var PET_2008_6AM = clippedpet.reproject({crs: 'EPSG:4326', scale: 250});
print('Projection, crs, and crs_transform:', PET_2008_6AM.projection());
Inspector Console Tasks
Use print(...) to write to this console.
ImageCollectio… JSON
ImageCollectio… JSON
ImageCollectio… JSON
ImageCollectio… JSON
ImageCollectio… JSON
Image (1 band) JSON
Projection, crs,… JSON
Projection JSON
ImageCollectio… JSON
ImageCollectio… JSON

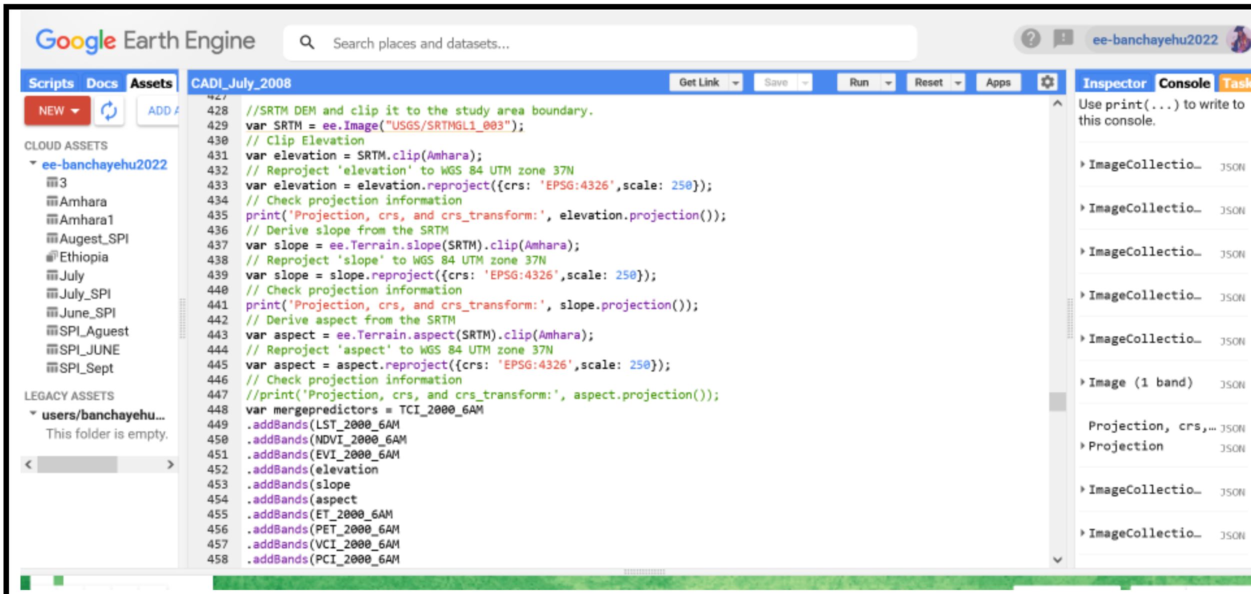
Google Earth Engine
CADI_July_2008
//SRTM DEM and clip it to the study area boundary.
var SRTM = ee.Image("USGS/SRTMGL1_003");
// Clip Elevation
var elevation = SRTM.clip(Amhara);
// Reproject 'elevation' to WGS 84 UTM zone 37N
var elevation = elevation.reproject({crs: 'EPSG:4326',scale: 250});
// Check projection information
print('Projection, crs, and crs_transform:', elevation.projection());
// Derive slope from the SRTM
var slope = ee.Terrain.slope(SRTM).clip(Amhara);
// Reproject 'slope' to WGS 84 UTM zone 37N
var slope = slope.reproject({crs: 'EPSG:4326',scale: 250});
// Check projection information
print('Projection, crs, and crs_transform:', slope.projection());
// Derive aspect from the SRTM
var aspect = ee.Terrain.aspect(SRTM).clip(Amhara);
// Reproject 'aspect' to WGS 84 UTM zone 37N
var aspect = aspect.reproject({crs: 'EPSG:4326',scale: 250});
// Check projection information
//print('Projection, crs, and crs_transform:', aspect.projection());
var mergepredictors = TCI_2000_6AM
.addBands(LST_2000_6AM
.addBands(NDVI_2000_6AM
.addBands(EVI_2000_6AM
.addBands(elevation
.addBands(slope
.addBands(aspect
.addBands(ET_2000_6AM
.addBands(PET_2000_6AM
.addBands(VCI_2000_6AM
.addBands(PCI_2000_6AM

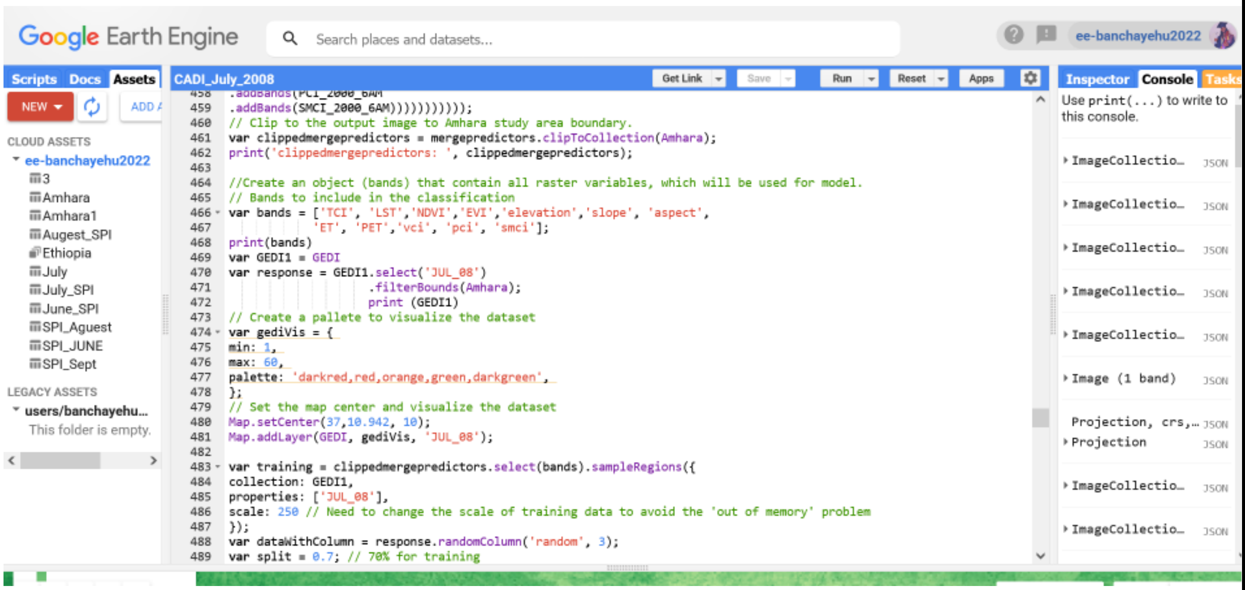
Google Earth Engine
CADI_July_2008
.addBands(SMCI_2000_6AM))))))))))));
// Clip to the output image to Amhara study area boundary.
var clippedmergepredictors = mergepredictors.clipToCollection(Amhara);
print('clippedmergepredictors: ', clippedmergepredictors);
//Create an object (bands) that contain all raster variables, which will be used for model.
// Bands to include in the classification
var bands = ['TCI', 'LST','NDVI','EVI','elevation','slope', 'aspect',
'ET', 'PET','vci', 'pci', 'smci'];
print(bands)
var GEDI1 = GEDI
var response = GEDI1.select('JUL_08')
.filterBounds(Amhara);
print (GEDI1)
// Create a pallete to visualize the dataset
var gediVis = {
min: 1,
max: 60,
palette: 'darkred,red,orange,green,darkgreen',
};
// Set the map center and visualize the dataset
Map.setCenter(37,10.942, 10);
Map.addLayer(GEDI, gediVis, 'JUL_08');
var training = clippedmergepredictors.select(bands).sampleRegions({
collection: GEDI1,
properties: ['JUL_08'],
scale: 250 // Need to change the scale of training data to avoid the 'out of memory' problem
});
var dataWithColumn = response.randomColumn('random', 3);
var split = 0.7; // 70% for training

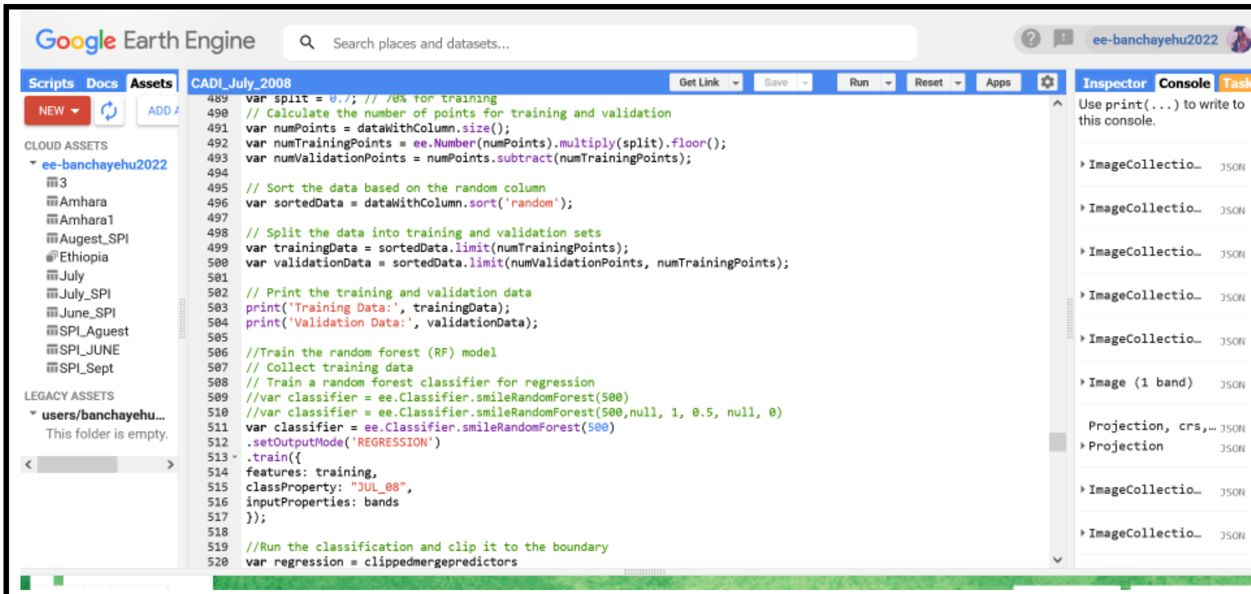
Google Earth Engine
Search places and datasets...
ee-banchayehu2022
Scripts Docs Assets
CADI_July_2008
Get Link
Save
Run
Reset
Apps
Inspector Console Tasks
NEW
ADD
CLOUD ASSETS
ee-banchayehu2022
3
Amhara
Amhara1
Augest_SPI
Ethiopia
July
July_SPI
June_SPI
SPI_Aguest
SPI_JUNE
SPI_Sept
LEGACY ASSETS
users/banchayehu...
This folder is empty.
// Calculate the number of points for training and validation
var numPoints = dataWithColumn.size();
var numTrainingPoints = ee.Number(numPoints).multiply(split).floor();
var numValidationPoints = numPoints.subtract(numTrainingPoints);
// Sort the data based on the random column
var sortedData = dataWithColumn.sort('random');
// Split the data into training and validation sets
var trainingData = sortedData.limit(numTrainingPoints);
var validationData = sortedData.limit(numValidationPoints, numTrainingPoints);
// Print the training and validation data
print('Training Data:', trainingData);
print('Validation Data:', validationData);
//Train the random forest (RF) model
// Collect training data
// Train a random forest classifier for regression
//var classifier = ee.Classifier.smileRandomForest(500)
//var classifier = ee.Classifier.smileRandomForest(500,null, 1, 0.5, null, 0)
var classifier = ee.Classifier.smileRandomForest(500)
.setOutputMode('REGRESSION')
.train({
features: training,
classProperty: "JUL_08",
inputProperties: bands
});
//Run the classification and clip it to the boundary
var regression = clippedmergepredictors
Use print(...) to write to this console.
ImageCollectio...
Image (1 band)
Projection, crs,...
Projection
JSON

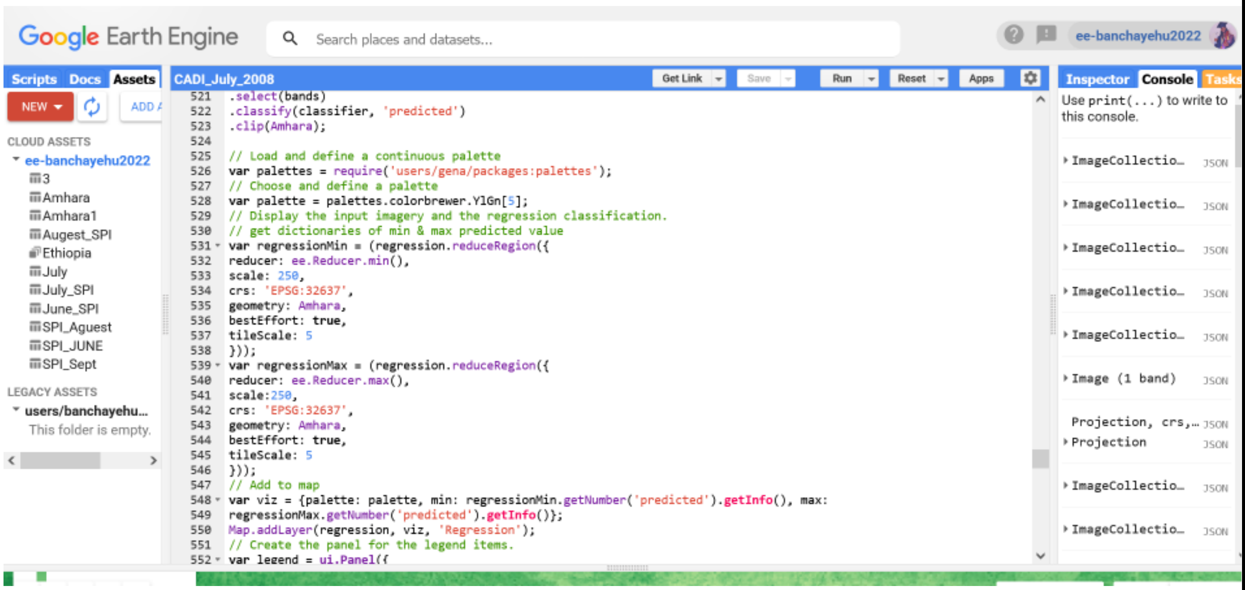
Google Earth Engine
Search places and datasets...
ee-banchayehu2022
Scripts Docs Assets
CADI_July_2008
Get Link
Save
Run
Reset
Apps
Inspector Console Tasks
.select(bands)
.classify(classifier, 'predicted')
.clip(Amhara);
// Load and define a continuous palette
var palettes = require('users/gena/packages:palettes');
// Choose and define a palette
var palette = palettes.colorbrewer.YlGn[5];
// Display the input imagery and the regression classification.
// get dictionaries of min & max predicted value
var regressionMin = (regression.reduceRegion({
reducer: ee.Reducer.min(),
scale: 250,
crs: 'EPSG:32637',
geometry: Amhara,
bestEffort: true,
tileScale: 5
}));
var regressionMax = (regression.reduceRegion({
reducer: ee.Reducer.max(),
scale:250,
crs: 'EPSG:32637',
geometry: Amhara,
bestEffort: true,
tileScale: 5
}));
// Add to map
var viz = {palette: palette, min: regressionMin.getNumber('predicted').getInfo(), max:
regressionMax.getNumber('predicted').getInfo()};
Map.addLayer(regression, viz, 'Regression');
// Create the panel for the legend items.
var legend = ui.Panel({
Use print(...) to write to this console.
ImageCollectio...
Image (1 band)
Projection, crs,...
Projection
JSON


Google Earth Engine
CADI_July_2008
style: {
position: 'bottom-left',
padding: '8px 15px'
}
});
// Create and add the legend title.
var legendTitle = ui.Label({
value: 'SPI)',
style: {
fontWeight: 'bold',
fontSize: '18px',
margin: '0 0 4px 0',
padding: '0'
}
});
legend.add(legendTitle);
// create the legend image
var lon = ee.Image.pixelLonLat().select('latitude');
var gradient = lon.multiply((viz.max-viz.min)/100.0).add(viz.min);
var legendImage = gradient.visualize(viz);
// create text on top of legend
var panel = ui.Panel({
widgets: [
ui.Label(viz['max'])
],
});
legend.add(panel);
// create thumbnail from the image
var thumbnail = ui.Thumbnail({
image: legendImage,
params: {bbox:'0,0,10,100', dimensions:'10x200'},

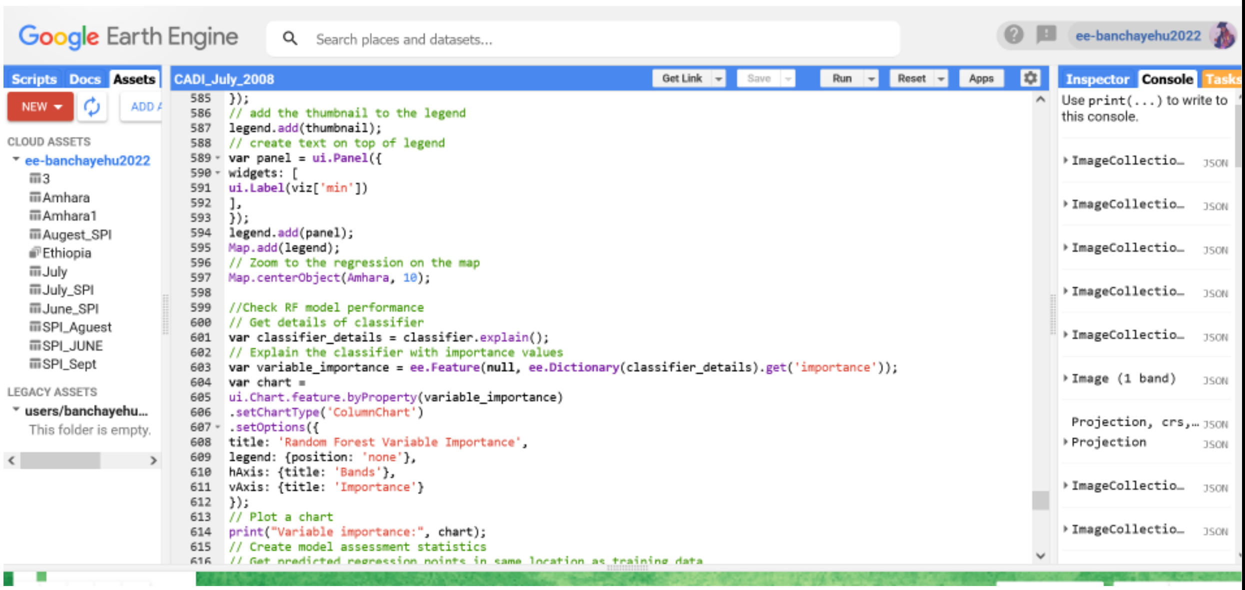
Google Earth Engine
CADI_July_2008
});
// add the thumbnail to the legend
legend.add(thumbnail);
// create text on top of legend
var panel = ui.Panel({
widgets: [
ui.Label(viz['min'])
],
});
legend.add(panel);
Map.add(legend);
// Zoom to the regression on the map
Map.centerObject(Amhara, 10);
//Check RF model performance
// Get details of classifier
var classifier_details = classifier.explain();
// Explain the classifier with importance values
var variable_importance = ee.Feature(null, ee.Dictionary(classifier_details).get('importance'));
var chart =
ui.Chart.feature.byProperty(variable_importance)
.setChartType('ColumnChart')
.setOptions({
title: 'Random Forest Variable Importance',
legend: {position: 'none'},
hAxis: {title: 'Bands'},
vAxis: {title: 'Importance'}
});
// Plot a chart
print("Variable importance:", chart);
// Create model assessment statistics

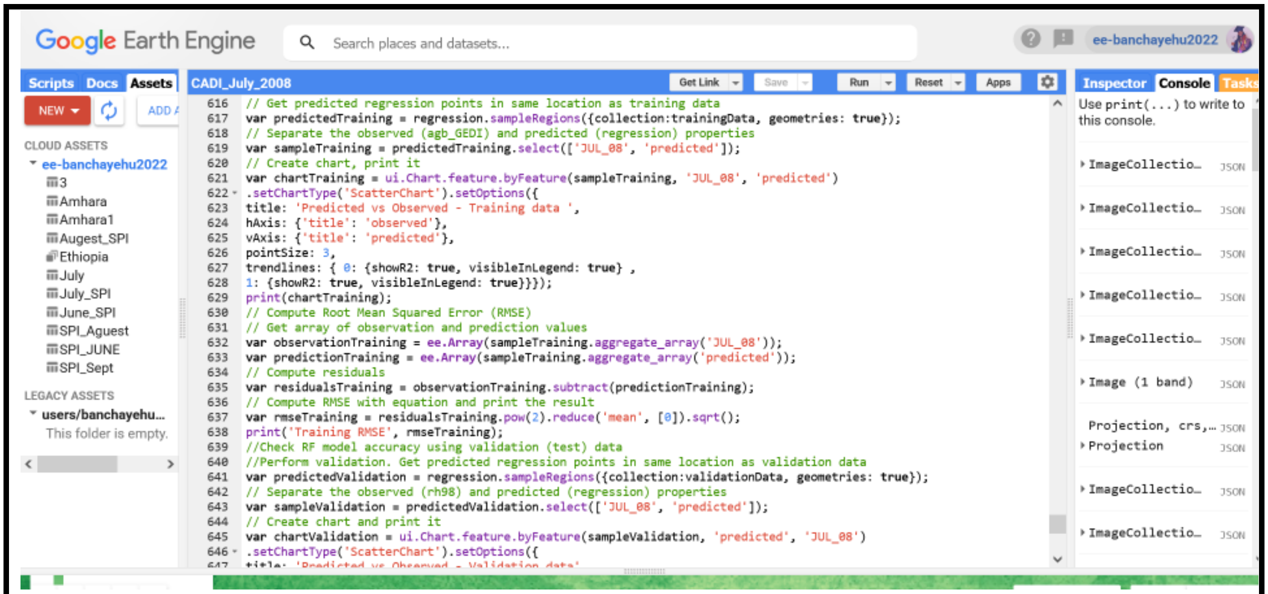
Google Earth Engine
Search places and datasets...
ee-banchayehu2022
Scripts Docs Assets
CADI_July_2008
Get Link Save Run Reset Apps
Inspector Console Tasks
NEW
ADD
CLOUD ASSETS
ee-banchayehu2022
3
Amhara
Amhara1
Augest_SPI
Ethiopia
July
July_SPI
June_SPI
SPI_Aguest
SPI_JUNE
SPI_Sept
LEGACY ASSETS
users/banchayehu...
This folder is empty.
// Get predicted regression points in same location as training data
var predictedTraining = regression.sampleRegions({collection:trainingData, geometries: true});
// Separate the observed (agb_GEDI) and predicted (regression) properties
var sampleTraining = predictedTraining.select(['JUL_08', 'predicted']);
// Create chart, print it
var chartTraining = ui.Chart.feature.byFeature(sampleTraining, 'JUL_08', 'predicted')
.setChartType('ScatterChart').setOptions({
title: 'Predicted vs Observed - Training data ',
hAxis: {'title': 'observed'},
vAxis: {'title': 'predicted'},
pointSize: 3,
trendlines: { 0: {showR2: true, visibleInLegend: true} ,
1: {showR2: true, visibleInLegend: true}}});
print(chartTraining);
// Compute Root Mean Squared Error (RMSE)
// Get array of observation and prediction values
var observationTraining = ee.Array(sampleTraining.aggregate_array('JUL_08'));
var predictionTraining = ee.Array(sampleTraining.aggregate_array('predicted'));
// Compute residuals
var residualsTraining = observationTraining.subtract(predictionTraining);
// Compute RMSE with equation and print the result
var rmseTraining = residualsTraining.pow(2).reduce('mean', [0]).sqrt();
print('Training RMSE', rmseTraining);
//Check RF model accuracy using validation (test) data
//Perform validation. Get predicted regression points in same location as validation data
var predictedValidation = regression.sampleRegions({collection:validationData, geometries: true});
// Separate the observed (rh98) and predicted (regression) properties
var sampleValidation = predictedValidation.select(['JUL_08', 'predicted']);
// Create chart and print it
var chartValidation = ui.Chart.feature.byFeature(sampleValidation, 'predicted', 'JUL_08')
.setChartType('ScatterChart').setOptions({
Use print(...) to write to this console.
ImageCollectio... JSON
ImageCollectio... JSON
ImageCollectio... JSON
ImageCollectio... JSON
ImageCollectio... JSON
Image (1 band) JSON
Projection, crs,... JSON
Projection JSON
ImageCollectio... JSON
ImageCollectio... JSON

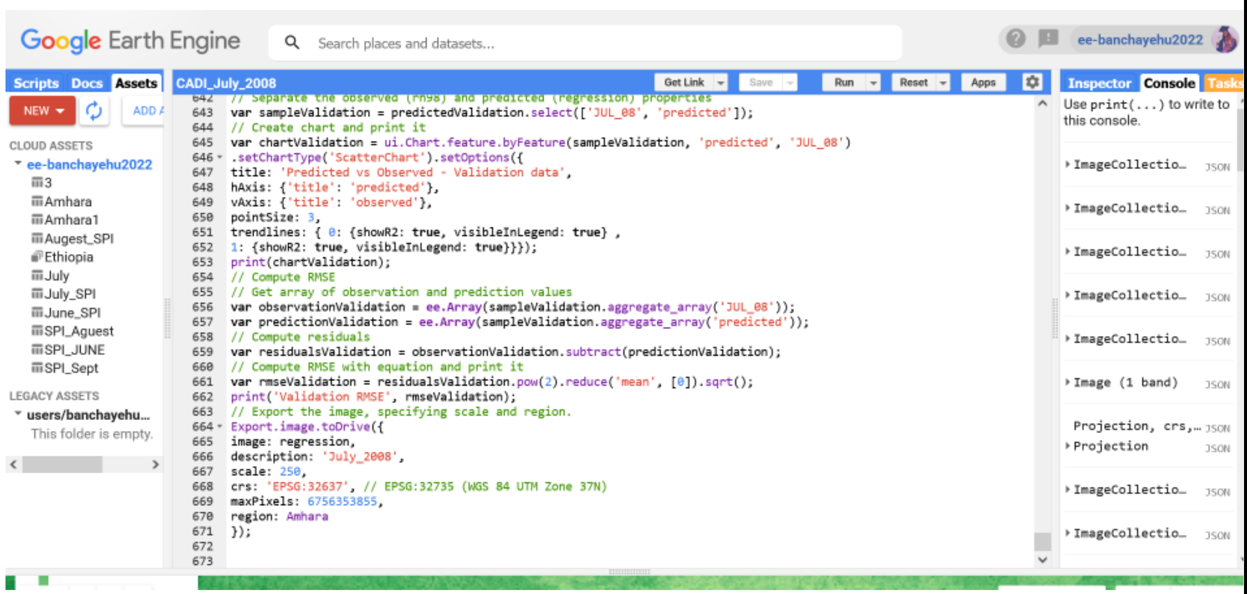
Google Earth Engine
Search places and datasets...
ee-banchayehu2022
Scripts Docs Assets
CADI_July_2008
Get Link Save Run Reset Apps
Inspector Console Tasks
NEW
ADD
CLOUD ASSETS
ee-banchayehu2022
3
Amhara
Amhara1
Augest_SPI
Ethiopia
July
July_SPI
June_SPI
SPI_Aguest
SPI_JUNE
SPI_Sept
LEGACY ASSETS
users/banchayehu...
This folder is empty.
var sampleValidation = predictedValidation.select(['JUL_08', 'predicted']);
// Create chart and print it
var chartValidation = ui.Chart.feature.byFeature(sampleValidation, 'predicted', 'JUL_08')
.setChartType('ScatterChart').setOptions({
title: 'Predicted vs Observed - Validation data',
hAxis: {'title': 'predicted'},
vAxis: {'title': 'observed'},
pointSize: 3,
trendlines: { 0: {showR2: true, visibleInLegend: true} ,
1: {showR2: true, visibleInLegend: true}}});
print(chartValidation);
// Compute RMSE
// Get array of observation and prediction values
var observationValidation = ee.Array(sampleValidation.aggregate_array('JUL_08'));
var predictionValidation = ee.Array(sampleValidation.aggregate_array('predicted'));
// Compute residuals
var residualsValidation = observationValidation.subtract(predictionValidation);
// Compute RMSE with equation and print it
var rmseValidation = residualsValidation.pow(2).reduce('mean', [0]).sqrt();
print('Validation RMSE', rmseValidation);
// Export the image, specifying scale and region.
Export.image.toDrive({
image: regression,
description: 'July_2008',
scale: 250,
crs: 'EPSG:32637', // EPSG:32735 (WGS 84 UTM Zone 37N)
maxPixels: 6756353855,
region: Amhara
});
Use print(...) to write to this console.
ImageCollectio... JSON
ImageCollectio... JSON
ImageCollectio... JSON
ImageCollectio... JSON
ImageCollectio... JSON
Image (1 band) JSON
Projection, crs,... JSON
Projection JSON
ImageCollectio... JSON
ImageCollectio... JSON

APPENDIX 3: Guiding Interview Questions

BAHIR DAR UNIVERSITY

FACULTY OF SOCIAL SCIENCES

DEPARTMENT OF GEOGRAPHY AND ENVIRONMENTAL STUDIES

FIELD OF GEO- INFORMATION SCIENCE

INTERVIEW

Interview Questions for Experts at the Agriculture and Food Security Offices in the Study area

Dear interviewee,

My Name is Banchayehu Molla; currently I am doing Master degree in Geo Information Science at Bahir Dar University. Now I am conducting research for my Msc thesis on Developing an Earth Observation Derived Combined Drought Index for Agricultural drought monitoring in Amhara region, Ethiopia. This interview questions have been prepared only for academic purposes. Your response is crucial for the success of this study. Therefore, as this research is only for academic purpose, I kindly request that you provide your genuine and thoughtful responses and all the information you provide is confidential, thus the researcher will guaranty your full security. Rest assured that any information you share during this interview were treated with utmost confidentiality and used exclusively for the purposes of this study.

Guiding interview questions for key informants

1. Can you briefly describe your role and experience related to agricultural drought monitoring?
2. Can you provide an overview of the agricultural drought conditions in your area?
3. Which zones of the region is mostly affected by drought?
4. How the Agriculture and Food Security Office monitor drought conditions?
5. Can you provide an overview of the current drought monitoring practices?
6. Which existing drought indices or metrics, if any, are currently being used for agricultural drought monitoring in the Amhara region?
7. How do you perceive the effectiveness of the existing agricultural drought monitoring systems in the region?
8. What are the main challenges and limitations of the existing drought monitoring approaches?
9. What are the limitations or challenges you have encountered in monitoring drought events?
10. Can you please provide information on drought years from the last 22 years that occurred from 2000 to 2021?
11. Which one was the most devastating event?
12. How the frequency of agricultural drought was looks like in the past drought years?

The insights and information you provided were crucial for the successful completion of my study. I sincerely appreciate your cooperation and voluntary participation in this study.